ESPOO 2006 VTT PUBLICATIONS 610

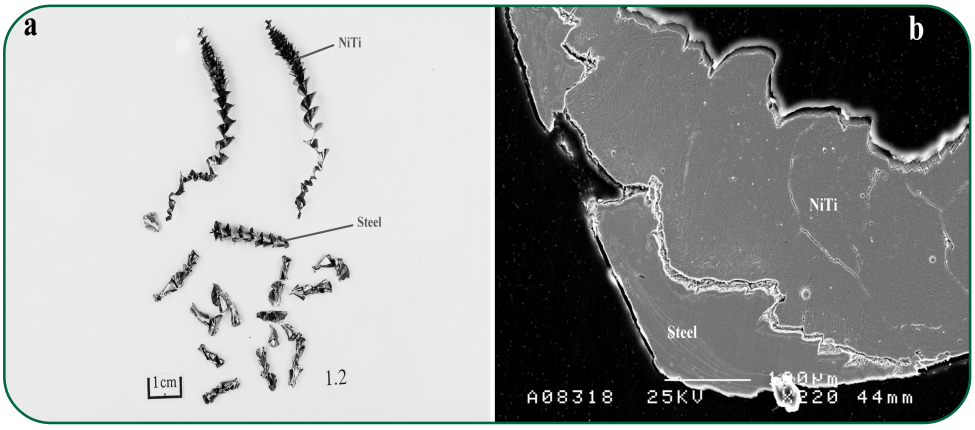

Jukka Paro

Machinability effects of stainless steels with a HIPed NiTi coating in high-efficiency machining operations

VTT PUBLICATIONS 610

Machinability effects of stainless steels with a HIPed NiTi coating in high-efficiency machining operations

Jukka Paro

Thesis for the degree of Doctor of Technology to be presented with due permission for public examination and criticism at Helsinki University of Technology in auditorium K216 on October 20 2006, at 12 o'clock.

ISBN 951–38–6853–2 (soft back ed.)
ISSN 1235–0621 (soft back ed.)

ISBN 951–38–6854–0 (URL: http://www.vtt.fi/publications/index.jsp)
ISSN 1455–0849 (URL: http://www.vtt.fi/publications/index.jsp)

JULKAISIJA – UTGIVARE – PUBLISHER

VTT, Vuorimiehentie 3, PL 1000, 02044 VTT
puh. vaihde 020 722 111, faksi 020 722 4374

VTT, Bergsmansvägen 3, PB 1000, 02044 VTT
tel. växel 020 722 111, fax 020 722 4374

VTT Technical Research Centre of Finland, Vuorimiehentie 3, P.O. Box 1000, FI-02044 VTT, Finland
phone internat. +358 20 722 111, fax +358 20 722 4374

VTT, Metallimiehenkuja 8, PL 1000, 02044 VTT
puh. vaihde 020 722 111, faksi 020 722 3349

VTT, Metallmansgränden 8, PB 1000, 02044 VTT
tel. växel 020 722 111, fax 020 722 3349

VTT Technical Research Centre of Finland, Metallimiehenkuja 8, P.O. Box 1000, FI-02044 VTT, Finland
phone internat. +358 20 722 111, fax +358 20 722 3349

Technical editing Anni Kääriäinen

Otamedia Oy, Espoo 2006

Paro, Jukka. Machinability effects of stainless steels with a HIPed NiTi coating in high-efficiency machining operations [Isostaattisella kuumapuristusmenetelmällä NiTi-pinnoitetun ruostumattoman teräksen suurtehotyöstön lastuttavuusvaikutuksia]. Espoo 2006. VTT Publications 610. 51 p. + app. 82 p.

Keywords stainless steels, machinability, machine tools, wear, surface coating, grinding, turning, drilling, nickel-titanium alloys

Abstract

The machinability effects of new high-strength stainless steels are researched due to specific properties arising from their structure. In grinding operations, HIPed (Hot Isostatically Pressed) austenitic 316L, duplex 2205 and super duplex 2507, and as-cast 304 stainless steel, in turning HIPed 316L, duplex stainless steel 2205 and X5 CrMnN 18 18 stainless steel, and in drilling HIPed PM (Powder Metallurgic) Duplok 27 and duplex stainless steel ASTM8190 1A and X2CrNi 1911 with HIPed NiTi coating were researched in revised machining testing environments using tool life testing, chip and workpiece surface morphology analysis. Chips, workpiece surfaces and cutting tools were analysed by SEM and EDS.

High toughness, workhardening and low heat conductivity have a synergistic effect in inducing machinability difficulties e.g. decreased product quality, shorter tool life, increased power consumption and decreased chip evacuation. An increased amount of alloying elements is found to decrease machinability in the form of increased cutting force and workhardening rate of the machined surface, and decreased tool life and surface roughness. Also, the machinability of PM-produced stainless steels is decreased because of the increased amount of hard oxide particles included in the microstructure of PM-produced stainless steel. The formation of BUE (Built-up Edge) is found, affecting the machinability and tool life of tested high-strength stainless steels.

In grinding operations HIPed austenitic 316L and duplex 2205 stainless steel are rated according to cutting force, workhardening rate and the amount of microvoids and microcracks in ground surfaces. In turning operations HIPed 316L, duplex stainless steel 2205 and X5 CrMnN 18 18 stainless steels are

assessed in machinability order. The machinability of conventional cast duplex stainless steel ASTM8910 and HIPed duplex stainless steel Duplok27 were sorted according to the PRE-value (Pitting Resistance Equivalent).

Finally in this study, the suitability of coated cemented carbide tools in the drilling of conventionally produced cast stainless steels with HIPed NiTi-coating was investigated. In drilling of difficult-to-cut X2CrNi 19 11 stainless steel with a pseudo-elastic coating, effective cutting parameters that maintain an adhesion layer between the NiTi coating and the stainless steel intact with an advantageous surface finish were generated.

Paro, Jukka. Machinability effects of stainless steels with a HIPed NiTi coating in high-efficiency machining operations [Isostaattisella kuumapuristusmenetelmällä NiTi-pinnoitetun ruostumattoman teräksen suurtehotyöstön lastuttavuusvaikutuksia]. Espoo 2006. VTT Publications 610. 51 s. + liitt. 82 s.

Avainsanat stainless steels, machinability, machine tools, wear, surface coating, grinding, turning, drilling, nickel-titanium alloys

Tiivistelmä

Uusien lujien ruostumattomien terästen ominaisuuksilla on suuri vaikutus niiden lastuttavuuteen. Tässä työssä tutkittiin isostaattisella kuumapuristuksella (HIP) valmistettujen austeniittisen 316L, duplex 2205 ja super duplex 2507 sekä valetun 304 ruostumattomien terästen hiontaa, HIP-menetelmällä valmistetun 316L ruostumattoman teräksen ja X5 CrMnN 1818 -typpiteräksen sorvausta sekä HIP-menetelmällä valmistetun Duplok 27 -teräksen ja ruostumattoman duplex-teräksen ASTM8190 1A porausta. Lisäksi tutkittiin HIP-menetelmällä valmistetun NiTi-pinnoitteella pinnoitetun X2CrNi 1911 ruostumattoman teräksen porausta. Lastuttavuutta selvitettiin sovelletuin testein tutkimalla terän kestoaikaa, analysoimalla lastujen ja työkappaleen pinnan morfologiaa. Lastuja, työkappaleiden pintoja sekä teriä tukittiin pyyhkäisyelektronimikroskoopilla (SEM) ja energiadispersiivisellä alkuaineanalyysillä (EDS).

Tutkittujen terästen ominaisuuksista suuri sitkeys, muokkauslujittuminen sekä matala lämmönjohtavuus aiheuttavat lastuttavuusongelmia. Runsaan seostuksen on todettu huonontavan lastuttavuutta, sillä lastuamisvoimat kasvavat, terien kestoajat lyhentyvät, koneistetut pinnat muokkauslujittuvat sekä työkappaleen pinnanlaatu huononee. Pulverimetallurgisesti valmistetuttujen ruostumattomien terästen mikrorakenteen kovat oksidit vaikeuttavat myös koneistettavuutta. Irtosärmän muodostumisen todettiin myös heikentävän testattujen terästen lastuttavuutta.

Tässä työssä havaittiin suurten lastuamisvoimien sekä hiotun pinnan muokkauslujittumisen ja mikrohalkeamien ja -säröjen muodostumisen vaikuttavan 316L sekä duplex 2205 ruostumattoman teräksen hiottavuuteen. Sorvaustutkimuksissa selvitettiin 316L:n, 2205:n sekä X5 CrMnN 1818:n lastuttavuuteen vaikuttavia

tekijöitä, terän kestoaikoja sekä kulumismekanismeja. Porauksessa arvioitiin myös perinteisen valetun duplex-teräksen sekä HIP-menetelmällä valmistetun duplex ruostumattoman teräksen lastuttavuutta PRE-arvon (Pitting Resistance Equivalent) avulla. Lopuksi selvitettiin pinnoitettujen kovametalliporien soveltuvuutta pseudo-elastisella NiTi-pinnoitteella pinnoitettujen valettujen ruostumattomien terästen poraukseen. Työssä löydettiin menetelmät ja lastuamisarvot, joilla voidaan saavuttaa riittäviä terien kestoaikoja ja pitää NiTi-pinnoitteen ja ruostumattoman teräksen välinen adheesiokerros vaurioitumatta sekä reikien pinnanlaatu hyvänä.

Preface

This thesis is based on the work carried out mainly in the Laboratory of Production Engineering at the Helsinki University of Technology (HUT) from 1993–1999. Publications I and II were accomplished during the "Machining of New Strength Stainless Steels" project in close co-operation with the Laboratory of Engineering Materials funded by the Academy of Finland. Publications III and IV were produced during the author's work at the Graduate School of Concurrent Mechanical Engineering (GSCME). This work was financially supported by Tekniikan edistämissäätiö (TES). The appended Publications V, VI and VII were prepared during several machining projects at VTT.

I would like to express my gratitude to Professor Veijo Kauppinen and Professor Hannu Hänninen for their guidance and invaluable support. Laizhu Jiang Ph.D. is thanked for his close co-operation during the course of this work. The encouragement of Dr.Tech. Jyrki Kohopää is also especially appreciated. Professor Mauri Airila (GSCME) is also especially acknowledged. I am also grateful to my colleagues for their helpful collaboration over the years.

Finally, warm thanks are owed to my dear family, wife Marjut and daughters Emmi and Anni, for their patience and support.

Geneve, June 2006

Jukka Paro

Contents

List of publications

This dissertation consists of an introductory report and seven appended publications (I–VII).

I Jiang, L., Paro, J., Hänninen, H., Kauppinen, V. & Oraskari, R. 1996. Comparison of grindability of HIPped austenitic 316L, duplex 2205 and super duplex 2507 and as-cast 304 stainless steels using alumina wheels. Journal of Materials Processing Technology 62(1996), pp. 1–9.

II Jiang, L., Hänninen, H., Paro, J. & Kauppinen, V. 1996. Active wear and failure mechanisms of TiN-coated high speed steel and TiN-coated cemented carbide tools when machining powder metallurgically made stainless steels. Metallurgical and Materials Transactions A, Vol. 27 A September 1996, pp. 2796–2808.

III Paro, J., Hänninen, H. & Kauppinen, V. 2001. Tool wear and machinability of X5 CrMnN 18 18 stainless steels. Journal of Materials Processing Technology, 119(2001), pp. 14–20.

IV Paro, J., Hänninen, H. & Kauppinen, V. 2001. Tool wear and machinability of HIPed P/M and conventional cast duplex stainless steels. Wear 249(2001), pp. 279–284.

V Paro, J.A., Gustafsson, T.E. & Koskinen, J. 2004. Drilling of conventional cast stainless steel with HIPed NiTi coating. Journal of Materials Processing Technology, 153–154(2004), pp. 622–629.

VI Paro, J.A., Gustafsson, T.E. & Koskinen, J. 2003. Chip morphology in drilling of conventional cast stainless steel with HIPed NiTi coating. Proceedings of the 3rd International Conference on Research and Development in Mechanical Industry, RaDMI 2003, Hotel Plaža, 19–23 September, Herceg Novi, Serbia and Montenegro. 8 p.

VII Paro, J.A., Gustafsson, T.E. & Koskinen, J. 2005. Deformation effects on the interface between X2CrNi 19 11 stainless steel and HIPed NiTi coating in machining. Proceedings of the 18th International Conference on Production Research, 31st July – 4th August 2005, Salerno, Italy. 5 p.

Original findings

The experimental data and analyses of this thesis report are directed towards evaluating the high-efficiency machining and machinability of new high-strength stainless steels, especially in modern machine tools and with modern tool materials. The following features of this thesis are believed to be original:

- The machinability effects of high-strength stainless steels with modern machine tools and cutting tools were studied over a wide range of machining parameters in grinding, turning and drilling operations.

- When using alumina wheels, the workhardening of the workpiece surface and the formation of microcracks decreases the grindability of HIPed austenitic 316L, duplex 2205 and super duplex 2507 and as-cast 304 stainless steels.

- When turning HIPed austenitic 316L, duplex 2205 using TiN-coated cemented carbide tools, the dominant tool wear mechanisms are fatigue-induced failure and diffusion wear.

- When the machining of PM-produced stainless steel is compared to that of conventionally produced stainless steel, the tool life is found to decrease. PM-produced stainless steel shows a higher workhardening rate, thus decreasing the tool life. On the other hand, the formation of BUE is increased when conventionally produced stainless steel is used.

- The presence of BUE decreases the machinability of X5CrMnN 18 18 stainless steels by causing decreased surface roughness and evidence of microcracks at the worked surface. The increase of nitrogen content was found to decrease the workhardening rate of the workpiece surface.

- The macroscopic geometry of stainless steel chip with a HIPed NiTi coating differs from conventional stainless steel chip and a combined chip structure is built. On the other hand, when effective cutting speeds and feed rates were utilized, optimal drill performance is achieved without a deterioration in coating properties.

List of symbols and abbreviations

a	Depth of cut
BUE	Built-Up Edge
CBN	Cubic Boron Nitride
CVD	Chemical Vapour Deposition
d	The diameter of the rotating tool or workpiece
f	Feed rate
EDS	Energy Dispersive Spectroscopy
EDM	Electric Discharge Machining
F_n	Normal force component
F_t	Tangential force component
F_x	Cutting force component in the direction of the x-axis
F_y	Cutting force component in the direction of the y-axis
F_z	Cutting force component in the direction of the z-axis
G	Grinding ratio
HEM	High Efficiency Machining
HIP	Hot Isostatically Pressed
HSC	High-Speed Cutting

HSM	High-Speed Machining
HSS	High-Speed Steel
k_v	Factor
K_v	Workability co-efficient
n	Rotation speed
OM	Optical Microscope
PCD	Polycrystalline Diamond
PM	Powder Metallurgy
PRE	Pitting Resistance Equivalent PRE = wt% Cr+ 3.3 x wt% Mo + 13x wt% N
R_a	Surface roughness (Mean Arithmetic Deviation)
SEM	Scanning Electron Microscopy
SMA	Shape Memory Alloy
T	Tool life
VB	Flank wear value
v, v_c	Cutting speed
v_f	Feed speed
V	Cutting volume
z	The number of cutting edges

1. Introduction

There is a tendency in the field of machined materials towards stainless steels with higher strength and higher corrosion resistance. Duplex stainless steels are often applied (Schintlmeister & Wallgram 1999). High-efficiency machining and the machinability of high-strength stainless steels are considered to be the most important future trends affecting machining operations. Duplex stainless steels have a lower nickel content than austenitic stainless steels, and an austenite plus ferrite structure. Increased strength with enhanced properties for service in a corrosive environment provides difficulties from a machinability point of view.

The characteristics of stainless steels raised from the austenitic structure are high toughness, low thermal conductivity and high workhardening co-efficient (Peckner & Bernstein 1977). From a machinability point of view the most important characteristic is the workhardening. Because of the low thermal conductivity, the chips are formed on the basis of catastrophic failure in narrow shear surfaces (Dolinšek 2003). When carbide tools are used these characteristics cause the formation of BUE and low values of tool life. Cutting forces are also increased and the unfavourable formation of tough chips appears (Dolinšek 2003).

Tool materials, such as CVD-coated (Chemical Vapour Deposition) with hard Al_20_3 coatings, are often preferred (Belejchak 1997). The need for a hard tool surface coating is especially required when HIPed stainless steels containing hard inclusions are to be machined.

Near-equiatomic nickel-titanium alloys (NiTi) have many attractive properties for engineering applications, such as pseudo-elasticity and good cavitation resistivity, in addition to their more well-known shape memory properties (Li & Sun 2002, Starosvetsky & Gotman 2001). In drilling stainless steel with a pseudo-elastic coating material, machinability difficulties are involved with the pseudo-elastic properties of the coating material. Nevertheless, both technical and commercial limitations arise when NiTi is considered as a material for large engineering components. Consequently, interest in NiTi-coating technologies, for example for stainless steels, is on the rise. The cutting process of NiTi-based shape memory alloys is influenced by their high ductility and high degree of workhardening, and the unconventional strain-stress behaviour (Weinert & Petzoldt 2004).

The investigation of machining austenitic stainless steels in different cutting processes has been initiated by industry, where the need for effective tools and demands for reliable data on cutting parameters extends far beyond the experiences or recommendations given by tool producers (Dolinšek 2003). The machinability studies are often carried out by vT-tests in turning, milling and drilling operations. Tool wear is studied by using optical microscopy to define the amount of flank and crater wear. The interaction between tool and chip can be effectively studied using SEM.

There are several tendencies affecting the technology and methods used in the metalworking industry. Highly efficient machining strategies are used, and HEM (High Efficiency Machining) is used as a machining method. In HEM machine tools, modern tools are used with sufficient cutting parameters. HEM focuses on optimising cutting efficiency to maximise material removal rate. Compared to HSM (High Speed Milling), lower spindle speeds and increased chip thicknesses are used. The modern tools and tool materials available for this research were specifically designed cutting tools for HEM machine tools. The machine tool reliability and productivity is controlled by optimising machining parameter selection and acceptable and adequate sufficient parameters are used. Also, nowadays modern machine tools are very complex mechatronical systems and their capability and efficiency are mainly determined by their kinematics, structural dynamics, computer numerical control system and the machining process (Altintas et al. 2005 and Weck et al. 2003).

The hypothesis of this work is that tool wear mechanisms and workhardening of the chip and workpiece surface also affect machinability behaviour in the drilling of stainless steels with a HIPed NiTi coating. The aim of the present research was to provide information about the effects, e.g. tool life, cutting forces and surface roughness, arising in the machining of new high-strength stainless steels in high-efficiency machining operations with respect to machining method, the amount of alloying elements and workpiece coating. The machinability tests of these materials were carried out with the machine tools installed in the Laboratory of Production Engineering at HUT.

The new high-strength stainless steels HIPed austenitic 316L, duplex 2205, super duplex 2507 and as-cast 304 were tested firstly in conventional grinding and turning operations (Publications I and II). The effect of nitrogen content in

turning operation of high nitrogen X5 CrMnN 18 18 stainless steels is presented in Publication III.

The machining operations with a high-performance machine tool were carried out when a machining centre equipped with modern drilling tools was applied (Publications IV–VII). The machinability of HIPed stainless steel Duplok27 and the conventionally produced cast stainless steel ASTM A890 1A was compared in Publication IV. The machinability effects of stainless steel with HIPed NiTi coating are presented in Publications V, VI and VII.

The machine tools and cutting tools used in the present study are widely commercially available without any special laboratory-oriented features, and also SEM is mainly used for sample visualisation in drilling tests with modern cutting tools. The results gained in the laboratory are also applicable in real machining operations of high-strength stainless steel components.

2. Experimental materials and procedure

2.1 Materials

Several duplex stainless steels and new high-strength stainless steels typically used in process industry applications were included in this study. The workpiece materials for the grinding tests were HIPed austenitic stainless steel PM 316L, duplex stainless steel PM 2205, super duplex 207 and as-cast 304. The workpiece materials for the turning tests were HIPed austenitic stainless steel PM 316L, HIPed duplex stainless steel PM 2205 and X5CrMnN 18 18 high nitrogen stainless steels. The test materials for the drilling tests were HIPed duplex stainless steel Duplok 27, cast duplex stainless steel A 890 1A, and cast stainless steel X2CrNi 1911 with a HIPed NiTi coating, the composition of which in wt-% is 55/45. The chemical compositions of the tested steels are given in Table 1.

Duplex stainless steels are increasingly used as an alternative to conventional stainless steels. The main advantages of the duplex grades are good resistance to stress corrosion cracking and also to corrosion fatigue in environments containing chlorides (Nyström 1995). Powder metallurgy (PM) materials are considered to have poor machinability, a behaviour explained by three contradictory theories, namely interrupted cutting, hard inclusions and reduced thermal conductivity (Agapiou et al. 1988). For austenitic stainless steels, it is difficult to combine the improvement of corrosion resistance with good machinability.

Improvements in machinability are often obtained by an increase in sulphur content. In order to combine high corrosion resistance properties with improved machinability, a Cu-enriched alloy has been developed (Coudreuse et al. 1997). Stainless steels containing malleable oxides form the latest generation of steels with improved machinability (Bletton et al. 1990). By modifying the composition of the non-metallic inclusions and controlling the shape, size and distribution of the inclusions, considerable improvements in the machinability of 2205 duplex stainless steel are obtained (Arnvig et al. 1994).

Duplex stainless steels show different technological behaviour when compared to other classes of stainless steel. Therefore, new geometry and cutting parameters are defined for duplex stainless steels (Pellegrini et al. 1997). Duplex

stainless steels have a machinability profile that differs somewhat from that of austenitic steels with a similar corrosion resistance, and they are not as difficult to machine with high-speed steel tools as with cemented carbide tools (Arnvig et al. 1994).

Table 1. Chemical composition (wt%) of the test materials.

Material	**Test performed**	**C wt%**	**Si wt%**	**Mn wt%**	**P wt%**	**S wt%**	**Cu wt%**	**Cr wt%**	**Ni wt%**	**Mo wt%**	**V wt%**	**Al wt%**	**N wt%**	**O wt%**
PM 316L	grinding, turning	0.05	0.68	1.44	0.022	0.009	0.19	16.7	11.0	2.7	0.11	0.021	0.12	0.12
PM2205	grinding, turning	0.03	0.07	1.42	0.022	0.008	0.013	22.1	5.3	3.0	0.07	0.016	0.21	0.014
PM2507	grinding	0.03	0.30	0.30	0.035	0.009	0.16	25.0	7.0	4.0	0.08	0.020	0.30	0.015
AC304	grinding	0.03	0.40	1.20	0.040	0.015	0.176	18.4	9.2		0.06	0.025	0.10	0.001
X5CrMnN18 8 (G88216)	turning	0.05	0.29	18.89				18.13	0.43	0.11	0.08		0.57	
X5CrMnN18 8 (DDT63)	turning	0.05	0.49	19.8				18.6	0.61	0.08	0.13		0.91	
Duplok 27	drilling	0.03	0.02	0.7	0.02	0.001	2.3	26.5	7.0	3.0			0.3	
A890 1A	drilling	0.03	0.74	0.63	0.026	0.006	3.01	25.0	5.54	2.03				
X2CrNi 1911	drilling	0.03	0.4	1.20	0.04	0.015		18.4	9.2		0.06			

According to Charles (1994) the most interesting characteristics of duplex stainless steels include:

- A low thermal expansion coefficient that makes these materials suitable for use in thermal cycling conditions.
- Higher thermal conductivity than in austenitic grades makes the duplex grades good candidates for heat exchanger applications.
- Strongly magnetic behaviour due to the presence of about 50 per cent ferrite, enabling the use of magnetic clamping during machining.

Chemical compositions of some duplex stainless steels are presented in Table 2.

Table 2. Chemical composition of duplex stainless steels designed for new applications (Charles 1994).

	Chemical Composition [wt%]					**Applications**
	Cr	**Ni**	**Mo**	**N**	**Others**	
CLI UR 35 N Cu	23	5	0.1	0.1	2 Cu	Improved machinability
AVESTA 2205 NRG	22	5.6	3	0.13	0.02 S	-”-
CLI UR 52 NRS	25	6.5	3	0.2	0.02S-1.6Cu	
SUMI-TOMO	22.5	10	–	0.1	3 Si	Nitric acid
AVESTA 2308 PM	22.5	9	2.4	0.02	0.04 Ti-0.06Al-2Si	Bars/ forgings
NIPPON S.S.	17.5	4	–	0.05	1Cu-3Si-3Mn	Railway car
COREA 3W-1Mo	22	5.5	1	0.16	3W	General purpose

Recent industrial applications in raw material handling, food processing and environmental management show the considerable advantages of high nitrogen steels compared to regular wear-resistant materials (Rennhard 1998). Choosing

high nitrogen steels for jewellery is motivated by nickel allergy prevention, and a unique combination of corrosion resistance and strength is achieved in specific medical applications by new grade high nitrogen steels (Rennhard 1998 and Ilola 1999). According to Sundvall et al. (1998) nitrogen alloyed stainless steel grades are commonly used in modern process industry applications.

2.2 Test methods

The main testing methods showing the machinability behaviour used in this study were drilling, grinding and turning tests. The machinability of the test materials was determined by means of tool wear testing, cutting force measurements and analysis of the tool surfaces and chips with SEM. Tool wear was measured with optical microscopy, the tools and chips were analysed by SEM, and the workpiece surfaces using microhardness measurements.

The machinability tests were carried out using the existing machine tools of the laboratory of Production Technology, which are also conventional machine tools applicable to the Finnish metalworking industry. The machining experiments for new high-strength stainless steels were selected to clarify the machinability of recently developed steels. Machining tests were also carried out using commercially available appropriate tooling and fixtures. The test methods are described in Appendix I.

The most common machining operations were selected, and machining tests were carried out using turning, grinding and drilling operations. Conventional machine tools and cutting tools were selected. After machining, the cutting tools and chips were analysed using optical microscopy and SEM to determine tool wear and tool wear mechanisms.

Test methods were selected to find the effects of new high-strength stainless steels during machining operations. For conventional machining operations there are standardised tool wear tests. In this research, the machinability behaviour of new high-strength stainless steels with modern material analysing equipment is shown, and the revised machinability tests were carried out using tool life testing in turning, grinding and drilling operations. Tool wear was studied to define the amount of flank and groove wear.

2.2.1 Grinding experiments

The grinding experiments presented in Publication I were carried out using an Okamoto horizontal-grinding machine with Norton 43A6 GVX Al_2O_3 wheels of 200 mm diameter. A cutting speed of 30 m/s and a 0.25 m/min table speed were applied. The materials presented in Table 1 were cut into test pieces of 8 mm wide and 200 mm long. During grinding the radial wheel wear was measured using a Micro-HITE height gauging instrument. Grinding force components were measured with a Kistler piezo-electric dynamometer and the surface roughness was measured after grinding with a Taylor surface roughness instrument. After the grinding tests, metallographic examinations and analyses of the ground surfaces were performed by SEM together with energy dispersive spectroscopy (EDS). Workhardening of the specimen surface was investigated with an MHT-4 microhardness tester with a load of 20 g. The methods are described in Appendix I.

2.2.2 Turning experiments

The results of the turning tests using a VDF lathe with a 100 kW spindle motor are presented in Publication II. TiN-coated high-speed steel (HSS) T42, P30 cemented carbide inserts and SPUN 120308 inserts are applied in the turning of samples. The samples were 70 mm in diameter and 350 mm in length. A lathe with a quick-stop device at Imatra Steel works was applied for chip root samples. The turning experiments on X5CrMn 18 18 presented in Publication III were carried out using TiN- and Al_2O_3-coated cemented carbide inserts of type SNMG 120408-PM P15/K15. HSS tools were applied with cutting speeds of 15–55 m/min, and solid carbide tools were applied with cutting speeds of 100–250 m/min. A feed rate of 0.15 mm/r and a depth of cut of 1 mm were utilised.

The flank wear (VB) of the cutting tools was measured with a toolmaker's microscope. The criterion for tool life was either VB = 0.3 mm or catastrophic failure of the tool edge. Cutting forces were measured with a three-component piezo-electric force dynamometer. The possible bonding interface between the tool materials and chips was analysed using SEM and EDS analysis. Solid carbide inserts and chips were also analysed using SEM and EDS after the turning tests on X5CrMn 18 18 stainless steels. The measurement of the

hardness value of the machined surface was also performed. The methods are described in Appendix I.

2.2.3 Drilling experiments

The drilling experiments on HIPed and conventionally produced stainless steels are presented in Publication IV. These were carried out by using a modern horizontal machining centre, a Mazatech FH480 equipped with a 12 000 rpm spindle and conventional precision tool holders, allowing a cooling trough spindle with solid carbide drills of Titex Alpha4+ DX45 ∅8.5 mm, P40. Cutting speeds between 40–69 m/min with a feed rate of 0.2 mm/r were used. The methods are described in Appendix I.

The drilling experiments on conventional cast stainless steels with a HIPed NiTi coating are presented in Publications V, VI and VII. The same machining centre was equipped with TiCN- and TiN-coated Mitsubishi MZS850L with a diameter of Ø8.5 mm. A cutting speed of 50 m/min and feed rates of 0.1, 0.15, and 0.2 mm/rev were used. The drilling tests were done both with and without through-spindle cooling.

The flank wear (VB) of the solid carbide drills was measured with a toolmaker's microscope. The criterion for tool life was either VB = 0.3 mm or catastrophic failure of the drill. SEM was used to analyse tool wear from cemented carbide drills and chip morphology. Chips were investigated with a MHT-4 microhardness tester using a load of 20 g.

3. Summary of main results

3.1 Comparison of test methods

Machinability is often defined as the quality or state of being machinable by different machining methods such as turning, milling, grinding, etc. In machining it is generally desirable to produce a satisfactory part at the lowest possible cost (Cook 1975). Lindgren (1980) divides machinability tests into authentic and simulated tests. Machinability is often characterised by the following three aspects:

- easy metal removal; such as power requirement and chip forming characteristics (curl or break down)
- tool life (crater wear, flank wear and chipping)
- workpiece quality (surface roughness, dimensional accuracy).

In Publications I and II preliminary tests are shown applying grinding and turning operations in the machining of high-strength stainless steel. Tool wear rate and phenomena are studied.

Tool wear plays a vital role in influencing both the ease of cutting and the resultant machined surface (Liew et al. 2003). The high strength, low thermal conductivity, high ductility and high workhardening tendency of austenitic stainless steels are the main factors that make their machinability low. In machining, segmental chips are formed and the formation of BUE is present when carbide tools are used (Dolinšek 2003). In many cases, machining problems with austenitic stainless steels are associated with BUE formation, bad surface, burr formation and unfavourable chip size. In Publication I, grindability and ground stainless steel surfaces are studied.

Komanduri and Brown (1981) compiled a detailed classification of chips produced by non-homogenous cutting, named as wavy chip, discontinuous chip, segmental chip and catastrophic shear chip. According to von Turkovich (1981) the properties of materials manifest themselves in cutting forces, chip form (curl, segmentation, BUE, strain and strain rates (including fracture), chip-tool contact length, temperatures in the shear zone and along the chip-tool interface and the mechanical and metallurgical state of the new surface. In this study cutting

forces, chip forms and workhardening of chips and workpiece surfaces were found to be sufficient indicators of the machinability of the tested stainless steels. The macroscopic morphology of the chips and the workhardening are studied against the cutting parameters in Publications II and III.

The cutting force is one of the most important physical variables embodying relevant process information in machining. Such information can be used to assist in understanding critical machining attributes such as machinability, cutter wear or fracture, machine tool chatter, machining accuracy and surface finish (Tlusty & MacNeil 1975, Budak & Altintas 1994, Budak & Altintas 1995). The effects of thermal conductivity and shear strength where considered in tool life prediction with a modified Taylor equation is presented by Schäpermeier (1999). In the most commonly used tool condition monitoring systems, sensors measure cutting force components or quantities related to cutting force (power torque, distance/displacement and strain (Jemelniak 1999). The machinability of new high-strength stainless steels is verified by the means of cutting force measurements in Publications I to IV.

Many models and attempts have been made to analyse the mechanics of the orthogonal machining process (Stevenson & Stephenson 1998, Beno 1996). In analytical studies of the mechanics of the machining process, attention is usually restricted to the simplified orthogonal case where a layer of material is removed by a single, straight cutting edge set normal to the cutting velocity (Arsecularatne et al. 1998). In this study, the machinability of the new high-strength stainless steels was presented by vT-curves in Publications III to VI. A quantitative evaluation system of machinability, grindability and other workabilities based on specific cost productions is proposed by Taniguchi (1971), Yeo (1989) and Yeo (1995).

It is suggested by Höglund (1976) and Šalak et al. (2005) that plastic deformation is the main phenomenon in the cutting process, and that this deformation takes place at a microscopic scale under extreme conditions. It has also been suggested by Recht (1964), that thermally-aided adiabatic instabilities from the interaction of strain rate, flow stress and temperature could be responsible for the serrated or discontinuous chip behaviour during the machining of titanium or steel. Iwata and Kanji (1976) show the significance of

dynamic crack behaviour during the metal cutting process. As shown in Publications I and III, cracks were found in the worked surfaces.

Research work into the physics of machinability theory is as yet unable to completely define the metal cutting processes (Mackerle 1999, Mackerle 2003, Shaw 1985, Oxley 1988, Özel 2006). Machinability data simply recommend "reasonable" sets of tool materials, feeds, speeds, fluids, etc., for given machining requirements, or a list of specific tool-life values for a set of machining conditions (Cook 1975). Beno (1996) lists modern methods describing material behaviour during a cutting operation near the shear zone. Chick and Mendel (1998) have expressed a model using wear curves to predict the cost of changes in cutting conditions. The effect of cutting fluid on workpiece surface quality is studied in Publications V and VI, where the effect of using through-spindle cooling is tested.

The commonly used basis for tool life criteria according to Tipnis and Joseph (1975) is presented in Table 3.

Table 3. Commonly used basis for tool life criteria (Tipnis & Joseph 1975).

Basis	**Criteria**
State of Machined Surface	Dimensional Tolerance, Surface Finish, Surface and Functional Integrity, in terms of residual stresses, surface damage and affected functional properties
Rate of Material Removal	Rate of Material Removal Under Fixed Force
Ease of Chip Disposal	Chip Length, Breakability
Duration of Tool Life	Location of Tool Wear, Distortion, Deflection, Loss of Edge Geometry

The machinability of stainless steels is often compared to the pitting resistance equivalent value representing the alloying content of the steel. The Pitting Resistance Equivalent (PRE) index, PRE= wt%Cr+3.3x wt%Mo+30x wt% N is presented in Figure 1.

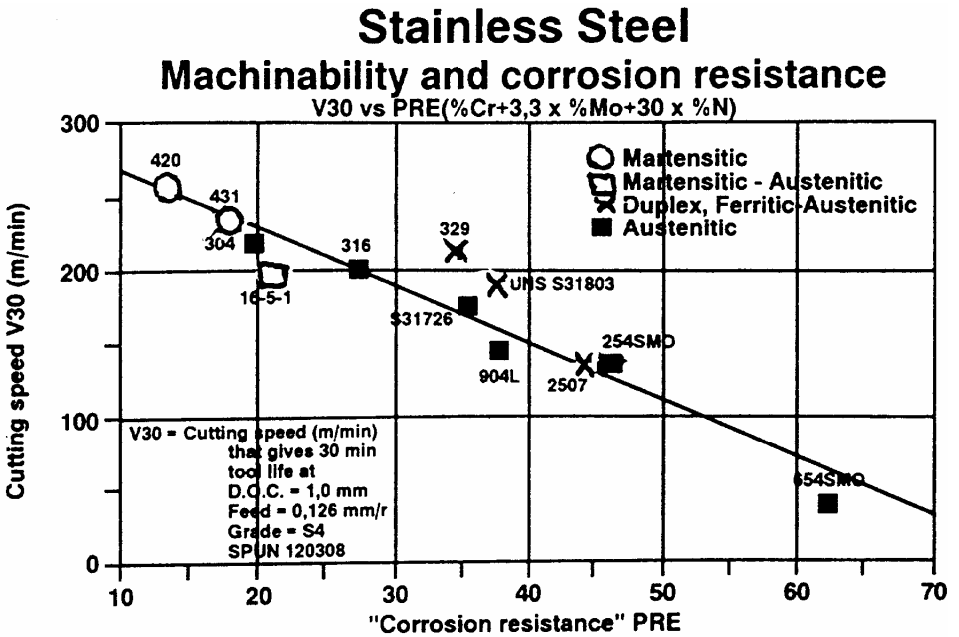

Figure 1. Machinability and corrosion resistance of stainless steels. V30 vs. PRE (Östlund 1994).

The machinability can be also expressed by the machinability by workability coefficient, K_v,which estimates material resistance to a cutting process. Tensile strength has been found to be the most useful attribute for determining the workability of stainless steels through this relationship (Hallum 1995).

$$K_v = -1.74 + 200/\sigma \quad (1)$$

3.2 Turning of new high-strength stainless steels

Stainless steels have always been considered difficult to machine. In the stainless steel family, duplex steels are particularly difficult to machine, generating more BUE and irregular wear than single-phase stainless steels (Roos 1997). The composition that provides high tensile strength and high corrosion resistance in stainless steels usually results in lower machinability than carbon steels, for example (Belejchak 1997).

It is suggested (Leffler et al. 1996) that the lower alloyed duplex grades, such as S32304, are comparatively easy to machine. In general, modern duplex grades tend to be more difficult to machine than the older grades, by virtue of higher austenite and nitrogen contents (Gunn 1997).

The machinability of PM 316L and PM 2205 was studied in this work. In turning operations, TiN-coated cemented carbide tools have a longer tool life when machining PM 316L than PM 2205 stainless steel. Selecting rapid and reliable manufacturing parameters and optimising these with respect to the machining task involved is a constant challenge for production planners and programmers. It is known that cutting tool material selection can be based on PRE-index classification (Jonsson 1994). The tested steels were ordered against the PRE-index in Publications I and II.

The shear instability in the cutting operation of stainless steel is often reflected in the formation of serrated chips. The mechanism of serrated chip formation has been explained in terms of the varying strength of the work material at the rake face (Sullivan et al. 1978). The chip formation process is studied in Publications II and III.

Workhardening has been recognised as an important feature in the poor machinability of austenitic stainless steel. According to Jiang et al. (1996), Sullivan et al. (1978) and Wright and Trent (1954), workhardening, together with low thermal conductivity, is believed to result in segmental chip formation. Workhardening of chips and machined surface was studied in Publications I–IV.

According to Chandrasekaran and Johansson (1994), notch wear at the depth of the cut is a serious problem during the machining of high alloyed austenitic stainless steels. Thick workhardened zones, stringy chips, harsh harmonics and high machining temperatures all take a toll on material removal rates, reducing insert life and increasing downtime (Belejchak 1997). Stainless steel producers currently often improve the machinability of austenitic stainless steels. Both austenitic and duplex stainless steels are supplied by stainless steel producers (Roos 1997).

3.3 The effect on grindability

When the grindability of PM 316L, PM 2205, PM 2507 and AC 304 were examined in terms of grinding ratio, grinding force and surface roughness using alumina wheels, the ratio decreased in the order AC 304, PM 316L, PM 2205 and PM 2507 steel; the grinding force increased in the following order: AC 304, PM 2205, PM 316L and PM 2507 steels; and surface roughness increased in the following order: PM 316L, PM 2205, PM 2507 and AC 304 steel.

Grinding methods utilise undefined cutting tool geometry in the form of grinding wheels or grinding paste. The cutting operations proceed via the interaction between the workpiece and hard grinding particle. According to Malkin (1984), material removal in grinding occurs via the interaction of abrasive grains in the grinding wheel with the workpiece at extremely high speeds and shallow penetration depths. The interaction between the grains on the grinding wheel and the workpiece can be placed into three categories: rubbing, blowing and cutting (Hahn 1962). Wear and the deformation of the grinding wheel are analysed using geometrical data (Tso & Yang 1998).

The workhardening behaviour of stainless steels during grinding increased in the following order: AC 304, PM 316L, PM 2205 and PM 2507. Also, a considerable number of microvoids were detected on the ground surfaces, increasing in the following order: PM 316L, PM 2205, PM 2507 and AC 304 steels.

Of the alloying elements in stainless steels, Ni and Mo promote diffusion wear of TiN-coated cemented carbide tools because of the replacing diffusion of Ni from the workpiece to the tool. It also causes diffusion of Co from the cemented carbide substrate to the workpiece, and diffusion of Mo from the workpiece to the substrate, partially replacing W. (König 1981.)

Difficult to cut, various high-strength stainless steels are produced by combinations of the following: Grain refinement by thermomechanical treatment, solid solution strengthening by lattice distortion through the addition of an alloying element, transformation strengthening by martensite transformation, workhardening by the formation of strain-induced martensite through rolling, strain ageing hardening by tempering or ageing of martensite,

and precipitation strengthening of inter-metallic compounds which are coherent with the matrix (Murata et al. 1993).

3.4 Turning of high-nitrogen stainless steels

The effect of nitrogen on the machinability of high-nitrogen stainless steels was studied in turning tests, as shown in Publication III. According to Ilola (1999), the strength of austenitic stainless steels at room temperature can be markedly increased with nitrogen alloying, without a significant reduction in toughness. By utilising alloying, small grain size, cold working and ageing strengthening methods, a yield strength of 3400 MPa can be achieved for austenitic stainless steels.

According to Ilola (1999), nitrogen-alloyed stainless steels have excellent fracture toughness over a wide temperature range. Although an increase in nitrogen content increases the yield strength, the fracture toughness is only slightly affected at room temperature (Speidel 1989).

Nitrogen alloying increases the fatigue strength of austenitic steels at room temperature in both high cycle and low cycle fatigue (Ilola 1999). The beneficial effects of nitrogen in low cycle fatigue can reach a limit at a relatively low nitrogen content, as happens with AISI 316LN with a nitrogen content of 0.12 wt% (Degaillaix et al. 1989). The creep resistance of austenitic steels is improved by nitrogen alloying (Ilola 1999), and nitrogen increases the creep rupture strength without decreasing the rupture ductility (Nakazawa et al. 1989).

Austenitic stainless steels are considered to be high-nitrogen stainless steels if they contain more than 0.4% nitrogen in solid solution (Speidel 1989). According to Wallén et al. (1992) and Romu (2000), the main reasons for the interest in nitrogen as an alloying element in austenitic stainless steels are to save on other expensive alloying elements such as nickel, and at the same time to introduce good property combinations to steels.

High-nitrogen steel with a higher nitrogen content is supposed to have lower machinability. According to Tervo (1998), the general trend appears to be that an increase in nitrogen content decreases the strain-hardening exponent, and

increases the strength factor. Nitrogen makes cutting forces greater due to dynamic strain ageing, whereas carbon and phosphorous make it smaller because of the formation of voids and cracks in the primary and secondary shear zones (Katayama & Hashimura 1990). In Publication III, a difference in cutting forces is shown between X5 CrMnN 18 18-trial materials. Instead of a tangential force of F_y = 2.2–2.5 kN in turning X5 CrMnN 18 18-trial material with 0.91% N, a lower tangential force of F_y = 2.2 kN is achieved when applying X5 CrMnN 18 18-trial materials with 0.57% N.

In the turning of high-nitrogen steels, presented in Publication III, the main failure mechanisms were catastrophic failure by tool nose breaking due to high cutting forces, and sharp edge chipping. Rapid tool wear and a tendency towards chipping have been studied on the major cutting edge. In turning tests of X5 CrMnN 18 18-trial material with a nitrogen level of N 0.91% using a cutting speed of v_c = 60 m/min, a tool life of about T = 31 min is achieved. Tool life decreases to T = 25 min at a cutting speed of 65 m/min. When increased cutting speeds are used, chip formation difficulties cause the chipping of tool material and catastrophic failure of the tool often occurs.

It has also been observed in turning tests that the machinability of high-nitrogen stainless steels is affected by BUE formation. The presence of BUE decreases the machinability of X5 CrMnN 18 18-trial materials. The formation of BUE worsens surface roughness and workpiece surfaces are strongly deformed. The workhardening of a workpiece surface decreases when nitrogen content is increased. According to Kubota et al. (1998), both yield strength and workhardening rate increase with increasing values of nitrogen concentration. The maximum microhardness value measured from X5 CrMnN 18 18-trial material with a nitrogen level of N 0.57% was approximately 600 HV, and with a nitrogen level of 0.91%, hardness values were just below 400 HV.

3.5 Drilling of HIPed and conventionally produced stainless steel

In Publication IV the difference between the machinability of HIPed PM and conventional stainless steel was studied in drilling experiments in the machining centre using solid carbide drills with an internal coolant supply. It is supposed by

Ezugwu et al. (1999) that in drilling operations there are complex sets of demands for the operation of tool and coolant. Coolant reduces the wear of the main flute. Spur and Stöferle (1979) have stated that chip form and dimensions have to be taken into account in those machining operations that have a small amount of chip room, such as drilling, broaching and milling.

When machining a number of alloys, a BUE may form on the tool and have a considerable influence on the tool wear rate, surface finish, and dimensional tolerances (Wallbank 1979). The study of the cutting angles of drills is of importance in the design and analysis of drills. Many models and analyses, such as calculation of force, temperature, wear, and chip ejection, are based on cutting angle analysis (Kaichun & Jun 1999).

According to Fujiwara et al. (1977), during drilling operations free-machining additives such as, S, Pb, Se and Te increase the machinability of austenitic stainless steels.

As observed in drilling tests using cutting speeds of 40–60 m/min and a feed rate of 0.2 mm/r, HIPed PM stainless steels show a shorter tool life than conventional cast stainless steels. When using solid carbide drills with an internal coolant supply, tool wear proceeded continuously and the tool life is between 5–12 min in machining of Duplok 27 stainless steel, and between 7–20 min in machining of A890 1A stainless steel.

According to Klocke et al. (1999), Klocke and Krieg (1999) and Gunn (1997), frittering and flaking of the coating takes place during the drilling of austenitic stainless steels.

It is also observed in drilling tests that the machinability of HIPed PM and conventional cast duplex stainless steels are affected by the formation of BUE. The formation of BUE causing adhesion wear is supposed to be the dominant failure mechanism of solid carbide drills. There is a higher tendency to form BUE in A890 1A than in Duplok 27 steel. Compared to that, at fast cutting speeds plastic deformation of the tool takes place, and in combination with flaking of the insert coating and frittering (Gunn 1997), the tool wear is also affected by the formation of BUE and flaking of the coating. Duplok 27 chips are more strongly deformed than A890 1A chips; the chip bottom of austenite in

Duplok 27 605 HV(20g) (original microhardness 370 HV(20g)) vs. austenite phase of A890 1A steel 505 HV(20g).

In many cases, machining problems with austenitic stainless steels are associated with BUE formation, bad surface, burr formation and unfavourable chip shape (Dolinšek 2003). In the drilling test of conventional cast stainless steels with a HIPed NiTi coating presented in Publications IV–VII, bad surface qualities from drilled holes were also found. Also, the drilling operation was affected by BUE formation.

4. Discussion

4.1 Comparison of test methods

In the reported tests and in the available literature, which is presented in Chapter 3 of this thesis, there is a lot of variation in how well different measuring methods and analysis techniques have worked. This is due to various factors affecting the results and because the result of the machining process depends on the properties of the machine tool, cutting tool, cutting tool material, workpiece dimensions features and workpiece material conditions, and also the peripheral equipment and human factors.

When machinability tests are carried out instead of standardised vT-testing, revised machinability test is often utilised, as in this research. The dynamic behaviour of machine tools and cutting tools is not considered in this research, though it has a remarkable effect on cutting results. Of course the machining parameters used in this research were selected to be sufficient and adaptable for the group of machine tools available in the laboratory of Production Technology at HUT. Tooling microscopes, length measuring devices are also presented widely in industry.

In the drilling tests, high-quality solid carbide drills fixed with high rotational accuracy tool adapters were used to decrease the effect of the dynamical behaviour of the rotating tools affecting the cutting tool wear. Tool holder rotational inaccuracy has been reported to decrease behaviour of rotating cutting in demanding machining conditions (Ranta et al. 1999).

4.2 The effect on grindability

Detailed studies of the grindability behaviour of PM 316L, PM 2205, PM 2504 and AC304 stainless steels with alumina wheels were carried out, and the results are presented in Publication I. Surface workhardening of ground stainless steels and the chemical interaction between them and alumina wheels was found. Attrition, abrasive and adhesive wear mechanisms were found affecting wear mechanisms. Grinding is particularly characterised by high friction between the

abrasive grits and the ground surface, and a high risk of thermal damage to the generated surfaces and to loading and wear of the grinding wheel could appear in the forms of thermal micro-cracks (Snoeys et al. 1978).

The effect of hard carbides of Cr and Mo on grinding wheel wear and the stainless steels used in this grinding research have a low content of C, and therefore the amount of carbides should be low.

A number of alumina particles were also found on the steels studied. The grinding forces were dependent not only on the workhardening of the workpiece, but also on the density of microcracks and microvoids forming during grinding. Grinding wheel wear has also an effect on the measured grinding force. Another factor which affects grinding force measurement is the sharpening of the grinding wheel. The balance of the grinding wheel and the vibrations of the grinding spindle have an effect on grinding wheel wear.

The grinding experiments were conducted on a surface grinding machine under reciprocating plunge grinding conditions. During grinding, radial wheel wear was measured using a Micro-HITE height measuring instrument. Based on these results, the grinding ratio (G) in the ready stage of wheel wear could be obtained as could the ratio of volumetric workpiece removal to volumetric wheel wear.

Grinding ratio, grinding force and surface roughness values were measured from the selected number of workpieces, and there is a possibility that the results could vary slightly as the amount of specimen increases, taking into account the uncertainty of the force measurement device, the surface roughness measurement device and the length measurement device. The grinding process related workpiece fixing, grinding wheel fixing and grinding strategy and grinding parameter controlling effects may inhibit fluctuations in the results.

The workhardening of stainless steels during grinding in this research was also researched from the selected amount of test pieces, based on microhardness values of distance from the ground surfaces and austenite and ferrite phases existing on the ground surfaces. The accuracy of microhardness tester depth measurement technology gives a level of displacement measuring accuracy resulting in measured microhardness values and plotted curves. Also, the surface

being tested generally requires a metallographic finish, the smaller the load used the higher the surface finish required.

Detailed metallographic examination and EDS analysis of ground surfaces gave results of scratches and grooves and transferred Al_2O_3 particles on the ground surfaces. Also, metallographic examination and EDS analysis of ground surface profiles showed the existence of Al_2O_3.

The formation of microcracks and microvoids affecting surface roughness, grinding forces and the ground surface morphology can be widely researched by means of SEM and EDS. Fluctuations in cutting fluid distribution during the grinding operation may also affect the grindability results.

4.3 Turning of new high-strength stainless steels

The turning tests of PM316 L and PM 2005 stainless steel, presented in Publication II, and X5CrMnN 18 18 stainless steel, presented in Publication III, of this research were carried out with a lathe powered with a 100 kW spindle motor and the tested HSS and solid carbide inserts were fixed with a tool holder of 25 mm. The setting of cutting depth was manual and feed rate values were set manually according to values provided by the machine tool. Rotational speed was checked by means of a rotameter. The flank wear (VB) of the cutting tools was measured with a toolmaker's microscope. During turning, the principal cutting force was measured with a piezoelectric turning dynamometer. Chip root samples were obtained by means of a quick stop device. Inserts and chip root samples were analysed by means of SEM and EDS. Chip root samples were also taken using the microhardness device presented in Appendix I.

During tool life testing of these researched difficult-to-machine materials, high cutting forces occurred, resulting in rapid tool wear. Increasing the amount of experiments, the vT-curve presentation may orientate slightly because of microscope interpretation of worn and damaged inserts. Also, the dynamic behaviour of the lathe head is supposed to cause fluctuations in the results of tool wear and tool life measurements.

Cutting force measurements were firstly used for showing serrated chip formation resulting in cutting force fluctuations, and secondly in turning experiments to point to the effect of nitrogen alloying on cutting force level. Various factors affect the results achieved with the force measurement device.

The wear topography and wear mechanisms of TiN-coated HSS and cemented carbide tools were researched with SEM and EDS methods from chip root samples, and the macroscopic morphology of chips showed the behaviour of stainless steel chip formation and BUE formation. According to Chang (2003), the formation of BUE is dynamically unstable and quite hard, causing rapid wear of the tool and gouging the face.

4.4 Drilling experiments

The drilling experiments presented in Publications IV–VII were carried out using the machining centre presented in Appendix I. A high-accuracy tool holder was used for fixing the tested drills. The tested machining parameters were controlled by numerical control of the machining centre. The tool wear of the drills was presented as a vT curve with selected cutting speeds. For the drilling tests of Duplok 27 and A890 1A, cutting speeds of 20–100 m/min were used with feed rates of 0.15–0.25 mm/revolution, and solid carbide drills with a diameter of Ø8.6 mm were used.

Drills and chips were analysed using SEM and EDS. Microhardness measurements of the chips were also performed. In the drilling experiments on stainless steels with a HIPed NiTi coating, HIP treatment was used to sinter coatings from NiTi powder onto a stainless steel block. The HIPing parameters were 900ºC, 100 MPa, and 3 h. The cooling rate was 4.6 K/min.

These tests used TiCN- and TiN-coated cemented carbide drills with a diameter of Ø8.5 mm, at a cutting speed of 50 m/min and feed rates of 0.1, 0.15, and 0.2 mm/rev. The chips and drilled holes were researched with SEM and EDS mapping. Several analyses from the NiTi coating and stainless steel samples showed the behaviour of this interface during the drilling operation. Weinert and Petzoldt (2004) examined the machinability of shape memory alloys by varying

different process parameters and the cooling lubricant concept, and evaluated the hardening of the machined subsurface zone.

To analyse the correlation of the measured parameters on the behaviour of the researched materials in the drilling tests, as was used by Belluco and Chiffre (2004), an analysis of variance was performed to investigate the effect of different cutting fluids on all measured parameters.

5. Summary of the thesis

The main objective of this thesis was to investigate the machinability effects of new high-strength stainless steels. The machinability of these new stainless steels is often poor. By selecting solid carbide cutting tools and machining parameters selected based on the revised machining presented in this research, sufficient tool lives and wear rates are achieved. The machinability effects arising when new high-strength stainless steels are machined with modern machine tools and cutting tools are researched in this thesis.

The test methods that were employed (drilling, grinding and turning tests) gave corresponding results for the machinability of new high-strength stainless steels. The results of the tests complement each other, and give a wider view of the workhardening of chips and machined surfaces with the mechanism of wear with applied machining parameters. Increasing the amount of alloying elements of stainless steels shows decreased machinability in grinding and turning operations. The formation of BUE was present in chip forming operations. Relevant machinability information of studied stainless steels is achieved. Machinability data and information affecting tool wear can be found in these tests, with electron microscopy investigations on chips and machined surfaces.

The grindability of HIPed austenitic 316L, duplex 2205 and super duplex 2507 and as-cast 304 were investigated. The grinding ratios, grinding forces and surface roughness were measured during grinding with alumina wheels. The effects on the grindability of workhardening, chemical interactions between the alumina wheel and the workpiece, and microcracks and microvoids were investigated. The workhardening behaviour of stainless steels was found to increase in following order, according to the amount of alloying elements and the production method of the steel: PM 316L, PM 2205, PM 2507 and AC 304.

The active wear and failure mechanisms of TiN-coated HSS and cemented carbide tools when machining powder metallurgically made 316L and 2205 stainless steels was examined by the turning test. In the cutting speed range of 100 to 250 m/min, fatigue-induced failure and diffusion wear was found to affect the tool life of TiN-coated cemented carbide tools.

In the turning and drilling operations tested, the presence of both BUE and workhardening were found to decrease the machinability of new high-strength stainless steels. HIPed and conventional cast stainless steel were compared in drilling operations, where PM-produced stainless steel Duplok 27 was found to be more difficult to machine than ASTM A 8910 stainless steel. Chips of Duplok 27 were found to be more strongly deformed than A890 1A chips. The formation of BUE causing adhesion wear was supposed to be the dominant failure mechanism of tools.

The effect of nitrogen was studied in the turning tests of high-nitrogen X5 CrMnN 18 18 stainless steels. The workhardening of a workpiece surface is decreased when the nitrogen content decreases from a nitrogen level of 0.91% to a level of 0.57%. Catastrophic failure of the tool nose was found. The machinability was also decreased by the presence of BUE.

Finally, in the drilling operations of conventionally cast stainless steel X2CrNi 19 11 with HIPed NiTi, effective cutting speeds were found of 50 m/min and feed rates of 0.1–0.2 mm/r without a deterioration in coating properties. The deformation effects of NiTi-coating and as well as stainless steels were found from chips and workpiece. An intact interface layer between the stainless steel and the NiTi-coating was also found on the deformed chips.

The first paper (Publication I) about the grindability of HIPed stainless steels was carried out in co-operation with the laboratories of Production Engineering and Engineering Materials at HUT. Lic.Tech. Risto Oraskari has been studying grinding technology and is currently working at the Helsinki Institute of Technology. The grinding experiments were carried out with the author and Dr.Tech. L. Jiang. The SEM analyses and metallography were done by Dr.Tech. L. Jiang. The author finished the paper during a research period financed by the Academy of Finland.

Publication II was also written in co-operation with the laboratories of Production Engineering and Engineering Materials at HUT. The turning experiments were carried out by the author and Dr.Tech. L. Jiang. The SEM analyses and metallography were mainly done by Dr.Tech. L. Jiang. The paper was finished and figures produced by the author during a research period financed by the Academy of Finland.

The research work presented in Publications III and IV was carried out during a period financed by the Graduate School of Concurrent Mechanical Engineering, supervised by Prof. Mauri Airila at HUT.

Publications V, VI and VII were written by the author. The presented research work was carried out at VTT Industrial Systems. The SEM and EDS analyses were carried out in co-operation with Tom E. Gustafsson M.Sc.

6. Summary of the appended papers

Publication I presents a comparison of the grindability of HIPed austenitic 316L, duplex 2205, super duplex 2507 and as-cast 04 stainless steels, using alumina wheels. Machinability was studied by grinding ratio, grinding force and surface roughness measurements. The ground surfaces were analysed by SEM and workhardening rates were measured.

Publication II compares the active wear and the failure mechanism of TiN-coated High-Speed Steel and Cemented Carbide tools when machining PM stainless steels. The machinability was studied by the turning of PM 316L and PM 2205 stainless steels. Chip samples were provided by a quick-stop device. Wear topography and the wear or failure mechanisms of tools were studied by SEM and EDS analyses.

Publication III compares the machinability of X5CrMnN 18 18 stainless steel with two different nitrogen levels. Solid carbide tools and chips were analysed by SEM. Machinability was studied by analysing chip morphology and the workhardening rate of the machined surface.

Publication IV compares the tool wear and machinability of HIPed PM with conventional cast stainless steel. The machinability testing was carried out in a machining centre using solid carbide drills with internal cooling. VT-curves are presented and machinability is compared to the Pitting Resistance Equivalent (PRE) index. The chips and drills are examined by SEM.

Publication V investigates the suitability of TiN and TiCN-coated cemented carbide tools in the drilling of conventionally cast stainless steel with a HIPed NiTi-coating. The machinability testing was carried out in a machining centre using solid carbide drills with internal cooling. The deformation of the stainless steel and NiTi chip is studied with SEM and EDS.

Publications VI and VII investigate chip morphology in the drilling of conventional cast stainless steel with a HIPed NiTi-coating. The machinability testing was carried out in a machining centre using solid carbide drills with external and internal cooling. The chip formation and surface quality is studied with SEM and EDS.

References

Agapiou, J.S., Halldin, G.W. & DeVries, M.F. 1988. On the Machinability of Powder Metallurgy Austenitic Stainless Steels. Journal of Engineering for Industry. Transactions of the ASME 110(1988)11, pp. 339–343.

Altintas, Y., Brecher, C., Weck, M. & Witt, S. 2005. Virtual Machine Tool. Annals of the CIRP 54(2005)2.

Arnvig, P.-E., Leffler, B., Alfonsson, E. & Brorson, A. 1994. Machinability, Corrosion Resistance and Weldability of an Inclusion Modified Duplex Stainless Steel. Proceedings of the 4th International Conference, Duplex 94 Stainless Steels, Vol. 1, Materials and Properties, Glasgow, Scotland.

Arsecularatne, J., Fowle, R. & Mathew, P. 1998. Prediction of Chip Flow Direction, Cutting Forces and Surface Roughness in Finish Turning. Journal of Manufacturing Science and Engineering 120(1998)2, pp. 1–12.

Belejchak, P. 1997. Machining Stainless Steel. Advanced Materials & Processes, December 97, Vol. 152, Issue 6, pp. 23–25.

Belluco, L. & De Chiffre, L. 2004. Evaluation of vegetable-based oils in drilling austenitic stainless steels. Journal of Materials Processing Technology 148(2004), pp. 171–176.

Beno, J. 1996. Untersuchungen zur Spanentstehungstelle. Wt-Produktion und Management 86(1996), pp. 462–467.

Bletton, O., Duet, R. & Pedarre, P. 1990. Influence of Oxide Nature in the Machinability of 316L Stainless Steels. Wear 139(1990), pp. 179–193.

Budak, E. & Altintas, Y. 1994. Peripheral Milling Conditions for Improved Dimensional Accuracy. International Journal of Machine Tools Manufacture 34(1994)7, pp. 907–918.

Budak, E. & Altintas, Y. 1995. Modelling of Avoidance of Static Form Errors in Peripheral Milling of Plates. International Journal of Machine Tools Manufacture 35(1995)3, pp. 459–476.

Chandrasekaran, H. & Johansson, J. 1994. Chip Flow and Notch Wear Mechanisms during the Machining of High Austenitic Stainless Steels. Annals of the CIRP 43(1994)1, pp. 101–105.

Chang, C. & Gwo-Chung, T. 2003. A force model of turning stainless steel with worn tools having nose radius. Journal of Materials Processing Technology 142(2003)10, pp. 112–130.

Charles, J. 1994. Structure and Mechanical Properties of Duplex Stainless Steels. Proceedings of the 4th International Conference, Duplex 94 Stainless Steels, Vol. 1, Materials and Properties, Glasgow, Scotland.

Chick, S. & Mendel, M.B. 1998. Using Wear Curves to Predict the Cost of Changes in Cutting Conditions. Journal of Manufacturing Science and Engineering. Transactions of the ASME 120(1998), pp. 166–168.

Cook, N. 1975. What is Machinability? Proceedings from an International Symposium on Influence of Metallurgy on Machinability. ASM 1975, pp. 1–10.

Coudreuse, L., Gagnepain, J. Ch. & Charles, J. 1997. UR 35N Cu: A Low Alloyed Duplex Stainless Steel with Improved Machinability and Corrosion-Abrasion Resistance. Stainless Steel World 1997, D97–129, pp. 1017–1020.

Degaillax, S., Dickson, J.L. & Foct, J. 1989. Effect of Nitrogen Content on Fatigue and Creep. Fatigue Behaviour of Austenitic Stainless Steels. In: Foct, J. & Henry, A. (Eds.). Proceedings of the International Conference on High Nitrogen Steels, HNS 88, Lille, France, 18–20 May 1988. London: The Institute of Metals. Pp. 199–203.

Dolinšek, S. 2003. Work-hardening in the drilling of austenitic stainless steels. Journal of Materials Processing Technology 133(2003)1–2, pp. 63–70.

Ezugwu, E., Wang, Z. & Machado, A. 1999. The Machinability of Nickel-Based Alloys: A Review. Journal of Materials Processing Technology, Vol. 86, No 1–3, pp. 1–16.

Fujiwara, T., Kato, T., Abeyama, S. & Nakamura, S. 1977. Effects of Free-Machining Additives on Machinability of the 18Cr-2Mo Stainless Steel. Proceedings of the International Symposium on Influence of Metallurgy on Machinability of Steel, 26–28 September, 1977. Tokyo, Japan. Pp. 231–240.

Gunn, R. 1997. Duplex Stainless Steels. Cambridge England: Abington Publishing. 204 p.

Hahn, R.S. 1962. On the Nature of the Grinding Process. 3rd MTDR Conference, Pergamon, Oxford. 129 p.

Hallum, D. 1995. What Mathematics Tells Us about Cutting Tools. American Machinist 139(1995)3, pp. 40–42.

Höglund, U. 1976. Cutting Edge Wear in Microscale Physical Conditions-Wear Processes. Annals of the CIRP, Vol. 25/1/1976, pp. 99–103.

Ilola, R. 1999. Effects of Temperature on Mechanical Properties of Austenitic High Nitrogen Steels. Acta Polytechnica Scandinavica, Mechanical Engineering Series No. 136. Doctor's Thesis. Espoo: Finnish Academy of Technology. 100 p.

Iwata, K. & Kanji, U. 1976. The Significance of Crack Behaviour in Chip Formation. Annals of the CIRP 25(1976)1, pp. 65–70.

Jemelniak, K. 1999. Commercial Tool Condition Monitoring Systems. International Journal of Advanced Manufacturing Technology (1999)15, pp. 711–721.

Jiang, L., Hänninen, H., Paro, J. & Kauppinen, V. 1996. Active Wear and Failure Mechanisms of TiN-coated High-Speed Steel and TiN-coated cemented carbide Tools when Machining Powder Metallurgically Made Stainless Steels. Metallurgical and Materials Transactions A, Vol. 27 A, pp. 2796–2808.

Jonsson, H. 1994. Rostfreien Stahl Drehen. Werkstatt und Betrieb 127(1994)1–2, pp. 68–70.

Kaichun, R. & Jun, N. 1999. Analysis of Drill Flute and Cutting Angles. International Journal of Advanced Manufacturing Technology (1999)15, pp. 546–553.

Katayama, S. & Hashimura, M. 1990. Effect of Carbon, Phosphorus and Nitrogen Contents in Steel on Machined Surface and Cutting Force. ISIJ International 30(1990)6, pp. 457–463.

Klocke, F. & Krieg, T. 1999. Umveltverträglich Zerspanen. Werkstatttechnik 89(1999)10, pp. 456–460.

Klocke, F., König, K. & Hanisch, D.O. 1999. Bohren kleiner Löcher in Austenischen Stahl. Werkstatttechnik 89(1999)5, pp. 223–227.

Komanduri, R. & Brown, R.H. 1981. On the Mechanics of Chip Segmentation in Machining. Journal of Engineering Industry (Trans. ASME), 1981, 103, pp. 33–51.

Kubota, S., Xia, Y. & Tomota, Y. 1998. Work-hardening Behaviour and Evolution of Dislocation-microstructures in High-nitrogen Bearing Austenitic Steels. ISIJ International, Vol. 38, No. 5, pp. 474–481.

König, W. & Messer, J. 1981. Influence of the Composition and Structure of Steels on Grinding Process. Annals of the CIRP 30(1981)2, pp. 547–552.

Leffler, B., Gunnarsson, S. & Svensson, M. 1996. Maskinbearbetning av rostfria stål. Kristianstad: Avesta Sheffield AB's Stiftelse för forskning. 222 p.

Li, Z. & Sun, Q. 2002. The initiation and growth of macroscopic martensite band in nano-grained NiTi microtube under tension. International Journal of Plasticity 18(2002), pp. 1481–1498.

Liew, W., Ngoi, B. & Lu, Y. 2003. Wear characteristics of PCBN tools in the ultra-precision machining of stainless steel at low speeds. Wear 254(2003)3–4, pp. 265–277.

Lindgren, B. 1980. Constant Feed Force Machinability Test, A Method Study. Dissertation. Göteborg: Chalmers University of Technology. 162 p.

Mackerle, J. 1999. Finite element analysis and simulation of machining a bibliography (1976–1996). Journal of Material Processing Technology 86(1999), pp. 17–44.

Mackerle, J. 2003. Finite element analysis and simulation of machining: an appendum a bibliography (1976–1996). Journal of Material Processing Technology 43(2003), pp. 103–114.

Malkin, S. 1984. Grinding of Metals: Theory and Application. Journal of Applied Metalworking. American Society for Metals 3(1984)2, pp. 95–109.

Murata, Y., Ohashi, S. & Uematsu, Y. 1993. Recent Trend in the Production and Use of High Strength Stainless Steels. ISIJ International, Vol. 33(1993)7, pp. 711–720.

Nakazawa, T., Abo, H., Tanino, M., Komatsu, H., Nishida, T. & Tashimo, M. 1989. Effects of Nitrogen and Carbon on Creep Properties of Type 316 Stainless Steels. In: Foct, J. & Henry, A. (Eds.). Proceedings of the International Conference on High Nitrogen Steels, HNS 88, Lille, France, 18–20 May 1988. London: The Institute of Metals (1989). Pp. 218–224.

Nyström, N. 1995. Plastic deformation of Duplex Stainless Steels. http://www2.lib.chalmers.se/cth/diss/doc/9495/Nystromagnus.html.01.12.00.

Oxley, P. 1988. Modelling Machining Processes with a View to Their Optimisation and to the Adaptive Control of Metal Cutting Machine Tools, Robot. Computer Integrated Manufacturing 4(1988)1/2, pp. 103–119.

Peckner, D. & Bernstein, I.M. 1977. Handbook of Stainless Steels. New York: McGraw-Hill.

Pellegrini, G., Di Caprio, G. & Pasagnella, R. 1997. Tool Performance in Continuous Cutting of Duplex Stainless Steels. Stainless Steel World, 58(1997), pp. 175–180.

Ranta, P., Paro, J. & Kauppinen V. 1999. Teränkiinnittimien pyörintätarkkuudesta, vaikutus työstöön ja työkalun asentovirheisiin. Publication TKK-KPT 4/99. Espoo: Helsinki University of Technology, Laboratory of Production Technology. 65 p.

Recht, R.F. 1964. Trans. ASME. Journal of Applied Mechanics, Paper no. 63, WA–67, pp. 189–193.

Rennhard, C.A.P. 1998. New Industrial Applications of HNS. In: Hänninen, H., Herzman, S. & Romu, J. (Eds.). Proceedings of the 5th International Conference on High Nitrogen Steels, HNS 98, Espoo – Finland and Stockholm – Sweden, 24–25 May 1998. Trans Tech Publications Ltd, Switzerland. Pp. 174–179.

Romu, J. 2000. Effect of Nitrogen Content on Precipitation Behaviour and Properties of P/M Austenitic Stainless Steels. Acta Polytechnica Scandinavica, Mechanical Engineering Series No. 141. Doctor's Thesis. Espoo: Finnish Academy of Technology. 140 p.

Roos, Å. 1997. Machinability of SANMAC SAF 2205. Stainless Steel World. KCI Publishing. D97–069, pp. 181–185.

Šalak, A., Selecká, M. & Daninger, M. 2005. Mach inability of Powder Metallurgy Steels. Cambridge, UK: Cambridge Int. Sci. Publ. Pp. 263–382.

Shaw, M.C. 1985. The Theory of Metal Cutting. Proceedings of the 25th International Machine Tool Design Res. Conference, Birmingham, 22–24, Apr. 1985. London: Macmillan Press. Pp. 33–36.

Schintlmeister, W. & Wallgram, W. 1999. CVD-Hartstoffschichten zum Drehen von Stahl. Werkstatt und Betrieb 132(1999)12, pp. 72–75.

Schäpermeier, E. 1999. Zerspanungsoptimierung beim Drehen von Stählen. München: Carl Hanser Verlag. 95 p.

Snoeys, R., Maris, M. & Peters, J. 1978. Thermally induced damages in grinding. Annals of the CIRP 27(1978)2, pp. 571–576.

Speidel, M.O. 1989. Properties and Applications of High Nitrogen Steels. In: Foct, J. & Hendry, A. (Eds.). Proceedings of the International Conference on High Nitrogen Steels, Lille, France, May 18–20 1988. London: Institute of Metals. Pp. 92–96.

Spur, G. & Stöferle, T. 1979. Handbuch der Fertigungstechnik. Band 3/1, Spanen. München: Carl Hanser Verlag. 592 p.

Starosvetsky, D. & Gotman, I. 2001. TiN coating improves the corrosion behaviour of superelastic NiTi surgical alloy. Surface and Coatings Technology 148(2001), pp. 268–276.

Stevenson, R. & Stephenson, D.A. 1998. The Effect of Prior Cutting Conditions on the Shear Mechanics of Orthogonal Machining. Journal of Manufacturing Science and Engineering 120(1998)2, pp. 13–20.

Sullivan, K.F., Wright, P.K. & Smith. 1978. Metallurgical Appraisal of Instabilities Arising in Machining. IP.D. 1978. Met. Technol., Vol. 5, pp. 181–189.

Sundvall, J., Olsson, J. & Holmberg, B. 1998. Applications of Nitrogen-Alloyed Stainless Steels. In: Hänninen, H., Herzman, S. & Romu, J. (Eds.). Proceedings of the 5th International Conference on High Nitrogen Steels, HNS 98, Espoo – Finland and Stockholm – Sweden, 24–25 May 1998. Trans Tech Publications Ltd, Switzerland. Pp. 181–186.

Taniguchi, N. 1971. On the Evaluation of Machinability and Other Workabilities Based on Specific Cost of Production. Annals of the CIRP, 19(1971)1, pp. 471–476.

Tervo, J. 1998. Wear Properties of High Nitrogen Austenitic Stainless Steels. Acta Polytechnica Scandinavica, Mechanical Engineering Series No. 128. Doctor's Thesis. Espoo: Finnish Academy of Technology. 88 p.

Tipnis, V. & Joseph, R. 1975. Testing for Machinability. Proceedings from an International Symposium on Influence of Metallurgy on Machinability. ASM 1975, pp. 11–30.

Tlusty, J. & MacNeil, P. 1975. Dynamics of Cutting Forces in End Milling. Annals of the CIRP 24(1975)1, pp. 21–25.

Tso, P.-L. & Yang, S.-Y. 1998. The Compensations of Geometrical Errors on Forming Grinding. Journal of Materials Processing Technology 73(1998)1–3, pp. 82–88.

von Turkovich, B.F. 1981. Survey on Material Behaviour in Machining. Annals of the CIRP 30(1981)2, pp. 533–540.

Wallbank, J. 1979. Structure of Built-up Edge Formed in Metal Cutting. Metals Technology, April 1979, pp. 145–153.

Wallén, B., Liljas, M. & Stenvall, P. 1992. A New High Molybdenum, High Nitrogen Stainless Steel. Materials & Design 13(1992)6, pp. 329–333.

Weinert, K. & Petzoldt, V. 2004. Machining of NiTi based shape memory alloys. Materials Science and Engineering A 378(2004), pp. 180–184.

Wright, P.K. & Trent, E.M. 1954. J. Iron Steel Inst., Vol. 177, pp. 406–410.

Yeo, S.H. 1995. A Tandem Approach to Selection of Machinability Data. Int. Journal Advanced Manufacturing Technology 10(1995)2, pp. 79–86.

Yeo, S.H. 1989. Towards Enchantment of Machinability, Data by Multiple Regression. Journal of Mechanical Working Technology 19(1989), pp. 85–99.

Östlund, S. 1994. Stainless Steel Turning. Stainless Steel Europe 6(1994)2, pp. 46–51.

Özel, T. 2006. International Journal of Machine Tools & Manufacture 46(2006), pp. 518–530.

Appendix I: Test devices

Grinding experiments (Publication I)

1. Materials

Workpiece materials

- PM316L, PM2205, PM2507 and AC304
- chemical compositions are presented in Table 1
- workpiece size
    - width x length: 8 x 200 mm^2
    - number of work pieces: 3 per material

Table 1. Chemical compositions of the stainless steels studied.

Code	%C	%Si	%Mn	%P	%S	%Cu	%Cr	%Ni	%Mo	%V	%Al	%N	%O
PM 316L	0.015	0.68	1.44	0.022	0.009	0.19	16.7	11.0	2.7	0.11	0.021	0.12	0.012
PM 2205	0.03	0.68	1.42	0.022	0.008	0.13	22.1	5.3	3.0	0.07	0.016	0.21	0.014
PM 2507	0.03	0.30	0.30	0.035	0.009	0.16	25.0	7.0	4.0	0.08	0.020	0.30	0.015
AC 304	0.03	0.40	1.20	0.040	0.015	0.17	18.4	9.2	-	0.06	0.025	0.10	0.001

Grinding wheel

- Norton 43A46 GVX
- diameter: Ø200 mm
- width: 12 mm
- grinding material: alumina Al_2O_3
- number of grinding wheels: 4

Grinding fluid

- 5% Castrol no. 7
- flow rate: 2 l/min

2. Machine tools

Surface grinding machine Okamoto PSG-5UAN

- grinding width and length: 200 x 500 mm^2
- distance between table and spindle: 500 mm
- hydraulic feed speed: 0.3–25 m/min
- automatic down feed: 0.004–0.03 mm
- grinding wheel dimensions
    - maximum diameter: Ø205 mm
    - wheel width: 19 mm
    - boring diameter: Ø50.8 mm
- power of the spindle motor: 1.5 kW

3. Measuring and analysing devices

Tesa Micro Hite I Height measuring device

- measuring area: 515 mm
- resolution: 0.001 mm
- accuracy: (3+6*L) µm, where L = meters

Kistler piezoelectric grinding dynamometer

Taylor Hobson surface roughness measurement device

Zeiss DSM 962 scanning electron microscope

- equipped with EDS link ISIS-system for qualitative chemical analysis

Microhardness measuring device MHT-4

- load: 20 g

Micrometer

4. Procedure

The microstructures of the test materials were characterised and photographed using a Nikon Epiphot optical microscope. Samples were polished mechanically and then etched with a mixture of HNO_3 (1 part), HCl (3 parts) and H_20 (4 parts).

The work pieces were held by a magnetic chuck. In the steady stage of wheel wear during grinding, the volumetric workpiece removal was calculated and radial wheel wear was measured using a Micro Hite device as a volumetric wheel wear for grinding ratio measurements. Wheel radius measurements were performed three times. Each material had its own grinding wheel.

The speed of the wheel was 30 m/s, the table speed was 0.25 m/s and the down feed was 0.015 mm/pass.

During grinding, F_n and F_c were recorded using a Kistler piezoelectric dynamometer and surface roughness was measured. After the grinding tests, metallographic examination and analyses of ground surfaces and profiles were performed using SEM and EDS.

5. Estimation of uncertainty of grinding ratio measurements

- test piece width and length measured with micrometer
- uncertainty: 0.005 mm
- material removal according to half of down feed value: 0.008 mm
- work piece material removal: $V_w \pm 0.018$ mm^3

- grinding wheel wear

$\Delta V = 2*3.14*\Delta r*\Delta w$
$\Delta r = (3+6*0.2)$ µm
$\Delta w = 0.005$ mm
$\Delta V = \pm 0.03$ mm^3
$\Delta G = \pm 0.018$ mm^3/± 0.03 mm^3 = ± 0.6

Turning experiments of PM316L and PM2205 (Publication II)

1. Materials

- bars with diameter of Ø70 mm and length of 350 mm
- bars of PM316L and PM 2205 with analyses according to Table 2
- heat treatment 3 hours at 1100 ºC

Table 2. Chemical compositions (wt. %) of HIP Stainless Steels: PM 316L and PM 2205.

Code	%C	%Si	%Mn	%P	%S	%Cr	%Ni	%Mo	%V	%Al	%Cu	%N	%O
PM 316L	0.05	0.68	1.44	0.022	0.009	16.7	11.0	2.7	0.11	0.021	0.19	0.12	0.012
PM 2205	0.03	0.66	1.42	0.022	0.008	22.1	5.3	3.0	0.07	0.016	0.13	0.21	0.014

2. Machine tool

Lathe VDF Heidenreich&Harbeck

- spindle power: 100 kW
- turning length: 750 mm
- max diameter: Ø300 mm
- rotation speed: max. 5000 1/min

Tools SPUN 120308

- HSS TiN Coeted Edgar Allen
- cutting speed: 15–55 m/min
- feed rate: 0.15 mm/r
- depth of cut: 1.0 mm

P30 cemented Carbide TiN coated

- cutting speed: 100–250 m/min
- feed rate: 0.15 mm/r
- depth of cut: 1.0 mm

Cutting fluid was not used

A quick stop device (Chip root experiments at Imatra Steel)

3. Measuring and analysing devices

Kistler piezoelectric turning dynamometer

Mitutoyo tool maker's microscope

Zeiss DSM 962 scanning electron microscope

- equipped with EDS link ISIS-system

Microhardness measuring device

MHT-4, load 20 g

4. Procedure

The test pieces were fixed using a chuck and tailstock. After turning, tool wear was measured from the insert until the criteria of 0.3 mm was reached. During machining cutting force components were recorded. Chip root samples were produced using a quick stop device.

The microstructures of the test materials were characterised and photographed using a Nikon Epiphot optical microscope. Samples were polished mechanically, and then etched with a mixture of HNO_3 (1 part), HCl (3 parts) and H_20 (4 parts).

Inserts and chips and chip root samples were analysed with SEM and EDS. Work piece samples were measured with a microhardness tester.

5. Estimation of uncertainty of tool wear measurements

- cutting parameters were set manually
- tool wear measurements were carried out using a tool maker's microscope
- accuracy 0.005 mm
- revised tests

Turning experiments of X5CrMnN18 18 (Publication III)

1. Materials with analysis according to Table 3

- one bar with a diameter of Ø125 mm and length of 620 mm, of high nitrogen steel 0.91%N
- one bar with a diameter of Ø130 mm and length of length 400 mm of high nitrogen steel 0.57%N

Table 3. Chemical compositions (wt.%) of X5 CrMnN 18 18 trial materials.

Melt	%C	%Si	%Mn	%Cr	%Mo	%Ni	%V	%N
G88216	0.05	0.29	18.89	18.13	0.11	0.43	0.08	0.57
DDt63	0.05	0.49	19.8	18.6	0.08	0.61	0.13	0.91

2. Machine tool

Lathe VDF Heidenreich&Harbeck

- spindle power: 100 kW
- turning length: 750 mm
- max diameter: Ø300 mm
- rotation speed: max. 5000 1/min

3. Cutting tools

Tools SNMG120408-PM

- P15/K15 cemented Carbide TiN- and Al_2O_3-coated
- cutting speed: 60, 65, 70 and 100 m/min
- feed rate: 0.24 mm/r
- depth of cut: 1.6 mm
- cutting fluid was not used

4. Measuring and analysing devices

Mitutoyo tool maker's microscope

Kistler piezoelectric turning dynamometer

Zeiss DSM 962 scanning electron microscope

- equipped with EDS link ISIS-system

The Zeiss DSM 962 scanning electron microscope used was equipped with an EDS link ISIS-system for qualitative chemical analysis in the microstructure of chips and work piece surface profiles.

Microhardness measuring device

MHT-4, load 20 g

5. Procedure

The test pieces were fixed using a chuck and tailstock. After turning the tool wear was measured from the insert until the criteria 0.3 mm was reached. During machining cutting force components were recorded.

The microstructures of the test materials were characterised and photographed using a Nikon Epiphot optical microscope. Samples were polished mechanically, and then etched with a mixture of HNO_3 (1 part), HCl (3 parts) and H_20 (4 parts).

SEM and EDS were used for qualitative chemical analysis in the microstructure of chips and work piece surface profiles. Workpiece samples were measured with a microhardness tester.

6. Estimation of uncertainty of tool wear measurements

- cutting parameters were set manually
- tool wear measurements were carried out using a tool maker's microscope
- accuracy: 0.005 mm
- revised tests

Drilling tests (Publication IV)

1. Materials

Materials with analysis according to Table 4 presented below.

- 4 plates of Duplok 27 (200 x 300 x 40 mm^3)
- 4 plates A8910 1A (200 x 300 x 40 mm^3)

Table 4. Chemical composition of the studied stainless steels (wt.%).

Code	%C	%Si	%Mn	%P	%S	%Cu	%Cr	%Ni	%Mo	%V	%Al	%N	%O
Duplok 27	0.03	0.2	0.7	0.02	0.001	2.3	26.5	7.0	3.0	-	-	0.3	-
A890 1A	0.03	0.74	0.63	0.026	0.006	3.01	25.0	5.54	2.03	-	-	-	-

2. Machine tool

Horizontal machining centre Mazatech FH480 with Mazatroll M Plus Control

- spindle revolution speed: 35–12000 1/min with spindle power of 22 kW
- spindle taper CAT 40
- feedrate: 32 m/min
- maximum workpiece size: diameter Ø610 mm, height 670 mm, weight 400 kg

3. Cutting tool

Solid carbide drills

- Titex Alpha4 + DX45

Tool adapter

- MST HiArt CT40-ART32-85S91

Cutting fluid

- Blaser BlasoCut –7%
- through spindle

4. Measuring and analysing devices

Mitutoyo tool maker's microscope

Zeiss DSM 962 scanning electron microscope

- equipped with EDS link ISIS-system

Microhardness measuring device

- MHT-4, load 20 g

5. Procedure

The work piece was fixed on a vice into the pallet of a machining centre. Drills were fixed using a high accuracy drilling tool holder. After drilling the drill wear was measured from the insert until the wear criteria of 0.3 mm was reached. During drilling cutting force components were recorded.

The microstructures of the test materials were characterised and photographed using a Nikon Epiphot optical microscope. Samples were polished mechanically, and then etched with a mixture of HNO_3 (1 part), HCl (3 parts) and H_20 (4 parts).

Drills and chips and chip root samples were analysed with SEM and EDS. Workpiece samples were measured with a microhardness tester.

6. Estimation of uncertainty of drill wear measurements

- cutting parameters were set manually
- tool wear measurements were carried out using tool maker's microscope
- accuracy: 0.005 mm
- revised tests

Drilling tests (Publications V–VII)

1. Materials

NiTi coated sample and capsule presented in Publication V

- X2CrNNi 1911 stainless steel block according the table below
- NiTi coating 55/45 wt.% of average thickness 5 mm

Table 5. The nominal composition of the steel used in the drilling experiment.

% C	% Mn	% S	% P	% Cr	% Ni	% Si	% V
0.03	1.20	0.015	0.04	18.4	9.2	0.4	0.06

2. Machine tool

Horizontal machining centre Mazatech FH480 with Mazatroll M Plus Control

- spindle revolution speed: 35–12000 1/min
- spindle power of 22 kW
- spindle taper: CAT 40
- feedrate: 32 m/min
- maximum workpiece size:
    - diameter Ø610 mm
    - height 670 mm
    - weight 400 kg

3. Cutting tool

Solid carbide drills

- Dijet DDS 850M with TiCN/TiN-coating, 8 pcs

Tool adapter

- MST HiArt CT40-ART32-85S91

Cutting fluid

- Blaser BlasoCut –7%
- through spindle

4. Measuring and analysing devices

Mitutoyo tool maker's microscope

JSM 6400 scanning electron microscope

- equipped with X-ray microanalysis system PGT PRISM with thin window

Microhardness measuring device

- MHT-4, load: 20 g

5. Procedure

The work piece was fixed on a vice into the pallet of a machining centre. Drills were fixed using a high accuracy drill holder. After drilling the drill wear was measured from the edges of the drill until the wear criteria of 0.3 mm was reached. Drills and chips and chip root samples were analysed with SEM and EDS. Workpiece samples were measured with a microhardness tester.

6. Estimation of uncertainty of tool wear measurements

- cutting parameters were set manually
- tool wear measurements were carried out using tool maker's microscope
- accuracy: 0.005 mm
- revised tests

PUBLICATION I

Comparison of grindability of HIPped austenitic 316L, duplex 2205 and super duplex 2507 and as-cast 304 stainless steels using alumina wheel

In: Journal of Materials Processing Technology 1996.
Vol. 62, pp. 1–9.

ELSEVIER

Journal of Materials Processing Technology 62 (1996) 1–9

Journal of Materials Processing Technology

Comparison of grindability of HIPped austenitic 316L, duplex 2205 and super duplex 2507 and as-cast 304 stainless steels using alumina wheels

Laizhu Jiang[a,*], Jukka Paro[b], Hannu Hänninen[a], Veijo Kauppinen[b], Risto Oraskari[c]

[a]*Laboratories of Engineering Materials, Helsinki University of Technology, Puumiehenkuja 3A, Espoo, Finland*
[b]*Laboratory of Workshop Technology, Helsinki University of Technology, Puumiehenkuja 3A, Espoo, Finland*
[c]*Helsinki Polytechnic Institute, Helsinki, Finland*

Received 16 September 1994; revised 21 September 1995

Industrial summary

The grinding ratios, grinding forces and surface roughnesses of HIPped austenitic (PM 316L), duplex (PM 2205) and super duplex (PM 2507) as well as as-cast (AC 304) stainless steels were measured during grinding using alumina wheels. It was observed that the grinding ratio decreased in the following order: AC 304, PM 316L, PM 2205 and PM 2507 steel, whilst the grinding force increased in the order: AC 304, PM 2205, PM 316L and PM 2507 steel. The surface roughness increased in the order: PM 316L, PM 2205, PM 2507 and AC 304 steel. It was observed also that the ground steel surfaces work-hardened in the following increasing order: AC 304, PM 316L, PM 2205 and PM 2507 steel. Abrasive plowing-wear grooves and adhesive built-up layers of alumina particles were observed on the ground surfaces of the steels, increasing in the following order: AC 304, PM 316L, PM 2205 and PM 2507 steel. Examination of the ground surface profiles of the workpieces showed that there were a considerable number of microcracks and microvoids on the ground surfaces of the steels, increasing in the following order: PM 316L, PM 2205, PM 2507 and AC 304 steel. Finally, the effects of work hardening, chemical interactions between the alumina wheel and the workpiece, as well as microcracks and microvoids, on the grindability of the stainless steels studied were investigated.

Keywords: Stainless steel; Alumina; Grinding ratio; Grinding force; Surface roughness

1. Introduction

Stainless steels are normally recognized as difficult materials to machine because of their high toughness, low thermal conductivity and high degree of work hardening. During grinding, however, the chemical interaction between a stainless-steel workpiece and a wheel, particularly an alumina wheel, may also play a crucial role in causing poor grindability. It has been reported that the poor wheel life when grinding stainless steels results mainly from a high tendency of adhesion between the workpiece and the alumina wheels [1], whilst it was also suggested much earlier that a high coefficient of friction between the workpiece and the abrasive may be responsible for a high rate of wheel wear [2]. Adhesive-wear mechanisms involve the oxidation of the workpiece and bonding between the oxidization products and the alumina [3]. It has been suggested that the chromium of stainless steel oxidizing into Cr_2O_3 could form a solid solution with Al_2O_3 and, therefore, promote bonding between stainless steels and alumina wheels. In addition, chromium would result in an increase of the friction coefficient and, therefore, in an increase of wheel wear [4].

It may be expected that not only the chemical composition, but also the microstructure of stainless steels, would exert some influences on their grindability. Although there have been some studies on the grindability of stainless steels [1,4,5], few studies have been concerned with comparison of the grindability of different types of stainless steels and with the effects of their microstructure. In this study, the grindability, i.e. the grinding ratio, the grinding force and the surface roughness of powder-metallurgically (PM) fabricated

* Corresponding author. Present address: R&D Centre, Sandvik Steel AB, 811 81 Sandviken, Sweden.

SSDI 0924-0136(95)02199-9

Table 1
Chemical compositions of the stainless steels studied (wt.%)

Code	C	Si	Mn	P	S	Cu	Cr	Ni	Mo	V	Al	N	O
PM 316L	0.05	0.68	1.44	0.022	0.009	0.19	16.7	11.0	2.7	0.11	0.021	0.12	0.012
PM 2205	0.03	0.68	1.42	0.022	0.008	0.13	22.1	5.3	3.0	0.07	0.016	0.21	0.014
PM 2507	0.03	0.30	0.30	0.035	0.009	0.16	25.0	7.0	4.0	0.08	0.020	0.30	0.015
AC 304	0.03	0.40	1.20	0.040	0.015	0.17	18.4	9.2		0.06	0.025	0.10	0.001

and hot-isostatically-pressed (HIPped) austenitic 316L, duplex 2205 and super duplex 2507 steels as well as as-cast 304 stainless steel, were measured during grinding using alumina wheels. Furthermore, the effects of the microstructure on the grindability of stainless steels were investigated.

2. Experimental

The grinding experiments were conducted on a straight surface grinder under reciprocating plunge grinding conditions. The alumina wheels used were type 43A46 GVX of 200 mm diameter and 12 mm width delivered by Norton Co., Sweden. The wheel speed was 30 m/s, the table speed was 0.25 m/s and the down feed was 0.015 mm/pass. Grinding fluid of 5% solution of Castrol no.7 in water was applied to the grinding zone at a flow rate of 2 l/min.

The workpiece materials were HIPped austenitic 316L (PM 316L), duplex 2205 (PM 2205), super duplex 2507 (PM 2507) and as-cast 304 (AC 304) stainless steels, the chemical compositions and microhardness values of the steels being given in Tables 1 and 2, respectively, and the microstructures of the steels being shown in Fig. 1(a)–(d), respectively. It can be seen that there is a considerable number of small oxide particles in the three HIPped stainless steels: much more than in AC 304 steel. Elongated ferrite phase areas are distributed in the AC 304 steel: it was impossible to measure the microhardness of the ferrite phase in this steel due to its fine structure. All the workpiece specimens were of 8 mm width, i.e., less than the wheel width, so that a recess developed in the wheel surface as a result of wheel wear, and of 200 mm length in the grinding direction. The specimens were held in place by a magnetic chuck, and positioned on the table so that the grinding marks of the ground surfaces were parallel to the longitudinal direction of the test specimens.

During grinding, the radial wheel wear was measured using a Micro-HITE surface measuring instrument. Based on these results, the grinding ratio, G, in the steady stage of wheel wear could be obtained as the ratio of the volumetric workpiece removal to the volumetric wheel wear [6]. The normal and tangential force components, F_n and F_t, during grinding were recorded with a Kistler piezo-electric grinding dynamometer and the surface roughness after grinding was measured with a Taylor surface roughness instrument. After the grinding tests, metallographic examinations and analyses of the ground surfaces and the profiles of specimens were performed by means of a scanning electron microscope (SEM) together with an energy dispersive spectroscopy (EDS). Work hardening of the specimen surface was investigated with a MHT-4 microhardness tester with a load of 20 g.

3. Results

3.1. Grinding ratio, grinding force and surface roughness

The grinding ratio, grinding force and surface roughness of four studied stainless steels are shown in Figs. 2–4, respectively. It can be seen that AC 304 steel has the highest grinding ratio followed by PM 316L, PM 2205 and PM 2507 steels while the grinding force, both the normal and tangential forces, increases in the following order: AC 304, PM 2205, PM 316L and PM 2507 steel. The surface roughness of ground stainless steels was found to increase in the following order: PM 316L, PM 2205, PM 2507 and AC 304 steel.

3.2. Work hardening of stainless steels during grinding

Work hardening of stainless steels during grinding can be seen in Fig. 5 based on the microhardness values of the workpiece as a function of distance from the ground surface. The microhardness values of the ground surfaces show that all the stainless steels tested work-hardened during grinding, if compared with the corresponding original microhardness values. In addi-

Table 2
Microhardness (HV) values of the stainless steels studied (load: 20 g)

Steel code	PM 316L	PM 2205		PM 2507		AC 304
Phase[a]	A	A	F	A	F	A
HV	250	300	330	310	340	260

[a] Phase: A-Austenite, F-Ferrite.

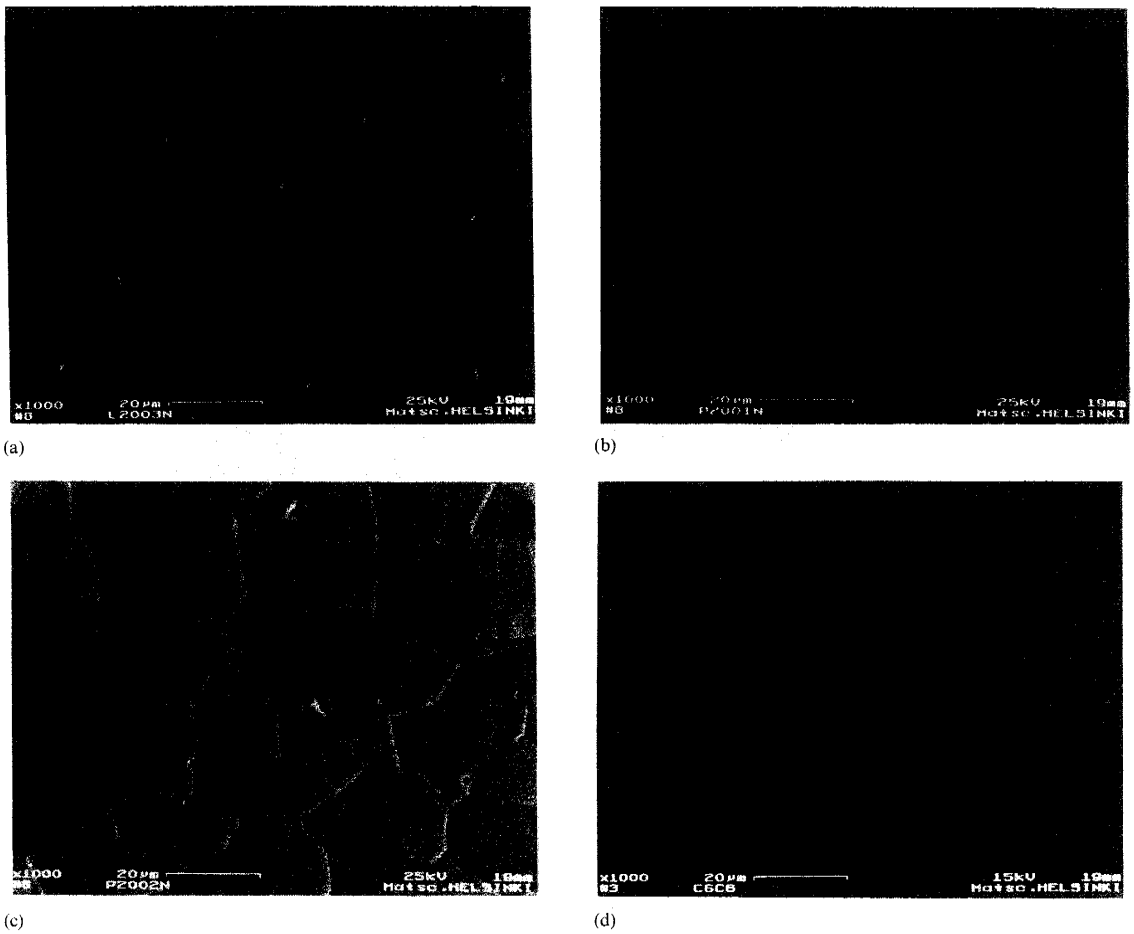

Fig. 1. BSE images of the microstructures of the stainless steels tested: (a) PM 316L steel; (b) PM 2205 steel; (c) PM 2507 steel, and (d) AC 304 steel.

tion, the austenite phase of PM 316L, PM 2205 and PM 2507 steels work-hardened more as compared with the ferrite phase of PM 2205 and PM 2507 steels and the austenite phase of AC 304 steel. Due to the elongated structure of the fine ferrite phase in AC 304 steel, it was impossible to measure the microhardness and, therefore, the work hardening of the ferrite phase of AC 304 steel.

3.3. Metallographic examination and EDS analysis of ground surface

Roughly speaking, all the ground surfaces of PM 316L, PM 2205, PM 2507 and AC 304 stainless steels, were predominantly covered by scratches and plowing wear grooves, indicating that the action of material removal of the stainless steels studied was mainly plastic flow. As an example, the morphology of the ground surface of PM 316L steel is shown in Fig. 6. In addition, the ground chip, Fig. 7, reveals that the chip-formation mechanism during grinding has been a shearing process.

Detailed SEM examinations and EDS analyses of the ground surfaces showed that there was a considerable number of alumina particles transferred from the alumina wheel to the ground surface, increasing in the following order: AC 304, PM 316L, PM 2205 and PM 2507 steel. As an example, the morphology of the ground surface and the element distribution on the surface of PM 2507 steel are shown in Fig. 8. It can be seen easily that the alumina particles adhere to the ground surface. There is some enrichment of molybdenum and silicon, some depletion of chromium and iron and a greater depletion of nickel and manganese at the sites of alumina particles, indicating that the bonding mechanism between the alumina wheel and the stainless

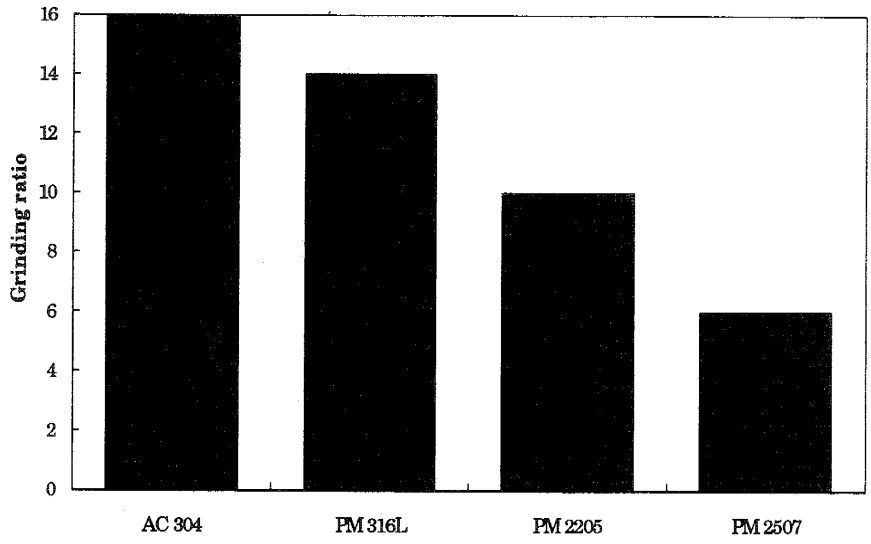

Fig. 2. Grinding ratio of stainless steels ground with alumina wheels.

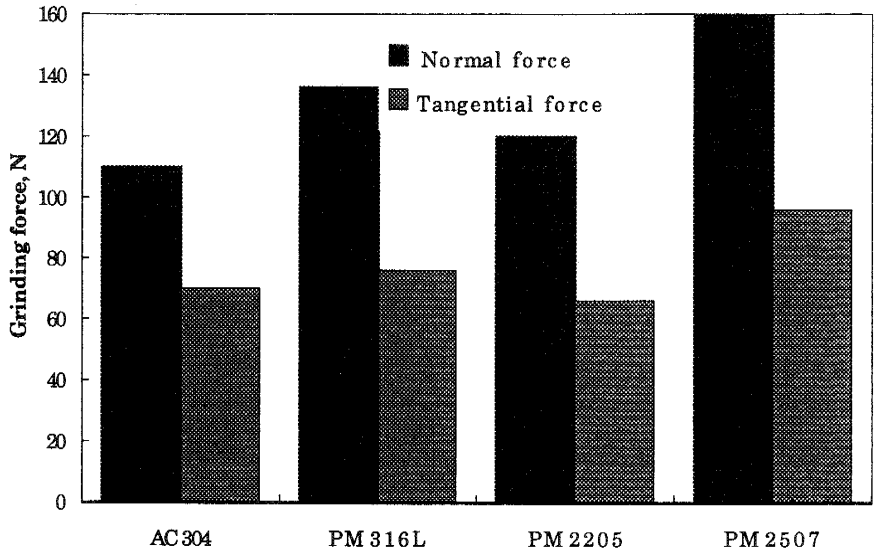

Fig. 3. Normal and tangential forces when grinding stainless steels using alumina wheels.

steels was due to the oxidation of mainly molybdenum and silicon and the consequent bonding between these oxides and Al_2O_3 from the alumina wheel.

3.4. Metallographic examination of ground surface profiles

Macrographs of the ground surface profiles of the steels studied are shown in Fig. 9(a)–(d). It can be seen that the ground surface of PM 316L steel is the smoothest, followed by those of PM 2205, PM 2507 and AC 304 steel.

Alumina particles, together with oxidation products of mainly molybdenum and silicon, were observed also in the profiles of the ground surfaces, Fig. 10, indicating further that some alumina particles are transferred from the alumina wheel to the stainless-steel surface during grinding.

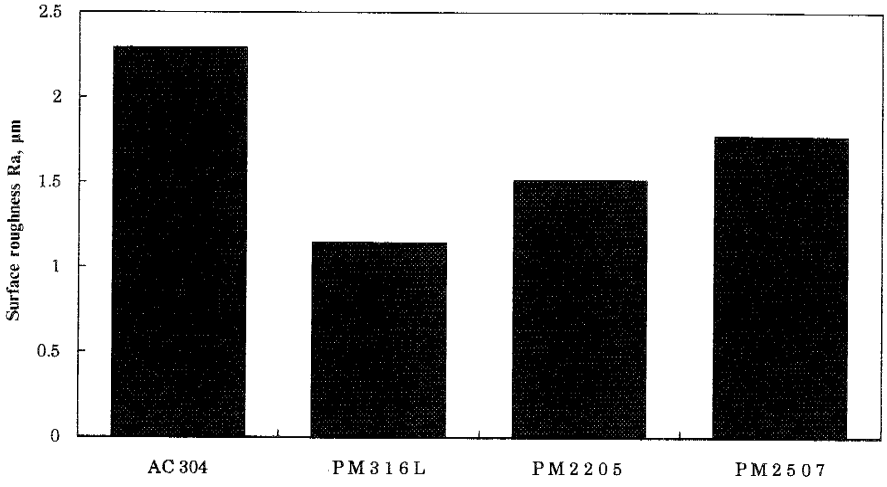

Fig. 4. Surface roughness R_a of stainless steels ground with alumina wheels.

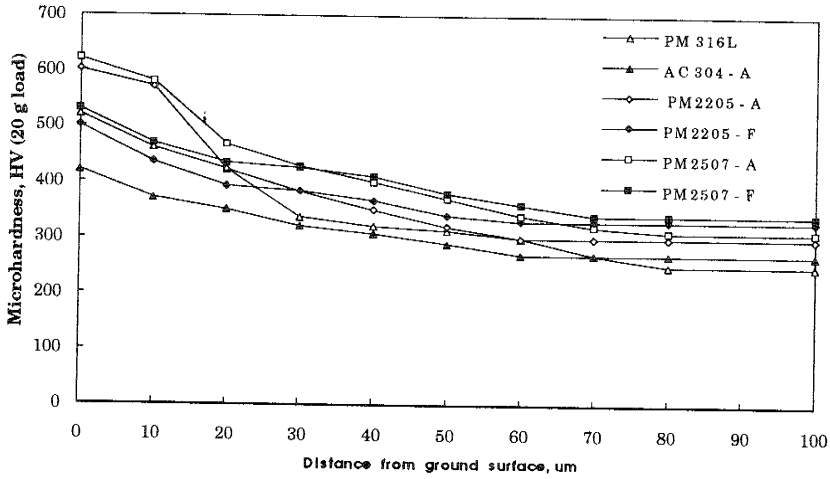

Fig. 5. Work hardening of stainless steels during grinding.

There was also a considerable number of microcracks and microvoids initiated on the ground surface of the steels studied. As an example, Fig. 11 shows microcracks and microvoids on the ground surface of AC 304 steel. These microcracks and microvoids may lead to the fracture of pieces of materials from the workpiece. Furthermore, it was observed that the density of microcracks and microvoids on the ground surface of the steels increased in the following order: PM 316L, PM 2205, PM 2507 and AC 304 steel.

There are two possible mechanisms for the formation of microcracks and microvoids on the ground surfaces of the steels studied.

1. Oxide inclusion initiation. During grinding, the hard oxide inclusions in the workpiece do not deform plastically, whilst the stainless steel matrix shows marked plastic flow. This mismatch of the strain between the hard oxide inclusions and the much softer matrix results in highly localized stresses at the interface leading to de-cohesion of the interface, microcracks and microvoids then being formed, as shown in Fig. 12 (a) and (b).

2. Mismatch of the deformability between the ferrite and the austenite phases. This mismatch results in highly localized stresses in the phase boundary leading to de-cohesion of the interface between the ferrite and the austenite phases and consequently to the formation of microcracks and microvoids, Fig. 13.

In PM 316L steel, only mechanism 1 was active, whilst in the rest of the steels studied, both mechanisms 1 and 2 were active in the formation of microcracks and microvoids on the ground surfaces.

4. Discussion

Due to the observed surface work hardening of ground stainless steels and the chemical interaction between them and the alumina wheels, it may be supposed that both attrition and adhesive wear occurs in alumina wheels when grinding stainless steels. Regarding the attrition wear, it may be expected that the wheel wear is the lowest and grinding ratio the highest when grinding AC 304 steel, followed by PM 316L, PM 2205 and PM 2507 steel, if considering the microhardness values of the ground steels. In addition, the presence of small hard oxide particles in the three HIPped stainless steels causes more excessive abrasive wear of alumina wheels as compared with that when grinding AC 304 steel. The adhesive wear was found to be dependent on the chemical interaction between the wheel and the workpiece. Due to the chemical interaction between the alumina wheel and the ground stainless steel, PM 2507 steel has the highest tendency to the adherence of alumina particles from the wheel, followed by PM 2205, PM 316L and AC 304 steels if the contents of molybdenum and silicon in the workpiece materials are considered. This was verified also by observations of the number of alumina particles on the ground surfaces of the steels studied. Based on the overall consideration of both attrition and adhesive wear, together with abrasive wear, it can be concluded that the wheel wear was the lowest and the grinding ratio the highest when grinding AC 304 steel, followed by PM 316L, PM 2205 and PM 2507 steels, while using alumina wheels.

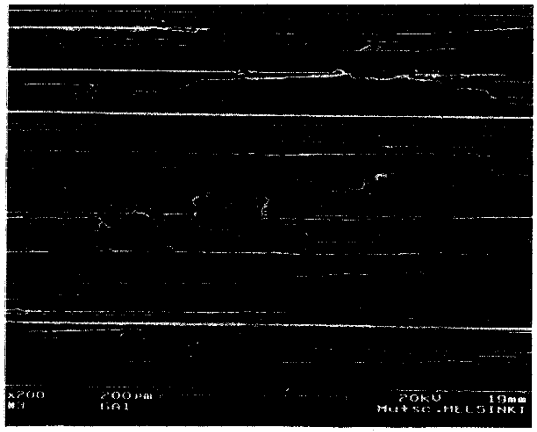

Fig. 6. Ground surface morphology of PM 316L steel showing scratches and plowing grooves.

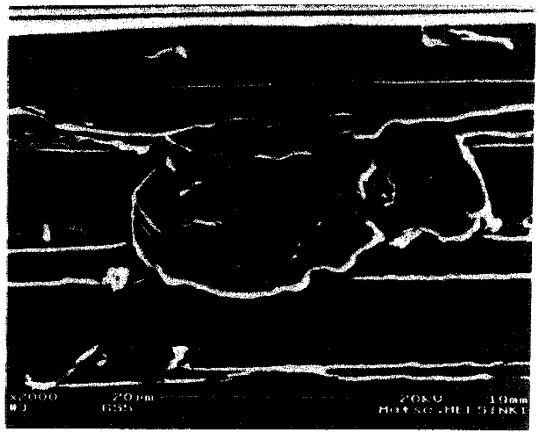

Fig. 7. Curled chip on the ground surface of PM 2507 steel showing a fine lamella structure formed as a result of shear instability.

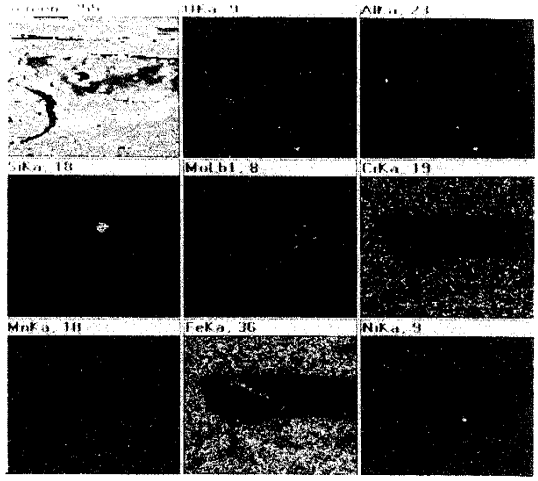

Fig. 8. EDS analyses of element distribution on the ground surface of PM 2507 steel.

The grinding forces were dependent not only on the work hardening of the workpiece, but also on the density of microcracks and microvoids forming during grinding of the workpiece. It was observed that the microhardness values of the ground steel surfaces increased in the following order: AC 304, PM 316L, PM 2205 and PM 2507 steel. The corresponding grinding forces would be expected to increase in the same order if considering only the effects of work hardening of the workpiece during grinding. However, the experimental results showed that the grinding forces increased in the order: AC 304, PM 2205, PM 316L and PM 2507 steel. The actual order of grinding forces when grinding PM 316L and PM 2205 steels may be due to the effects of microcracks and microvoids on the ground surface. It has been reported that the presence of microcracks and microvoids in the shear zone would lead to a reduction of cutting force during turning [7]: a similar conclusion may be applicable for grinding. In these tests, it was found that the area density of microcracks and microvoids on the ground surface of PM 2205 steel was much greater than that of PM 316L steel, resulting in

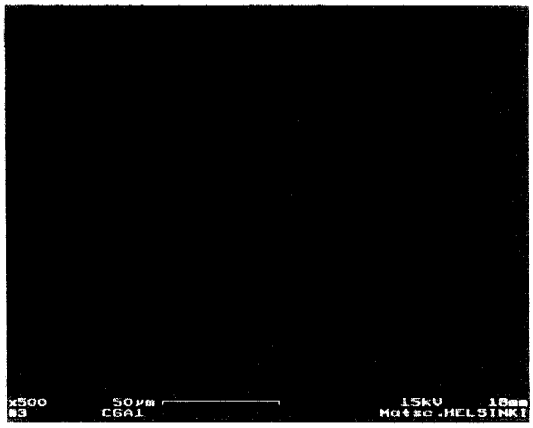

(a)

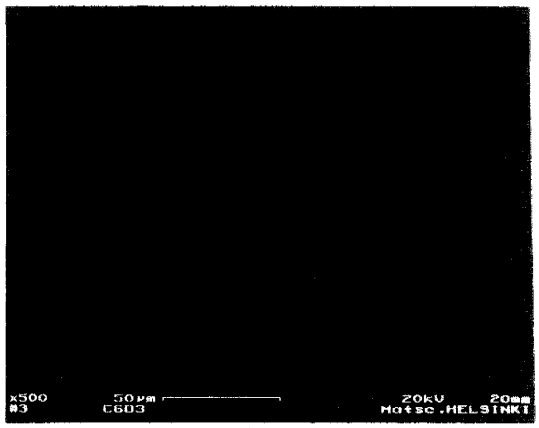

(b)

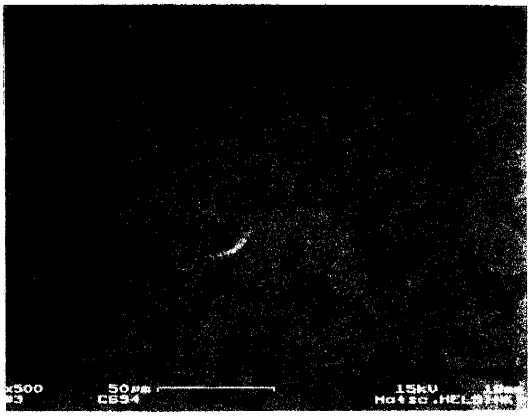

(c)

(d)

Fig. 9. BSE images of the morphology of the profiles of the ground surface of the stainless steels tested: (a) PM 316L steel; (b) PM 2205 steel; (c) PM 2507 steel, and (d) AC 304 steel.

the grinding forces when grinding PM 316L steel being greater as compared with those when grinding PM 2205 steel.

The surface roughness of the ground samples was dependent predominantly on the area density of micro cracks and microvoids on the ground surface. It was observed in these experiments that the area density increased in the following order: PM 316L, PM 2205, PM 2507 and AC 304 steel. There was no doubt that the density of microcracks and microvoids on the ground surface of PM 316L steel was the lowest because only oxide inclusions were responsible for the formation of microcracks and microvoids, whilst in addition to the oxide inclusions also the mismatch of strain between the ferrite and the austenite phases was responsible for the formation of microcracks and microvoids in PM 2205, PM 2507 and AC 304 steels. Due to the elongated shape of the ferrite phase in AC 304 steel, it may be expected that a higher stress concentration would arise and accordingly more (area density) microcracks and microvoids would be initiated when grinding AC 304 steel as compared with that when grinding both PM 2205 and PM 2507 steels. As an example, microcracks and microvoids on the ground surface of AC 304 steel are shown in Fig. 14. The area density of microcracks or microvoids initiated by the elongated ferrite phase in AC 304 steel was much higher as compared with that in PM 2507 steel (Fig. 13). Due to the higher alloy content of PM 2507 steel, the ductility and toughness of the ferrite phase is lower and the tendency for microcracks and microvoids to form is higher as compared with that of PM 2205 steel. Accordingly, it is understandable that surface roughness of ground steels increases in the following order: PM 316L, PM 2205, PM 2507 and AC 304 steel, i.e., in the same order as the density of microcracks and microvoids on the ground surface increases.

5. Conclusions

The grindability of PM 316L, PM 2205, PM 2507 and AC 304 stainless steels was examined in terms of grinding ratio, grinding force and surface roughness using alumina wheels. It was observed that the grinding ratio decreased in the following order: AC 304, PM 316L, PM 2205 and PM 2507 steel; the grinding force increased in the following order: AC 304, PM 2205, PM 316L and PM 2507 steel, and the surface roughness increased in the following order: PM 316L, PM 2205, PM 2507 and AC 304 steel.

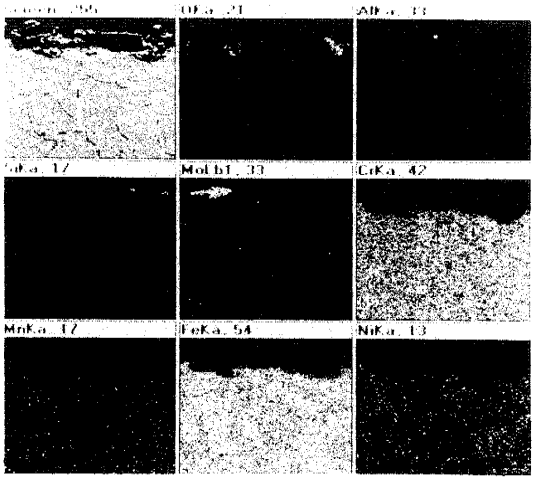

Fig. 10. EDS mapping analyses of the ground surface of PM 2507 steel.

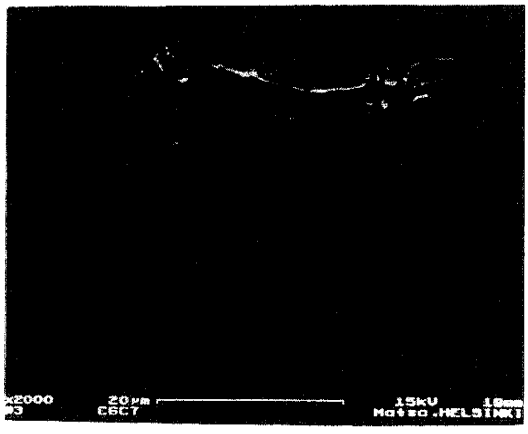

Fig. 11. Microcracks and microvoids on the ground surface of AC 304 steel.

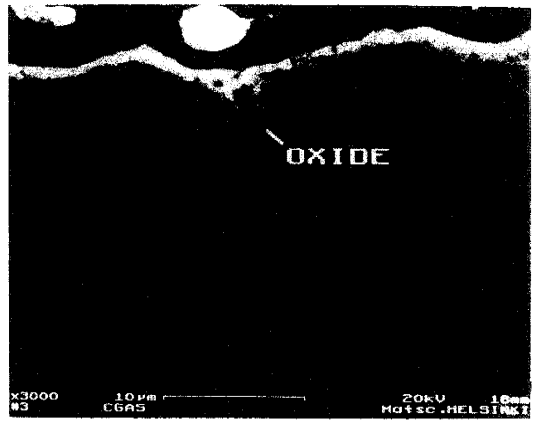

(a)

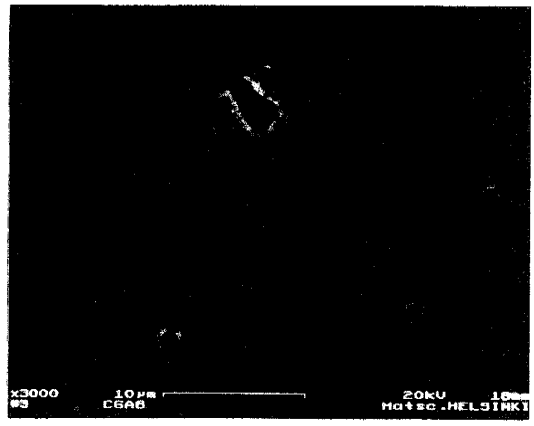

(b)

Fig. 12. Microvoid initiaton by oxide inclusions on the ground surface of PM 316L steel: (a) secondary electron image, and (b) back-scattered electron image.

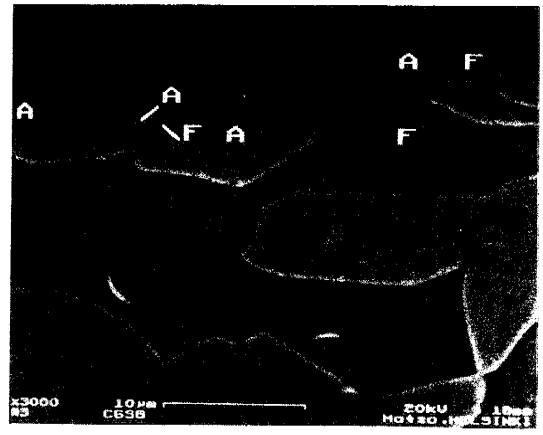

Fig. 13. Microcrack and microvoid initiation at the phase boundary between the austenite and the ferrite phases in PM 2507 steel.

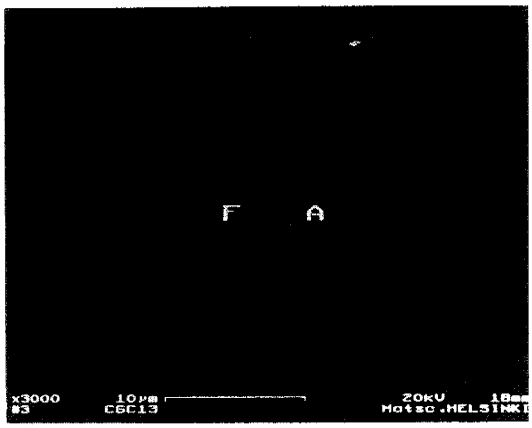

Fig. 14. Back-scattered electron image of microcracks and microvoids on the ground surface of AC 304 steel.

The work-hardening behaviour of stainless steels during grinding increased in the following order: AC 304, PM 316L, PM 2205 and PM 2507 steel. Alumina particles transferred from alumina wheels were detected on the ground surfaces. The mechanism of transfer may be the oxidation of mainly molybdenum and silicon of stainless steels and the subsequent bonding of alumina and these oxidation products. In addition, a considerable number of microcracks and microvoids was detected on the ground surfaces of the steels in the following increasing order: PM 316L, PM 2205, PM 2507 and AC 304 steel.

Acknowledgements

The financial support from TEKES (Technology Development Centre of Finland) is greatly acknowledged. Thanks are due to Rauma Materials Technology Co., Tampere, for supplying the workpiece materials. The assistance of Mr Alpo Hakola in Laboratory of Workshop Technology, Helsinki University of Technology, in the grinding tests is deeply appreciated. Active interest in this project from Dr Jari Liimatainen, Rauma Materials Technology Co., is also acknowledged.

References

[1] S. Yossifon and C. Rubenstein, *J. Eng. Ind., 103* (1981) 144–155.
[2] W.A. Mohun, *J. Eng. Ind., 84* (1962) 466–482.
[3] R. Komanduri, *Ann. CIRP, 2* (1976) 191–196.
[4] K. Miyoshi and D.H. Buckley, *Wear, 82* (1982) 197–211.
[5] S. Yossifon and C. Rubenstein, *Ann. CIRP, 31* (1982) 225–228.
[6] S. Malkin, *Grinding Technology: Theory and Application of Machining with Abrasives*, Ellis Horwood, Chichester, UK, 1989.
[7] L.H.S. Luong, *Met. Technol., 7* (1980) 465–470.

PUBLICATION II

Active wear and failure mechanisms of TiN-coated high speed steel and TiN-coated cemented carbide tools when machining powder metallurgically made stainless steels

In: Metallurgical and Materials Transactions A 1996.
Vol. 27A, pp. 2796–2808.

Active Wear and Failure Mechanisms of TiN-Coated High Speed Steel and TiN-Coated Cemented Carbide Tools When Machining Powder Metallurgically Made Stainless Steels

LAIZHU JIANG, HANNU HÄNNINEN, JUKKA PARO, and VEIJO KAUPPINEN

In this study, active wear and failure mechanisms of both TiN-coated high speed steel and TiN-coated cemented carbide tools when machining stainless steels made by powder metallurgy in low and high cutting speed ranges, respectively, have been investigated. Abrasive wear mechanisms, fatigue-induced failure, and adhesive and diffusion wear mechanisms mainly affected the tool life of TiN-coated high speed steel tools at cutting speeds below 35 m/min, between 35 and 45 m/min, and over 45 m/min, respectively. Additionally, fatigue-induced failure was active at cutting speeds over 45 m/min in the low cutting speed range when machining powder metallurgically made duplex stainless steel 2205 and austenitic stainless steel 316L. In the high cutting speed range, from 100 to 250 m/min, fatigue-induced failure together with diffusion wear mechanism, affected the tool life of TiN-coated cemented carbide tools when machining both 316L and 2205 stainless steels. It was noticed that the tool life of TiN-coated high speed steel tools used in the low cutting speed range when machining 2205 steel was longer than that when machining 316L steel, whereas the tool life of TiN-coated cemented carbide tools used in the high cutting speed range when machining 316L steel was longer than that when machining 2205 steel.

I. INTRODUCTION

AUSTENITIC and duplex stainless steels are normally recognized as materials difficult to machine, because of their following traits:

(1) high tensile strength and high work hardening rate and low thermal conductivity, leading to high cutting temperature and accelerated tool wear;
(2) high fracture toughness, resulting in poor chip breakability and poor surface finish; and
(3) strong bonding to the tool, especially to cemented carbide tools,[1] causing some pieces of material to be torn from the cutting tool and carried away by the chips.

Until now, the main mechanisms for tool wear when machining austenitic and duplex stainless steels are unclear, although there are some studies on them. It has been reported that the high work hardening rate, combined with low thermal conductivity, results in serrated chips when machining stainless steels.[2] The serrations of the chips cause vibration of the cutting forces and attrition wear of the cutting tool, especially the cemented carbide tool.[3] Besides vibration of the cutting forces, it has been recognized that a strong bonding between the tool and the workpiece material is also a necessary condition for attrition wear to occur. Little data concerning work hardening of stainless steels during machining have been presented until now. Also, the bonding mechanisms between stainless steel and the cutting tool, especially the cemented carbide tool, have not been investigated, although it has been generally accepted that the resulting high cutting temperature when machining both austenitic and duplex stainless steels is a very important factor causing bonding.

The machining cost of workpiece materials normally occupies at least 30 pct of the total cost of the final product. For the materials difficult to machine, such as stainless steels, it may be up to 50 pct. Powder metallurgy employing hot isostatic pressing (HIP) technology has recently been used to produce stainless steel products; this process, on one hand, reduces the machining costs because the size and shape of the products can be very close to the final product, but on the other hand, possibly causes the machinability of HIP steels to be poorer than that of the conventional steels due to considerable amounts of hard oxide particles. As the applications of HIP austenitic and duplex stainless steels are increasing due to their excellent mechanical properties and high corrosion resistance, it becomes more and more important to also know their machinability. The machinability of materials depends not only on their properties but also on the cutting tools. Although there are some new cutting tools available, both HSS and cemented carbide tools, with or without TiN coating, are still frequently used in the industry for turning. In this study, the tool lives and the cutting forces were measured in the turning tests of both HIP austenitic (PM 316L) and HIP duplex (PM 2205) stainless steels using TiN-coated HSS and TiN-coated cemented carbide tools in the low and high cutting speed ranges, respectively. Particular attention was paid to the wear and failure mechanisms of the cutting tools and the materials issues related to them.

LAIZHU JIANG, formerly with the Laboratory of Engineering Materials, Helsinki University of Technology, is with AB Sandvik Steel, 81811 Sandviken, Sweden. HANNU HÄNNINEN, Laboratory of Engineering Materials, and JUKKA PARO and VEIJO KAUPPINEN, Laboratory of Workshop Technology, are with the Helsinki University of Technology, 02150 Espoo, Finland.

Manuscript submitted September 7, 1994.

II. EXPERIMENTAL PROCEDURE

A. *Workpiece Materials*

The workpiece materials for turning tests were HIP austenitic stainless steel PM 316L and HIP duplex stainless

Table I. Chemical Compositions (Weight Percent) of HIP Stainless Steels: PM 316L and PM 2205

Code	C	Si	Mn	P	S	Cr	Ni	Mo	V	Al	Cu	N	O
PM 316L	0.05	0.68	1.44	0.022	0.009	16.7	11.0	2.7	0.11	0.021	0.19	0.12	0.012
PM 2205	0.03	0.66	1.42	0.022	0.008	22.1	5.3	3.0	0.07	0.016	0.13	0.21	0.014

steel PM 2205. Their chemical compositions are given in Table I.

The samples, 70 mm in diameter and 350 mm in length, were heat treated for 3 hours at 1100 °C and then water quenched. There is a considerable amount of small oxide particles distributed in both steels, mainly consisting of silicon, aluminum, and manganese, according to scanning electron microscope (SEM) observation and energy-dispersive spectroscopy (EDS) analyses. The microhardness value of austenite of PM 316L is about 240 HV, while those of ferrite and austenite phases of PM 2205 steel are about 330 and 300 HV, respectively.

B. *Tool Materials and Turning Conditions*

For turning tests of HIP stainless steels, PM 316L and PM 2205, TiN-coated HSS (T42) tools (Edgar Allen Tools Ltd., Sheffield, England) were employed in the low cutting speed range, from 15 to 55 m/min, and TiN-coated cemented carbide (P30) tools (Plansee Tizit, Austria) were employed in the high cutting speed range, from 100 to 250 m/min. The insert had the geometry of SPUN 120308 with a rake angle of 6 deg, clearance angle of 5 deg, cutting edge angle of 75 deg, cutting edge inclination of 0 deg, and nose radius of 0.8 mm. The turning tests were carried out on a center lathe with 100 kW spindle power with the cutting conditions given in Table II.

The flank wear VB of the cutting tools at every cutting speed was measured with a toolmaker's microscope. The criterion for tool life was VB = 0.3 mm or catastrophic failure of the tool edge. The principal cutting forces F_z were measured with a three-component piezoelectric force dynamometer. After turning, the wear topograph of the flank surfaces of the cutting tools was examined by an SEM together with EDS analysis. Chip root samples were obtained by means of a quick-stop device. They were mounted and cross sectioned for metallographic examinations of macrostructures and microstructures and, especially, of the possible bonding interface between the tool materials and the chips, by means of SEM and EDS analysis. The microhardness values at chip bottoms of both steels were measured with an MHT-4 microhardness tester with a load of 20 g to investigate work hardening behavior during turning.

III. EXPERIMENTAL RESULTS

A. *Tool Life*

The tool lives based on flank wear or catastrophic failure of the cutting edge when machining both PM 316L and PM 2205 steels in low and high cutting speed ranges are shown in Figure 1. It can be concluded that, according to these tests, TiN-coated HSS and TiN-coated cemented carbide tools exhibited catastrophic failure at cutting speeds over 45 and 200 m/min, respectively. The chips quickly became red hot in these cases. As can be seen from Figure 1, TiN-coated HSS tools exhibited longer tool life in the low cutting speed range when machining PM 2205 steel as compared with that when machining PM 316L steel, whereas TiN-coated cemented carbide tools presented longer tool life in the high cutting speed range when machining PM 316L steel as compared with that when machining PM 2205 steel.

Table II. Cutting Conditions

Cutting speed, m/min	15, 35, 45, 55 (low cutting speed range) 100, 150, 200, 250 (high cutting speed range)
Feed rate, mm/revolution	0.15
Depth of cut, mm	1.00
Cutting fluid	dry

B. *Cutting Force*

The principal cutting forces when machining PM 316L and PM 2205 steels in low and high cutting speed ranges are shown in Figures 2(a) and (b), respectively. It can be seen that the principal cutting forces when machining PM 2205 steel are lower than those when machining PM 316L steel in the low cutting speed range, whereas the opposite is true in the high cutting speed range.

C. *Wear Topograph and Wear Mechanisms of TiN-Coated HSS Tools*

1. *Abrasive wear at cutting speeds below 35 m/min*

The SEM observations of the worn tools revealed that the flank surfaces of HSS substrates of TiN-coated HSS tools showed abrasive grooves when machining PM 316L and PM 2205 steels at cutting speeds below 35 m/min. Some free carbides and built-up edges (BUEs) were found on the flank surfaces (Figures 3(a) and (b)), based on EDS analyses. These carbides and BUEs were believed to cause the abrasive groove wear on the flank surface of HSS substrate of the tool.[4,5] Additionally, it seems likely that the small hard oxides in these HIP stainless steels may also cause the abrasive wear on the HSS substrate of the tool, but the dimensions of the resulting groove may be too small to be resolved by an SEM.[5]

2. *Fatigue-induced failure at cutting speeds between 35 and 45 m/min*

The flank surfaces of TiN-coated HSS tools exhibited a considerable amount of fatigue-induced failure when machining both PM 316L and PM 2205 steels at cutting speeds between 35 and 45 m/min. For example, Figures 4(a) and (b) show the worn topograph of the flank surfaces of HSS substrate of TiN-coated HSS tool when machining PM 316L and PM 2205 steels at a cutting speed of 45 m/min, respectively.

It can be seen that the flank surface of HSS substrate of TiN-coated HSS tool when machining PM 2205 steel is less

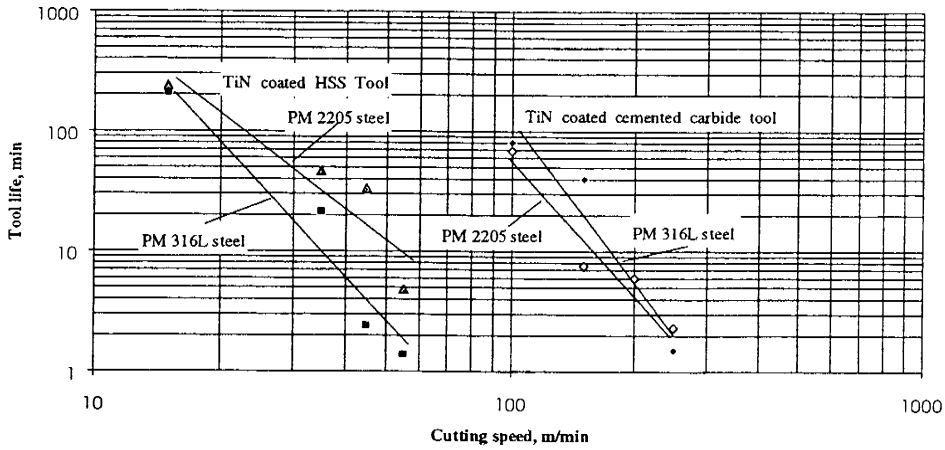

Fig. 1—Tool lives for TiN-coated HSS and TiN-coated cemented carbide tools in the low and high cutting speed ranges, respectively, when machining PM 316L and PM 2205 stainless steels.

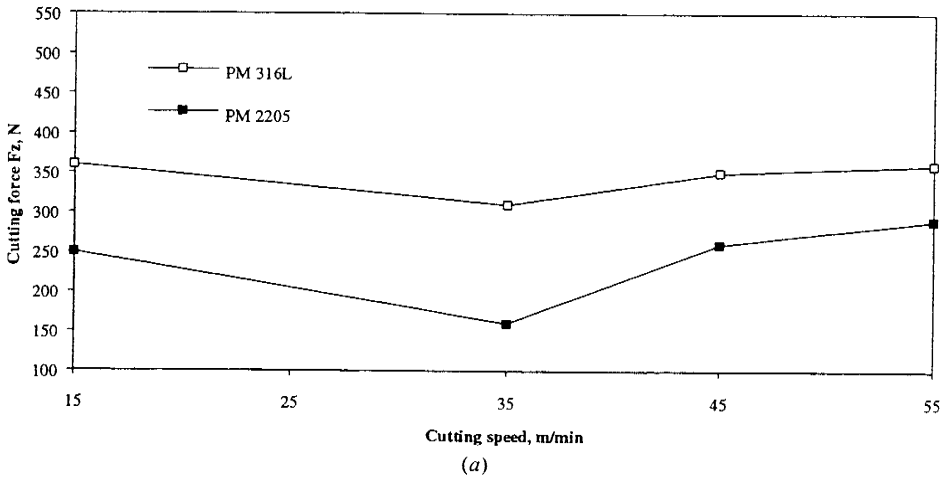

(*a*)

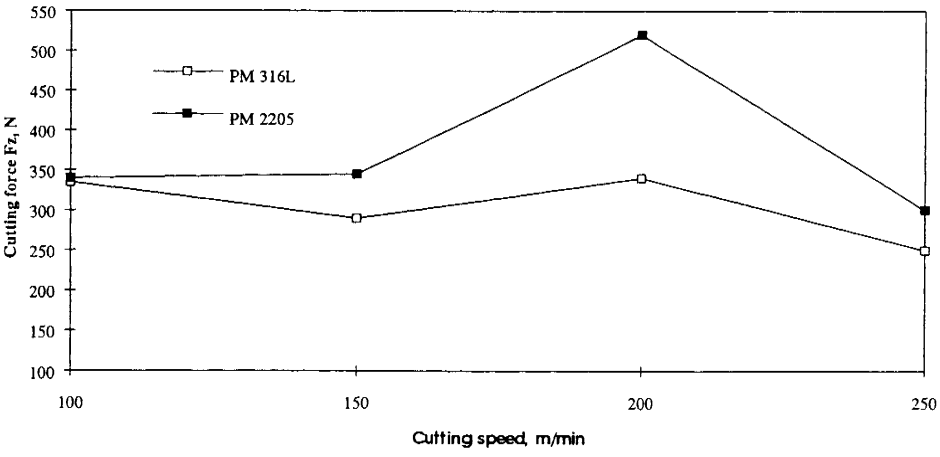

(*b*)

Fig. 2—Cutting forces when machining PM 316L and PM 2205 steels in low and high cutting speed ranges: (*a*) in the low cutting speed range using TiN-coated HSS tool; and (*b*) in the high cutting speed range using TiN-coated cemented carbide tool.

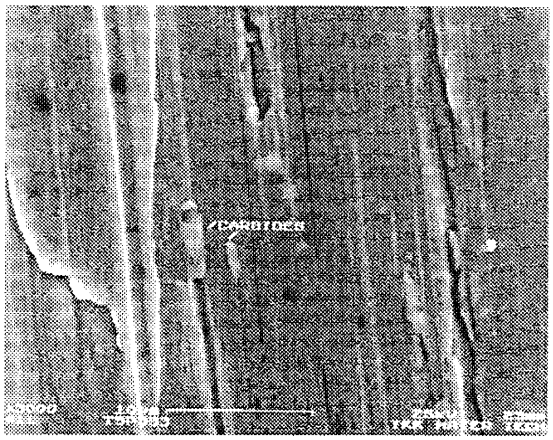

(*a*)

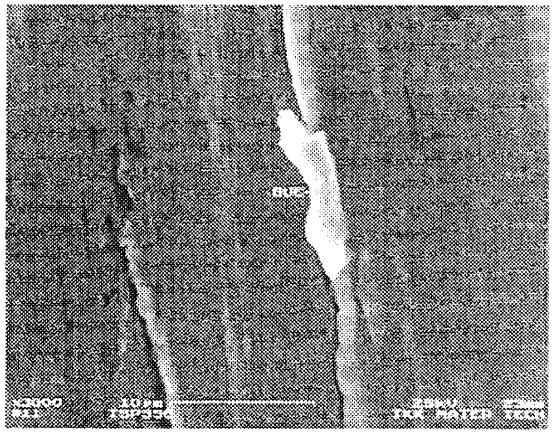

(*b*)

Fig. 3—(*a*) and (*b*) Abrasive groove wear on the flank surface of HSS substrate of TiN-coated HSS tool when machining PM 2205 steel at a cutting speed of 35 m/min.

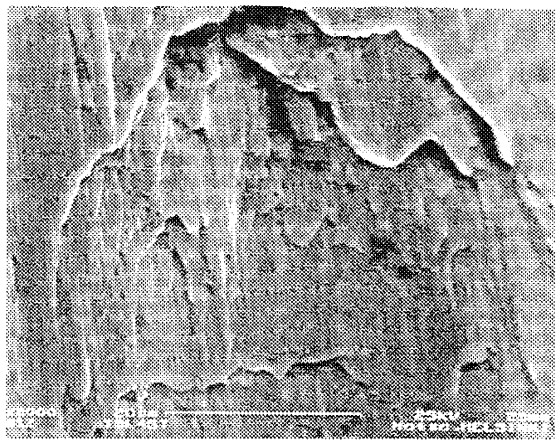

(*a*)

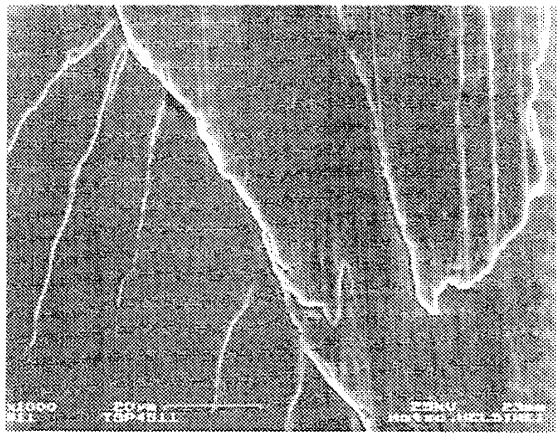

(*b*)

Fig. 4—Fatigue-induced failure on the flank surface of TiN-coated HSS when machining (*a*) PM 316L and (*b*) PM 2205 steels at a cutting speed of 45 m/min.

rough due to fatigue cracks as compared with that when machining PM 316L steel at the same cutting speed.

3. *Adhesive wear and diffusion wear at cutting speeds over 45 m/min*

At cutting speeds over 45 m/min, bonding occurred between the HSS substrate and the workpiece when machining both PM 316L and PM 2205 steels. As an example, the bonding between the HSS substrate and PM 316L is shown in Figure 5. This bonding resulted in adhesive and diffusion wear. Some pieces of HSS substrate torn away from the tool could be seen sticking on the chips. Diffusion of the tool elements, such as W and V, across the bonding interface into the chips was detected if no TiN coating was present in the interface (Figure 6), which indicates that diffusion wear of the tool occurred in this case. On the other hand, no diffusion was detected if a TiN coating was present on the HSS substrate and on the bonding interface, which indicates that TiN coating is able to protect HSS substrate from diffusion wear.

It was observed that the fatigue-induced failure mechanism was cooperative together with adhesive and diffusion wear mechanisms for TiN-coated HSS tool at cutting speeds over 45 m/min in the low cutting speed range, especially when machining PM 316L steel, resulting in the tearing away of some pieces of HSS substrate from the cutting tool.

D. *Wear Topograph and Wear or Failure Mechanisms of TiN-Coated Cemented Carbide Tools*

Fatigue-induced failure was the dominant failure mechanism of TiN-coated cemented carbide tool when machining PM 316L and PM 2205 steels in the whole high cutting speed range between 100 and 250 m/min. The catastrophic failure of the tool due to the fatigue cracks can be seen in Figure 7.

Besides fatigue-induced failure, a diffusion wear mechanism of TiN-coated cemented carbide tools was also active when machining PM 316L and PM 2205 steels in the whole high cutting speed range. For example, the wear mor-

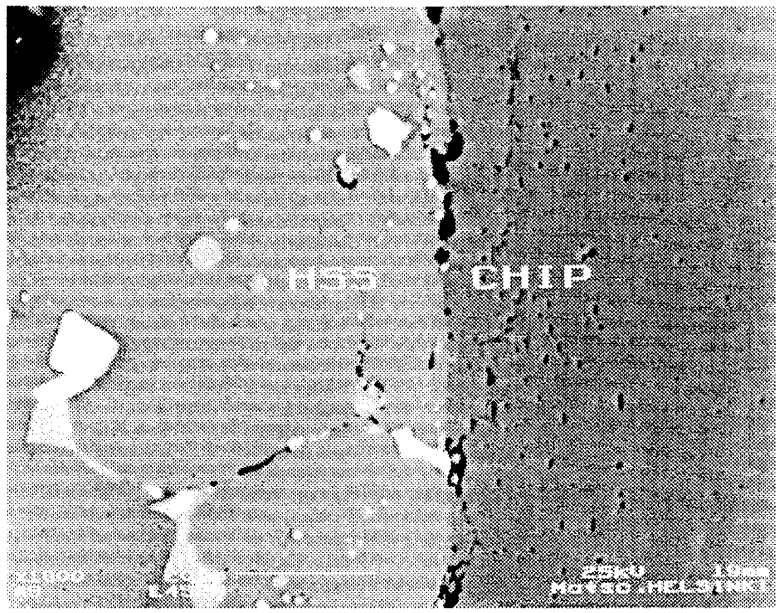

Fig. 5—Bonding between HSS substrate (left side) and the chip (right side) of PM 316L steel at a cutting speed of 45 m/min.

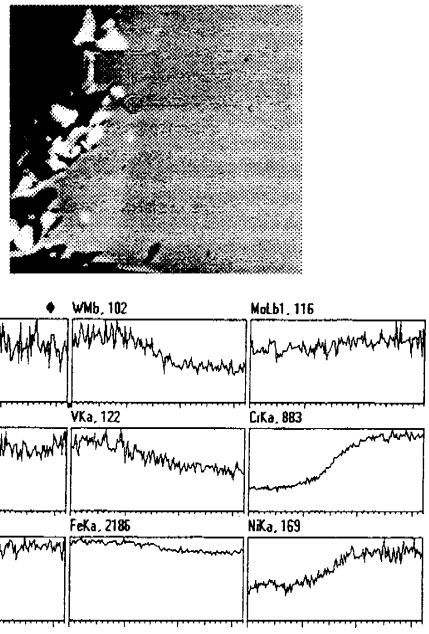

Fig. 6—Chemical composition across the bonding interface (HSS substrate on the left side and chip on the right side) without TiN coating present when machining PM 316L steel at a cutting speed of 45 m/min.

phology of the flank surface of TiN-coated cemented carbide tool when machining PM 316L steel at a cutting speed of 200 m/min, together with EDS analyses, is shown in Figure 8.

Oxide layers consisting mainly of Mn and Si can be observed bonding to TiN coating, while the workpiece layers are seen to bond to cemented carbide substrate on the flank surface. It can also be noticed that, of all the elements of the workpiece, only Ni and Mo diffused into the tool substrate, while only Co of the tool elements diffused into the workpiece. It is well known that both Ni and Co have similar crystal structure and close lattice constants at high-temperature leading to the substitutional diffusion: Ni diffuses from the workpiece into the tool substrate, while Co diffuses from the tool substrate into the workpiece. Molybdenum has the similar ability to form carbide as W, and accordingly, it is able to diffuse from the workpiece into the tool substrate, partially replacing W in the carbides.

Although the bonding of the stainless steel workpiece to the cemented carbide substrate may protect the flank surface of the cutting tool from abrasive wear, it will result in diffusion wear and also attrition wear (fatigue-induced failure) if fatigue cracks form inside the tool substrate. In general, bonding layers of stainless steel were detrimental to the performance of TiN-coated cemented carbide tool, because the main wear or failure mechanisms were the fatigue-induced failure and diffusion wear other than the abrasive wear in the high cutting speed range. No diffusion was detected within the areas of sticking oxide layers, which means that these layers can really act as protective films.

E. *Macroscopic Morphology of Chips*

1. *Low cutting speed range*

The macroscopic morphology of the chips of PM 316L and PM 2205 steels in the low cutting speed range is shown in Figures 9 and 10. It can be seen that the chips are generally continuous, showing serrations which become more and more pronounced as the cutting speed increases. The chips of PM 316L steel were thicker and more serrated as

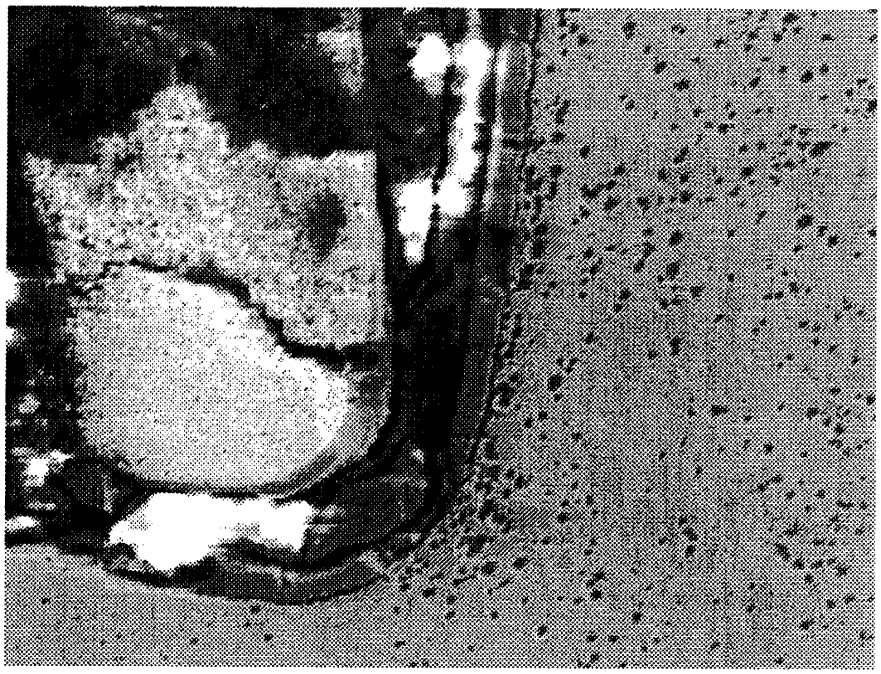

Fig. 7—Catastrophic failure of TiN-coated cemented carbide tool when machining PM 2205 steel at a cutting speed of 200 m/min.

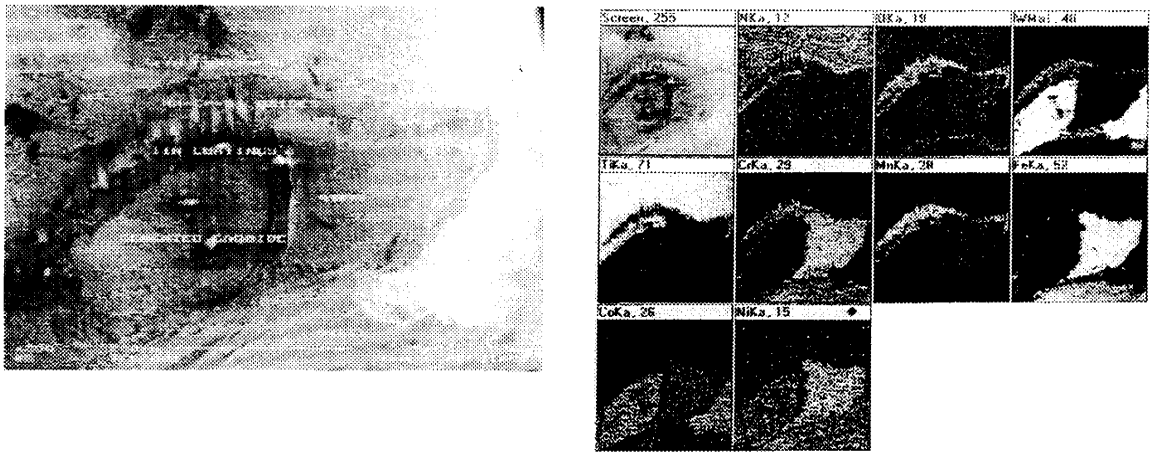

Fig. 8—Wear morphology and related EDS analyses of TiN-coated cemented carbide tool when machining PM 316L steel at a cutting speed of 45 m/min.

compared with those of PM 2205 steel at the same cutting speed. Accordingly, the cutting force when machining PM 316L steel was higher than that when machining PM 2205 steel at the same cutting speed.

2. *High cutting speed range*

The macroscopic morphology of the chips of PM 316L and PM 2205 steels in the high cutting speed range is shown in Figures 11 and 12. As compared with the chips in the low cutting speed range, the chips in the high cutting speed range are more markedly serrated. It can also be seen that the chips of PM 2205 steel are generally thicker than those of PM 316L steel at the same cutting speed. Accordingly, the principal cutting forces when machining PM 2205 steel were higher than those when machining PM 316L steel at the same cutting speed.

F. *Work Hardening of Stainless Steel during Machining*

Work hardening of stainless steel during machining can be seen from the hardness values of the chip bottom, because the chip bottom can be considered as the most markedly deformed zone inside the chips. The microhardness values of the chip bottom of PM 316L and PM 2205 steels

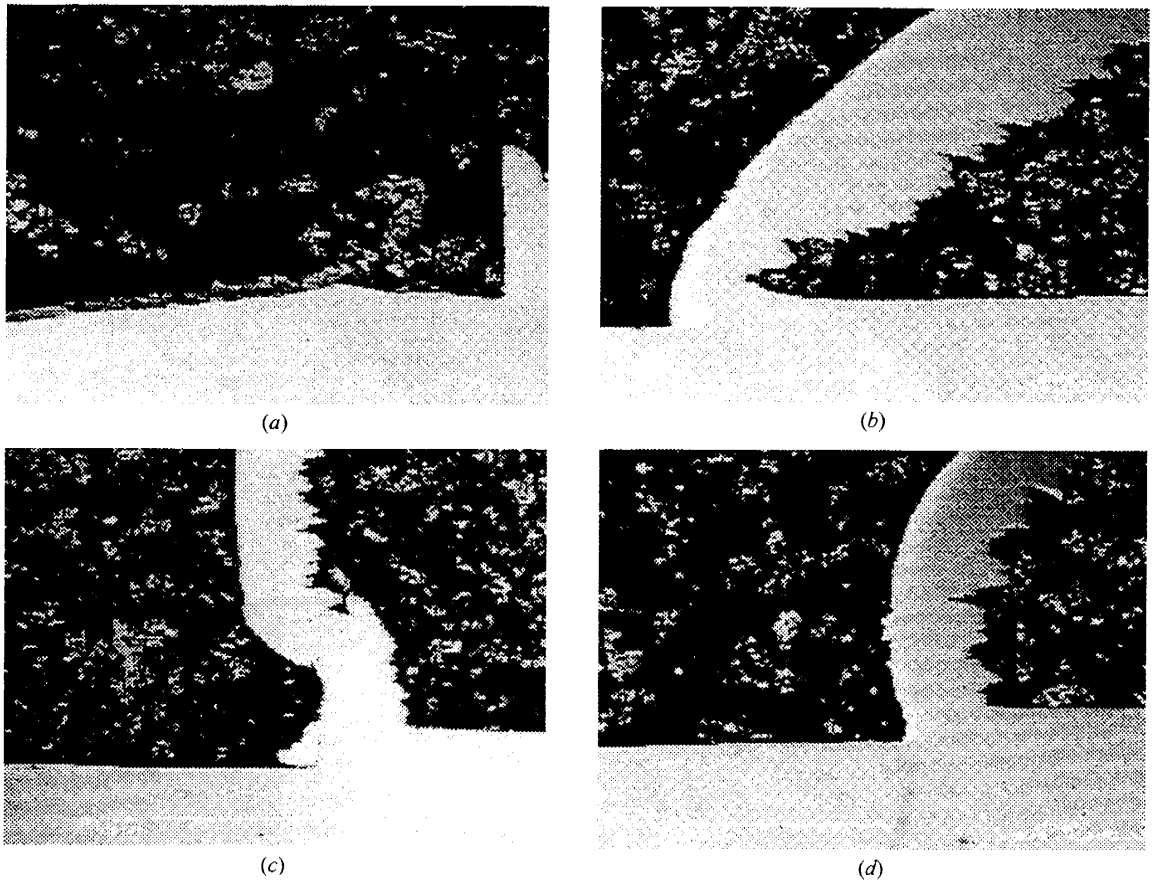

Fig. 9—(*a*) through (*d*) Macroscopic morphology of the chips of PM 316L steel in the low cutting speed range.

in the low cutting speed range, as an example, are shown in Figure 13. As compared with the original microhardness, it can be seen that the austenite phase of PM 316L steel and both the austenite and ferrite phases of PM 2205 steel undergo marked work hardening during machining. Further, it can be seen that the degree of work hardening (the change of microhardness value after turning) of PM 316L steel is much higher as compared with that of PM 2205 steel.

Similar conclusions can be drawn regarding the work hardening behavior of both steels during machining in the high cutting speed range.

IV. DISCUSSION

It was noticed in these tests that fatigue-induced failure was the dominant failure mechanism for TiN-coated HSS tools when machining PM 316L and PM 2205 steels at cutting speeds over 35 m/min in the low cutting speed range and for TiN-coated cemented carbide tools when machining these two steels in the whole high cutting speed range. It has been recognized that fatigue is induced by cyclic vibrations of the cutting forces which are related to the serrations of the chip.[3]

Based on the observations of the macroscopic morphology of the chips in the low cutting speed range, higher vibrations of the principal cutting force may be expected when machining PM 316L steel as compared with those when machining PM 2205 steel due to more serrated chips of PM 316L steel. As an example, the changes of output voltage of the piezoelectric force dynamometer when machining PM 316L and PM 2205 steels at a cutting speed of 55 m/min in the low cutting speed range are shown in Figures 14(a) and (b). There is a linear relationship between the cutting force and the output voltage, and therefore, the changes of the cutting force values can be seen from the changes of the values of the output voltage. Besides the larger amplitude, a higher vibration frequency of the principal cutting force was also recorded when machining PM 316L steel as compared with that when machining PM 2205 steel at the same cutting speed in the low cutting speed range. In the high cutting speed range, the chips were markedly serrated as compared with those in the low cutting speed range. However, little difference of the serrations of the chips of PM 316L and PM 2205 steels was observed in the high cutting speed range. Accordingly, while high frequencies and large amplitudes of the cutting force were

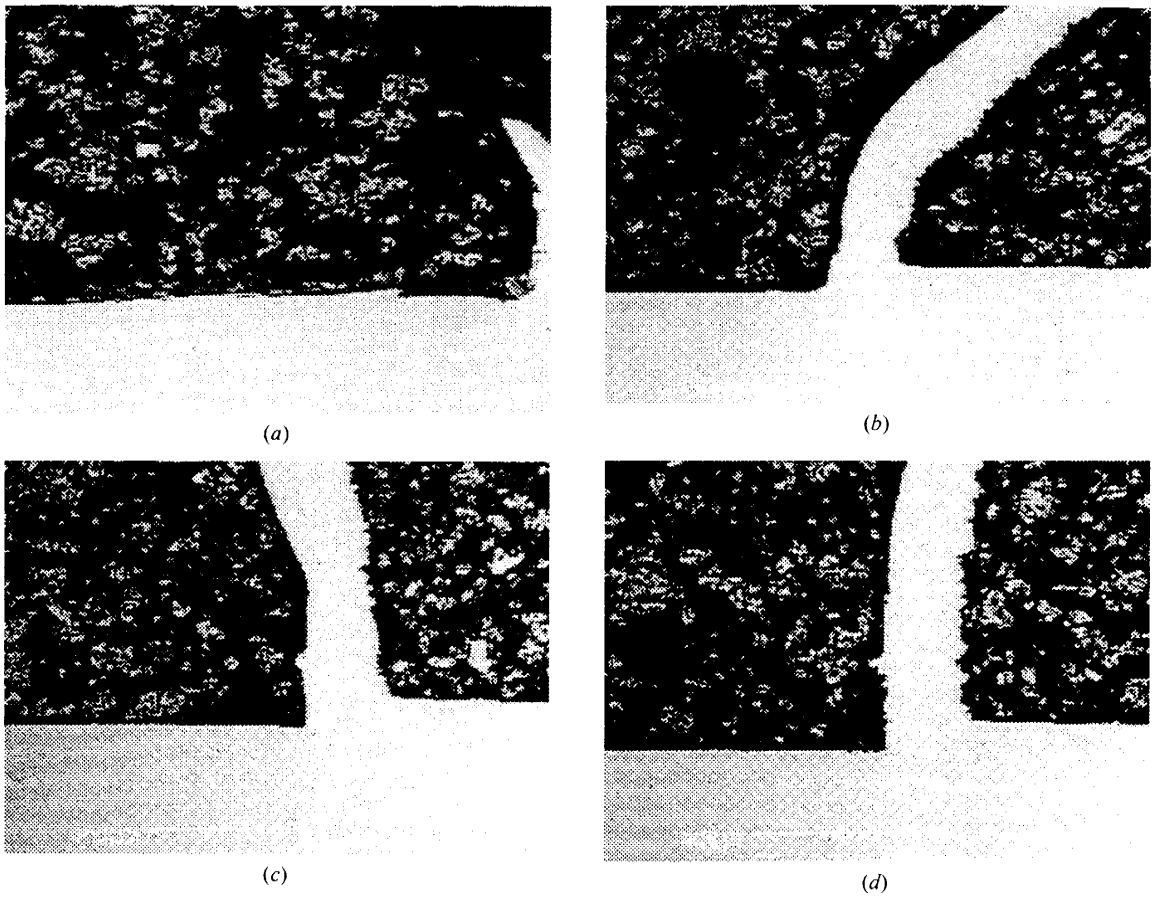

Fig. 10—(*a*) through (*d*) Macroscopic morphology of the chips of PM 2205 steel in the low cutting speed range.

recorded, there is little difference in the cutting force vibrations when machining both steels at the same cutting speed in the high cutting speed range, as shown in Figures 15(a) and (b) for PM 316L and PM 2205 steels, respectively.

It is normally accepted that deformation is concentrated to adiabatic shear bands if serrated chips are formed. As an example, the microstructure of a chip of PM 2205 steel at cutting speed of 200 m/min is shown in Figure 16. Heavy and slight deformation occur alternatively inside the chip. The heavy deformation zone seems like an adiabatic shear band. According to a previous study,[2] formation of heavily concentrated deformation zones in the chips of stainless steels was supposed to be due to high work hardening and low thermal conductivity. In addition, changes of the direction of strain in the different deformation zones (heavy and slight deformation) in the primary shear zone can also be recognized, which indicates that there have been cyclic changes of the shear angle of the stainless steel chips. The changes of shear angle may also be partially responsible for the serrations of the stainless steel chips, which agrees with an earlier study.[6]

The higher degree of work hardening would result in more concentrated deformation leading to more serrated chips. Also, the higher cutting temperature would promote the formation of serrated chips of the materials with low thermal conductivity. In the low cutting speed range, the cutting temperature when machining PM 316L and PM 2205 steels may not be very high, and only a slight difference of the cutting temperature when machining both steels may be expected. Accordingly, the work hardening degree may be the dominant factor affecting the degree of serration of the chips in the low cutting speed range. Based on the data concerning work hardening, it can be understood that the chips of PM 316L steel exhibit more marked serrations as compared with those of PM 2205 steel. In the high cutting speed range, however, the cutting temperature when machining both steels may be high and also a large temperature difference may be expected. Accordingly, the cutting temperature will, together with the high degree of work hardening, play an important role in producing serrated chips in the high cutting speed range. Due to much higher strength of PM 2205 steel, the cutting temperature when machining it is expected to be much higher than that when machining PM 316L steel in the high cutting speed range. The effect of the higher cutting temperature will

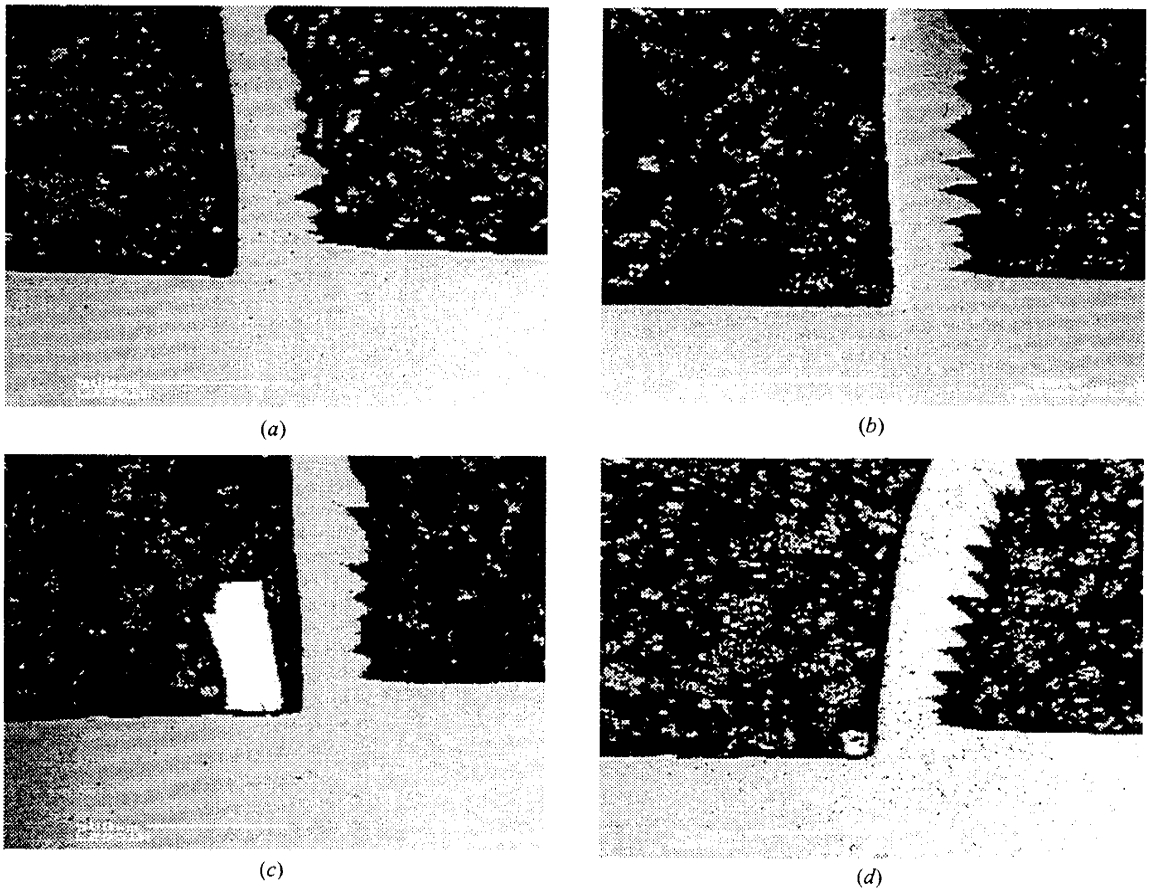

Fig. 11—(*a*) through (*d*) Macroscopic morphology of the chips of PM 316L steel in the high cutting speed range.

balance the effect of the lower degree of work hardening of PM 2205 steel on the degree of serration of the chips, resulting in chips with a degree of serration comparable to that of the chips of PM 316L steel in the high cutting speed range.

The tool life of TiN-coated HSS tool was longer when machining PM 2205 steel as compared with that when machining PM 316L steel in the low cutting speed range. At cutting speeds below 35 m/min, the abrasive wear mechanisms were dominant. Because of the higher work hardening degree of PM 316L steel, the fallen BUEs from PM 316L steel on the flank surface of the cutting tool are expected to have a slightly higher hardness and result in slightly more marked abrasive wear and, consequently, slightly shorter tool life as compared with those of PM 2205 steel. Although there were some other wear or failure mechanisms, fatigue-induced failure was the dominant and most rapid failure mechanism of TiN-coated HSS tools at cutting speeds over 35 m/min in the low cutting speed range. Based on macroscopic observations and hardness measurements of the chips of PM 316L and PM 2205 steels, it can be well understood that the chips of PM 316L steel exhibit a higher degree of serration leading to higher vibrations of the principal cutting force and therefore more marked fatigue of the cutting tools as compared with those of PM 2205 steel. Furthermore, it can be recognized that TiN-coated HSS tool has a longer tool life when machining PM 2205 steel as compared with that when machining PM 316L steel in the low cutting speed range.

In the high cutting speed range using TiN-coated cemented carbide tool, however, both fatigue-induced failure and diffusion wear mechanisms are cooperative and dominant in tool wear and failure. Based on the macroscopic observations of the chips, it can be seen that there was little difference in the serrations of the chips and accordingly little difference in the vibrations of the cutting forces when machining both PM 316L and PM 2205 steels in the high cutting speed range. Consequently, little difference of fatigue-induced failure of the tools can be expected to occur when machining both steels. The only mechanism contributing to the difference of tool lives when machining both steels is diffusion wear, which is markedly dependent on the cutting temperature. As discussed previously, the cutting temperature when machining PM 2205 steel may be expected to be much higher than that when machining PM 316L steel. Accordingly, the diffusion wear will be more

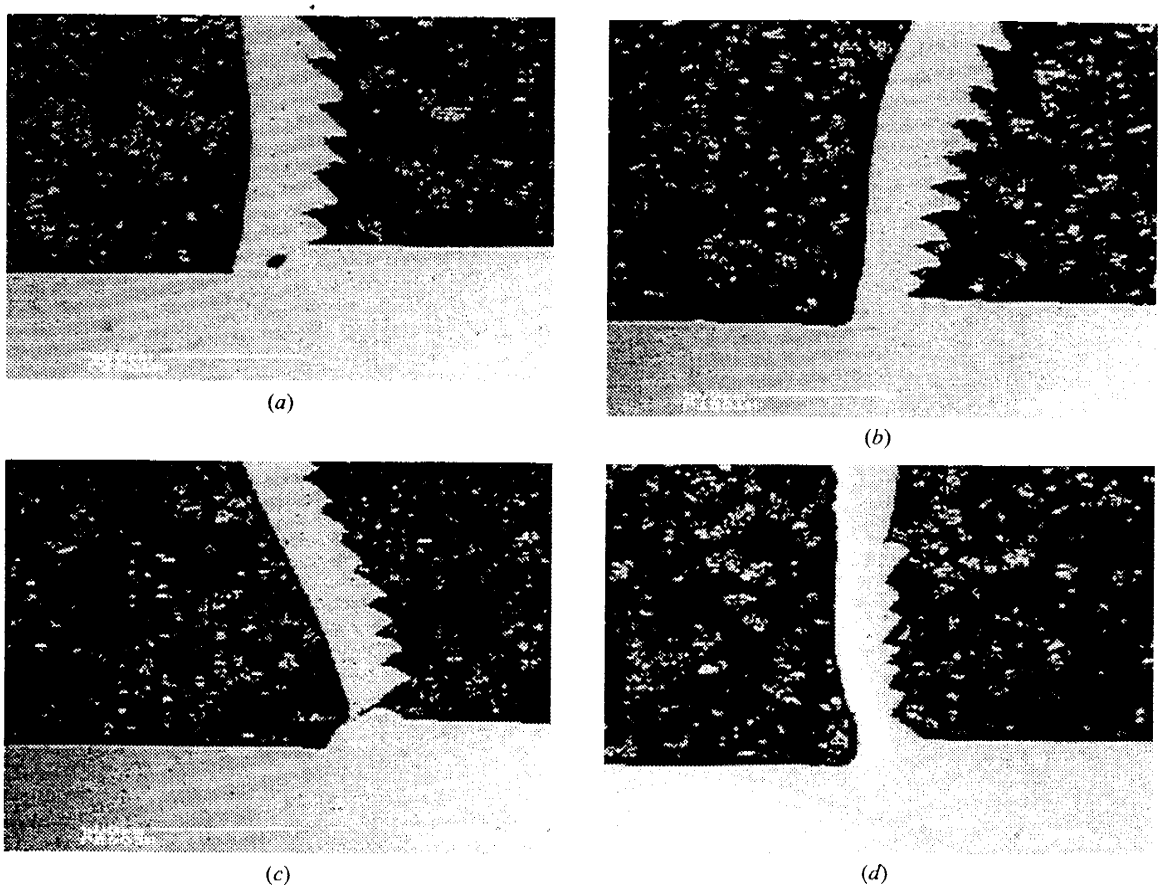

Fig. 12—(*a*) through (*d*) Macroscopic morphology of the chips of PM 2205 steel in the high cutting speed range.

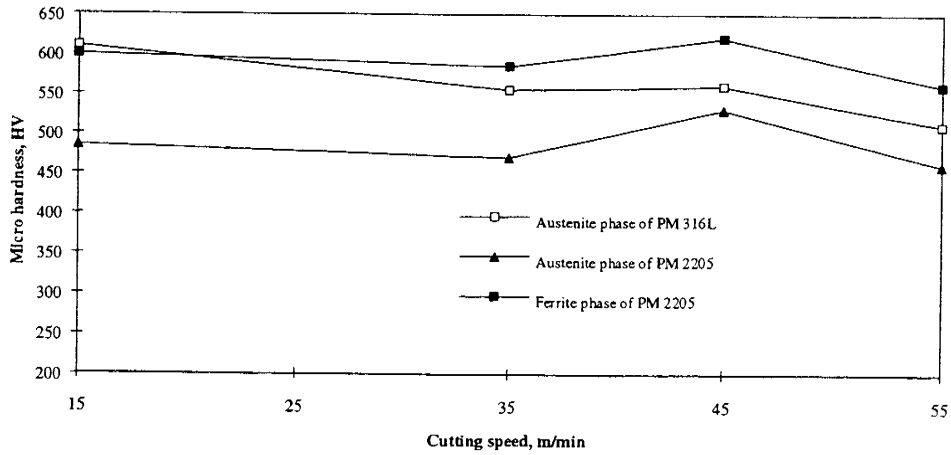

Fig. 13—Microhardness of austenite phase of PM 316L and both austenite and ferrite phases of PM 2205 steel at chip bottom in the low cutting speed range.

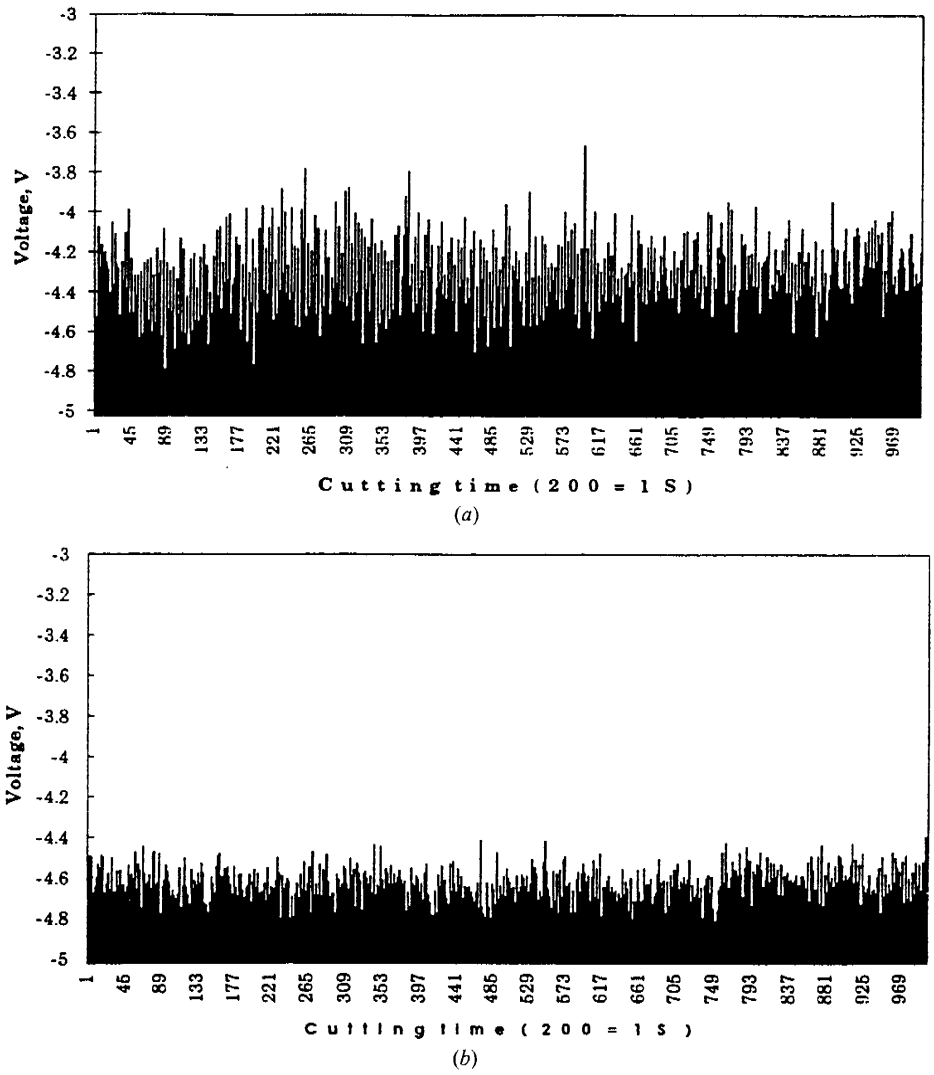

Fig. 14—Cyclic vibrations of cutting force when machining (*a*) PM 316L and (*b*) PM 2205 steels at a cutting speed of 55 m/min.

pronounced and, consequently, a shorter tool life for TiN-coated cemented carbide tool can be expected when machining PM 2205 steel as compared with those when machining PM 316L steel in the high cutting speed range.

The alloying elements of stainless steels may adversely affect the machinability and the performance of the cutting tools because of their strength-increasing role and particularly of the toughness-increasing role of Ni. Additional mechanisms contributing to the effects of the alloying elements on machinability of stainless steels or the performance of the cutting tool were investigated in this study by means of SEM and EDS analyses of TiN-coated cemented carbide tools in the high cutting speed range. It can be concluded that Ni and Mo promote diffusion wear because of the replacing diffusion of Ni from the workpiece and Co from the substrate of the tool and diffusion of Mo from the workpiece to the substrate, partially replacing W. No promotion of diffusion-induced wear of TiN-coated cemented carbide tool was caused by Cr.

V. CONCLUSIONS

TiN-coated HSS and TiN-coated cemented carbide tools were used for turning PM 316L and PM 2205 steels in the low and high cutting speed ranges, respectively. The tool lives and the cutting forces were measured, and the wear and failure mechanisms of the cutting tools were investigated. Particular attention was paid to the fatigue-induced failure. The following main conclusions can be drawn.

1. Abrasive wear, fatigue-induced failure, and diffusion

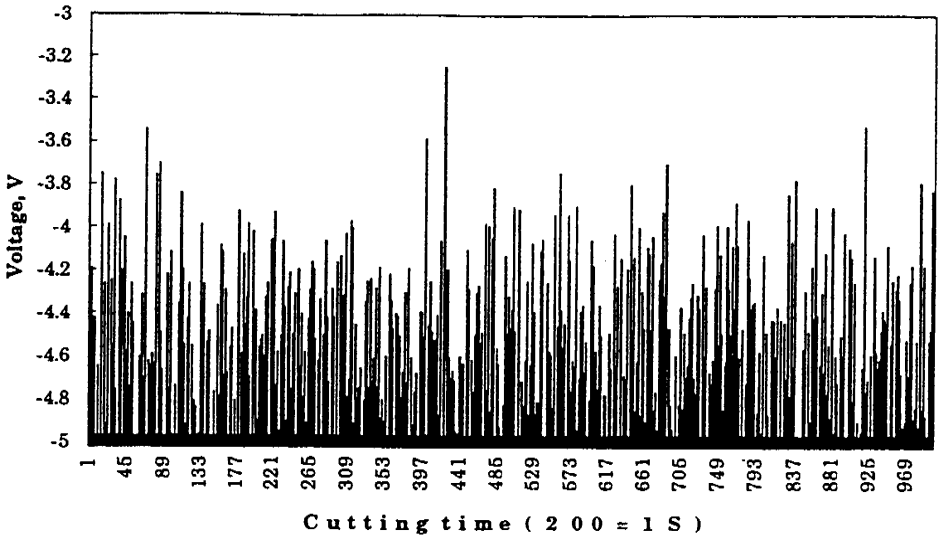

(*a*)

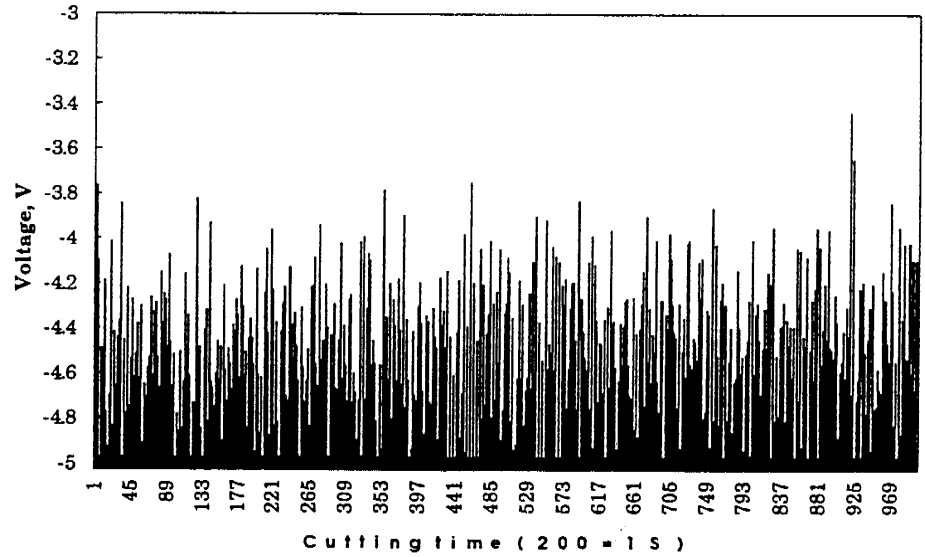

(*b*)

Fig. 15—Cyclic vibrations of cutting force when machining (*a*) PM 316L and (*b*) PM 2205 steels at a cutting speed of 100 m/min.

wear were dominant wear and failure mechanisms of TiN-coated HSS tools when machining PM 316L and PM 2205 steels at cutting speeds below 35 m/min, between 35 and 45 m/min, and over 45 m/min, respectively. In addition, fatigue-induced failure was also active at cutting speeds over 45 m/min in the low cutting speed range, especially when machining PM 316L steel.

2. Fatigue-induced failure, together with diffusion wear, was the dominant failure mechanism for TiN-coated cemented carbide tools in the whole high cutting speed range.

3. Fatigue affecting the cutting tool lives when machining PM 316L and PM 2205 steels was caused by serrated chips produced by low thermal conductivity and a high degree of work hardening of stainless steels. Higher frequency and larger amplitude values of the cutting force vibrations were recorded when machining PM 316L steel as compared with those when machining PM 2205 steel in the low cutting speed range. However, no major difference of the frequency and the amplitude values of the cutting force vibrations was recorded when machining both steels in the high cutting speed range.

4. TiN-coated HSS tool had longer tool life when machining PM 2205 steel as compared with that when machining PM 316L steel in the low cutting speed range, which was

Fig. 16—Cyclic deformation of a chip of PM 2205 steel at a cutting speed of 200 m/min.

attributed to the lower fatigue-induced damage when machining PM 2205 steel.

5. TiN-coated cemented carbide tool had longer tool life when machining PM 316L steel as compared with that when machining PM 2205 steel in the high cutting speed range, which was supposed to be due to the lower cutting temperature resulting in less diffusion wear when machining PM 316L steel.

6. Of the alloying elements in stainless steels, Ni and Mo promote diffusion wear of TiN-coated cemented carbide tools because of replacing diffusion of Ni from the workpiece to the tool and Co from the cemented carbide substrate to the workpiece and diffusion of Mo from the workpiece to the substrate, partially replacing W.

ACKNOWLEDGMENTS

The financial support from the Center of International Mobility (CIMO), Finland, to one of the authors (LZJ) is gratefully acknowledged. Thanks are due to Rauma Materials Technology Co., Tampere, for supplying the workpiece materials. The permission to use the facilities and the assistance of Mr. Alpo Hakola, Laboratory of Workshop Technology, Helsinki University of Technology, with the turning tests is acknowledged. Thanks are also due to Mr. Reima Väinöla, Imatra Steel Co., for the assistance of quick-stop tests. The active interest in this project of Dr. Jari Liimatainen, Rauma Materials Technology Co., is also acknowledged.

This article was originally presented and published in *Materials Issues in Machining—II* and *The Physics of Machining Process—II*, Conf. Proc., TMS, Warrendale, PA, 1994.

REFERENCES

1. E.M. Trent: *Metal Cutting*, 2nd ed., Butterworth and Co., London, 1984, p. 204.
2. M.C. Shaw: *Machinability*, The Iron and Steel Institute, London, 1967, p. 1.
3. K.F. Sullivan, P.K. Wright, and P.D. Smith: *Met. Technol.*, 1978, pp. 181-89.
4. S. Söderberg, S. Hogmark, H. Haag, and H. Wisell: *Met. Technol.*, 1983, pp. 471-80.
5. S. Söderberg and S. Hogmark: *Wear*, 1986, pp. 315-29.
6. P. Albrecht: *J. Eng. Ind. Trans. ASME*, 1962, vol. 84, pp. 405-17.

PUBLICATION III

Tool wear and machinability of X5 CrMnN 18 18 stainless steels

In: Journal of Materials Processing Technology 2001.
Vol. 119, pp. 14–20.
Reprinted with permission from Elsevier.

ELSEVIER

Journal of Materials Processing Technology 119 (2001) 14–20

Journal of Materials Processing Technology

www.elsevier.com/locate/jmatprotec

Tool wear and machinability of X5 CrMnN 18 18 stainless steels

Jukka Paro[a,*], Hannu Hänninen[b], Veijo Kauppinen[a]

[a]*Laboratory of Workshop Technology, Helsinki University of Technology, Puumiehenkuja 3, SF-02150 Espoo, Helsinki, Finland*
[b]*Laboratory of Engineering Materials, Helsinki University of Technology, Helsinki, Finland*

Abstract

In this study, active wear and failure mechanisms of TiN-coated cemented carbide tools when machining X5 CrMnN 18 18 austenitic stainless steel have been investigated. By nitrogen alloying austenite is stabilised and the strength of austenitic stainless steel is increased and work hardening is promoted. Stainless steels are often considered as poorly machinable materials. High strength and work hardening rate cause difficulties from the machining point of view. In this study turning tests carried out by using a test lathe and a cutting force measuring device are presented. Chips were analysed by scanning electron microscopy. The machinability of X5 CrMnN 18 18 austenitic stainless steels is examined based on tool life and cutting speed presented by vT-diagrams. The effect of cutting speed and nitrogen content is also analysed by cutting force measurements. Based on the cutting tests, cutting speeds of 40–200 m/min, feed rate of 0.15–0.25 mm and depth of cut of 1.6 mm for X5 CrMnN 18 18 stainless steels can be applied from machinability point of view. Higher nitrogen content decreases cutting force and decreases machinability. Tool wear criterion, VB-value of 0.3 mm, is reached after turning time of 10 min, when 60, 65 and 70 m/min and 0.24 mm/r feed rates are utilised.

Keywords: Tool wear; Machinability; Stainless steel

1. Introduction

Austenitic stainless steels are considered to be difficult to machine. Built-up edge (BUE) and irregular wear are often faced in machining operations. Difficulties from the machining point of view increase when duplex and high-strength stainless steels are to be machined. Machinability is often compared to the pitting resistance equivalent to pre-value representing the alloying content of the steel. High nitrogen stainless steels are common ultra-high strength stainless steels.

Nitrogen alloyed stainless steels exhibit a variety of exceptional properties like high strength, high ductility and resistance to stress corrosion cracking [1]. It is known that the effect of nitrogen on the flow stress of the steel is due to two strengthening mechanisms [2,3]. Nitrogen acts as an obstacle against dislocation movement causing solid solution hardening and the other mechanism is grain size hardening [1].

Nitrogen alloyed stainless steels show a high cold work capacity. Increased work hardening rate decreases machinability. The work hardening rate increases with increasing nitrogen content [1]. X5 CrMnN 18 18 ultra-high strength stainless steels with grain size of 30 μm have typically yield strength of 660 MPa and high nitrogen austenitic steel is able to work harden to 0.2% yield strength levels as high as up to 3000 MPa [1].

* Corresponding author. Tel.: +358-451-3524; fax: +358-451-3518.

2. Experimental part

2.1. Test materials

X5 CrMnN 18 18 trial materials were produced by VSG Energie- und Schmiedetechnik GmbH. X5 CrMnN 18 18 trial material samples examined in the turning tests are presented in Tables 1 and 2.

The mechanical properties of X5 CrMnN 18 18 trial materials were measured by tensile testing. Yield strength for X5 CrMnN 18 18 trial material with 0.91 wt.% N was 458 MPa. Microhardness values were tested for both X5 CrMnN 18 18 trial materials. The microstructures of X5 CrMnN 18 18 trial materials are presented in Figs. 1 and 2.

2.2. Turning experiments

The turning tests were carried out with a conventional lathe equipped for testing purposes. The VDF-lathe applied in experiments is powered by 100 kW main spindle motor and equipped with Kistler cutting force measuring device. Turning tests were carried out according to ISO standard for tool life testing of single point turning tools. Tool wear was measured by using optical microscope.

The cutting tools used in the tests were made by Sandvik Coromant AB, Sweden. Solid carbide inserts were of type

0924-0136/01/$ – see front matter
PII: S0924-0136(01)00877-9

Table 1
Workpiece dimensions of X5 CrMnN 18 18 trial materials and their melt numbers

Two bars of diameter 125 mm × 620 mm	Melt DDT63
One bar of diameter 130 mm × 400 mm	Melt G88216

Table 2
Chemical compositions (wt.%) of X5 CrMnN 18 18 trial materials

Melt	C	Si	Mn	Cr	Mo	Ni	V	N
G88216	0.05	0.29	18.89	18.13	0.11	0.43	0.08	0.57
DDT63	0.05	0.49	19.8	18.6	0.08	0.61	0.13	0.91

SNMG 120408-PM P15/K15. The insert was CVD coated with TiN and Al_2O_3 layers.

Cutting parameters for the turning tests of X5 CrMnN 18 18 trial materials were selected to achieve appropriate tool life. Tool wear criteria were the width of flank wear value of VB = 0.3 mm or catastrophic failure. Cutting speeds in tests were $v_c = 60$, 65, 70 and 100 m/min, depth of cut was $a = 1.6$ mm and feed rate was $v_f = 0.24$ mm/r.

2.3. Tool life testing

Tool life testing vT-curves are presented in Fig. 3. When turning with the cutting speed $v_c = 60$ m/min the breaking

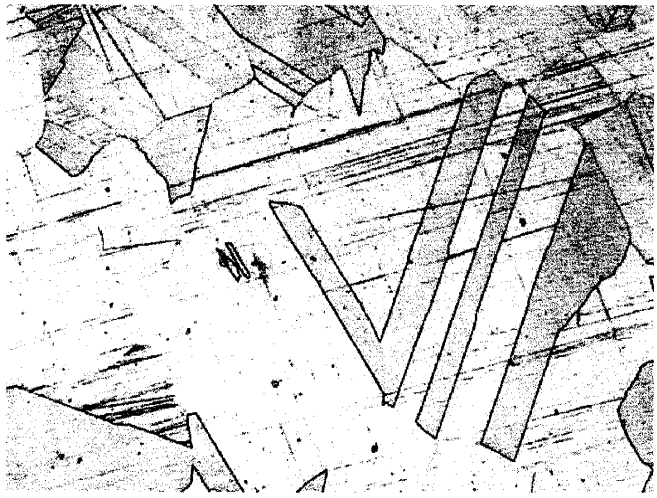

Fig. 1. Microstructure of X5 CrMnN 18 18 trial material with 0.91 wt.% N.

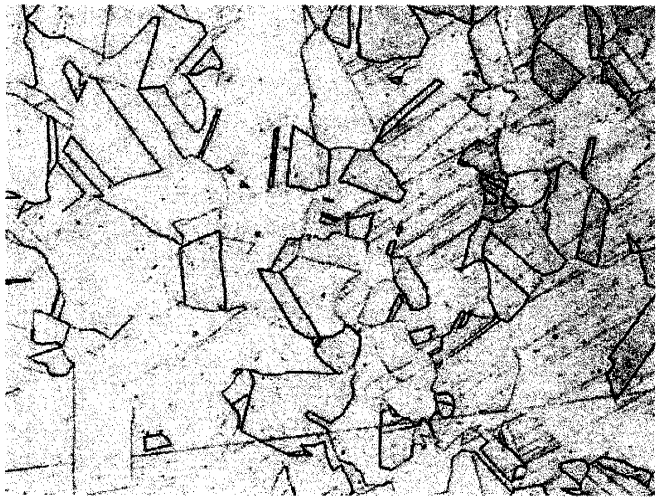

Fig. 2. Microstructure of X5 CrMnN 18 18 trial material with 0.57 wt.% N.

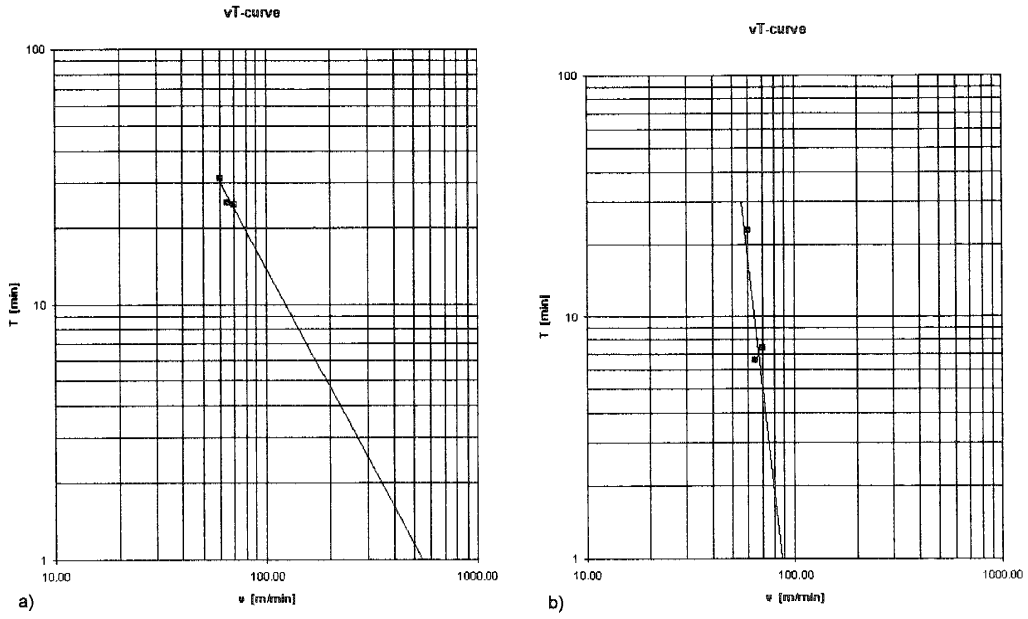

Fig. 3. Tool life testing vT-curves when machining X5 CrMnN 18 18 trial materials: (a) 0.91 wt.% N; (b) 0.57 wt.% N.

and chipping of tool nose begins after 20 min turning time. Continuous turning of the rapid tool wear proceeds and the surface roughness worsens and the chip formation becomes irregular. Increasing cutting speed v_c to a value of 65 m/min shows serrated chip formation until turning is to be interrupted after 25 min turning. The cutting speed v_c value of 70 m/min shows more problems in chip formation and surface roughness is decreased.

When turning the material with higher nitrogen level with the cutting speed of 60 m/min tool nose breaking occurs after 12 min tool life. Increasing the cutting speed to 70 m/min, the tool life is shortened and surface roughness

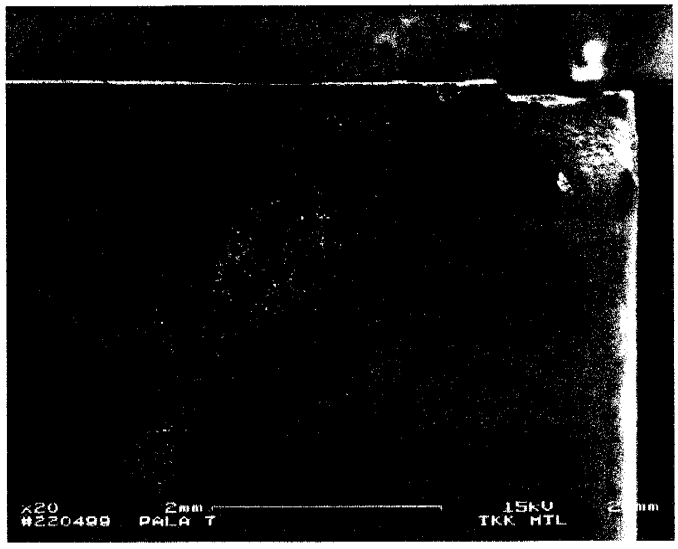

Fig. 4. The flank edge of solid carbide insert after machining time, $T = 4$ min in turning of X5 CrMnN 18 18 trial material, 0.91 wt.% N. Cutting speed, $v_c = 65$ m/min.

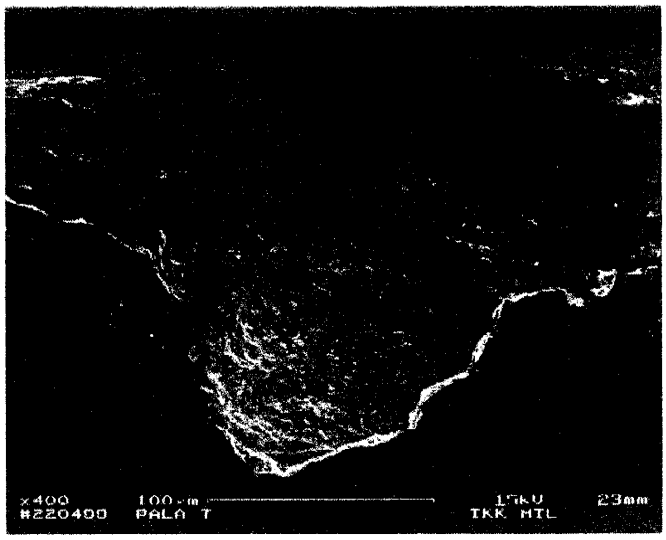

Fig. 5. The chipping of solid carbide insert in turning of X5 CrMnN 18 18 trial material with 0.57 wt.% N.

becomes worse. The main tool wear mechanisms are tool nose breaking and chipping of the cutting edge.

The test material with lower nitrogen level was much more complicated to machine. Tool lives shorter than 10 min were achieved. Catastrophic failure was the tool wear criterion interrupting the tool life testing experiment. Tool nose being partially damaged because of high stresses and forces, cutting circumstances are worsened at the cutting edge and BUE due to workpiece material adhesion to broken flank edge areas occurs.

2.4. Tool wear mechanisms

Solid carbide inserts used in turning test of trial materials are shown in Figs. 4 and 5, examined by scanning electron microscopy (SEM). Fig. 4 illustrates damaged insert representing typically worn tool in turning tests. Turning both X5 CrMnN 18 18 trial materials broken tool nose, chipping of the cutting edge and missing coating were observed.

It can be observed from Fig. 4 that tool nose breaking, chipping of cutting edge and wear of the coating occurred. Also deformation of the insert can be seen. In Fig. 5 on the small chipping area near the beginning of tool nose breakage area is observed adhered X5 CrMnN 18 18 trial material with 0.57 wt.% N.

The flow line like test material particles fixed into solid carbide insert indicates the incidence on BUE formation in the rake face area of turning tool.

2.5. Chip morphology

To analyse chip morphology SEM was used for X5 CrMnN 18 18 trial materials. Chips from cutting speeds of 60, 65 and 70 m/min from both testing materials were

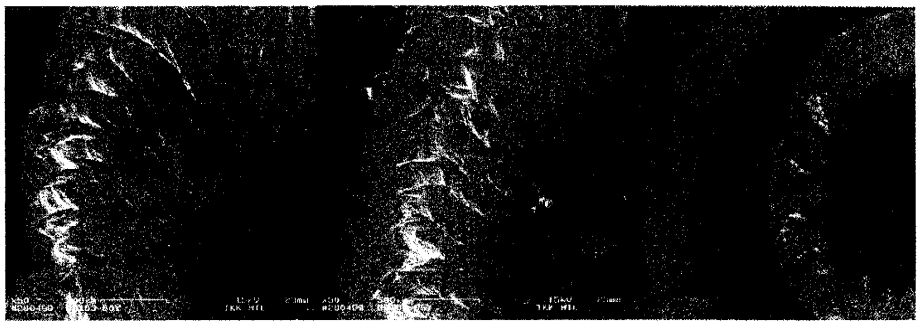

a) b) c)

Fig. 6. SEM-images of chips in the direction away from the workpiece. X5 CrMnN 18 18 trial material with 0.91 wt.% N. Cutting speeds: (a) $v_c = 60$, (b) 65 and (c) 70 m/min, depth of cut $a = 1.6$ mm and feed rate $v_f = 0.24$ mm/r.

a) b) c)

Fig. 7. SEM-images of the chips in the direction away from the workpiece. X5 CrMnN 18 18 trial material with 0.57 wt.% N. Cutting speeds: (a) $v_c = 60$, (b) 65 and (c) 70 m/min, depth of cut $a = 1.6$ mm and feed rate $v_f = 0.24$ mm/r.

analysed. Chips were strongly deformed to small short conical–helical chips or arc type chips. The chips from the test material with lower nitrogen content are presented in Fig. 6 and the chips from the test material with higher nitrogen content in Fig. 7. Chips are presented in the direction away from the workpiece.

The chips presented in Figs. 6 and 7 are machined from both X5 CrMnN 18 18 trial materials: increasing the cutting speed the chip changes from arc-like chip to spiral-like chip. Fig. 6 shows the chips from turning X5 CrMnN 18 18 trial material with 0.91 wt.% N; the chip becomes at the cutting speed $v_c = 60$ m/min arc-like and the cutting speed value $v_c = 70$ m/min spiral-like. In Fig. 6 X5 CrMnN 18 18 trial material with 0.57 wt.% N shows smaller arc-like chips and by the cutting speed $v_c = 70$ m/min spiral-like chips having smaller radius than chips of X5 CrMnN 18 18 trial material with 0.91 wt.% N. The serrated structure of chips can be observed. The thickness of serrated structure observed by means of optical microscopy is about 0.2 mm.

Chip surface sliding against the rake face of the tool was examined by SEM and it is shown in Figs. 8 and 9. Outside the chips in the direction of the workpiece shear bands and

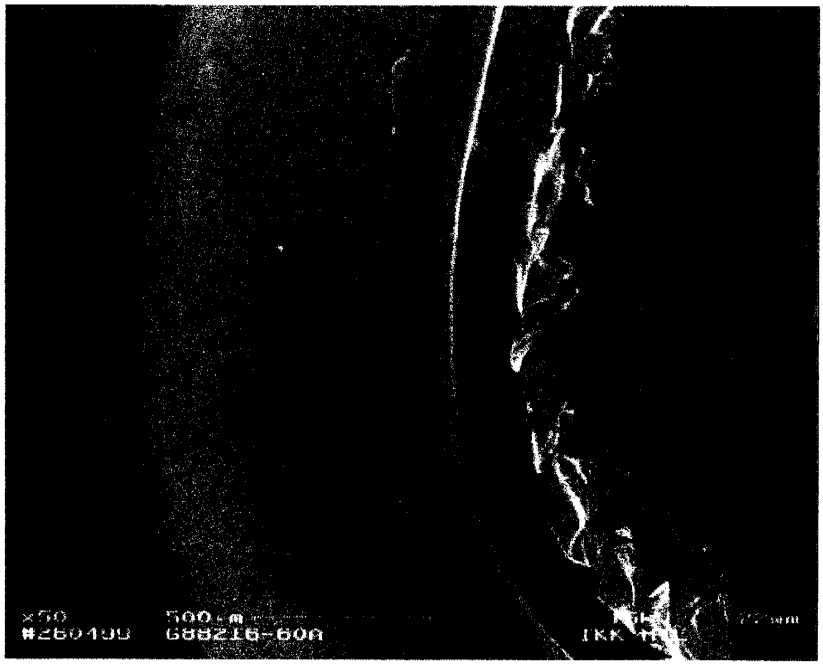

Fig. 8. SEM-image in the direction towards the workpiece. X5 CrMnN 18 18 trial material with 0.91 wt.% N. Cutting speed $v_c = 65$ m/min, depth of cut $a = 1.6$ mm and feed rate $v_f = 0.24$ mm/r.

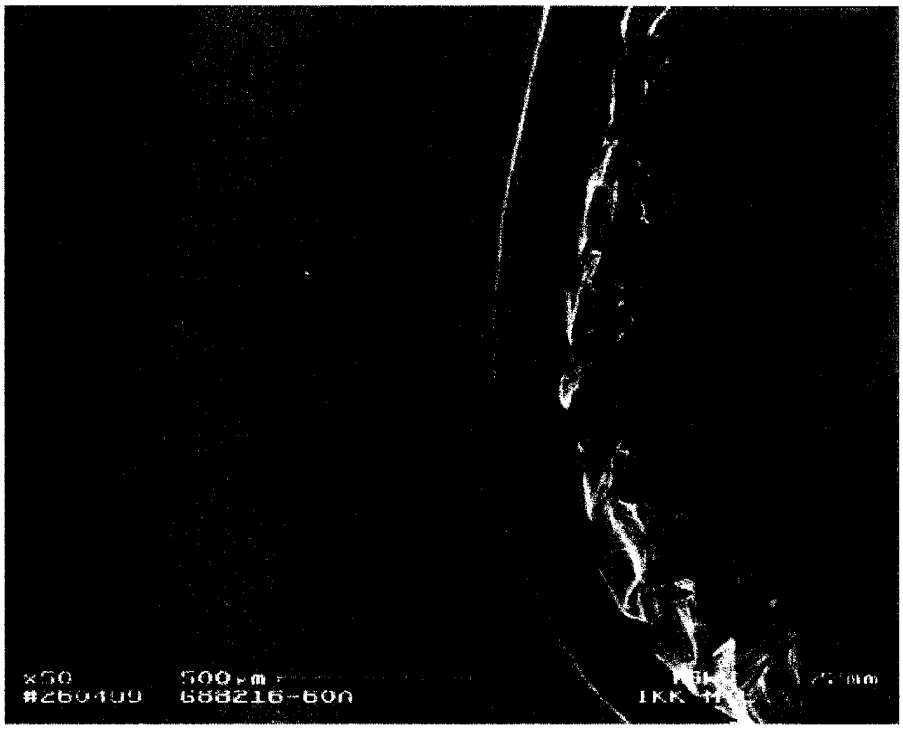

Fig. 9. SEM-image in the direction towards the workpiece. Chip from X5 CrMnN 18 18 trial material with 0.57 wt.% N. Cutting speed $v_c = 65$ m/min, depth of cut $a = 1.6$ mm and feed rate $v_f = 0.24$ mm/r.

strongly deformed chip is observed. Serrated structure having width of 0.2 mm is seen.

2.6. Cutting forces

Cutting forces of X5 CrMnN 18 18 trial materials are presented in Tables 3 and 4. There was a difference in cutting forces when machining X5 CrMnN 18 18 trial material with 0.57 wt.% N.

Table 3
Cutting force components of X5 CrMnN 18 18 trial material with 0.91 wt.% N

v_c (m/min)	F_y (kN)	F_x (kN)	F_z (kN)
60	2.4–2.9	1.2–1.5	0.7
65	2.4–3.0	1.2–1.6	0.7–0.8
70	2.5–3.5	1.3–2.9	0.7–1.2
100	2.3–3.5	1.2–2.5	0.7–1.0

Table 4
Cutting force components of X5 CrMnN 18 18 trial material with 0.57 wt.% N

v_c (m/min)	F_y (kN)	F_x (kN)	F_z (kN)
60	2.2	1.0	0.6
65	2.2	1.0	0.6
70	2.2	1.0	0.6
100	1.8	0.8	0.5

3. Discussion

Rapid tool wear and tendency to chipping was studied on major cutting edge. In turning tests of X5 CrMnN 18 18 trial material with 0.91 wt.% N using cutting speed $v_c = 60$ m/min, tool life of about $T = 31$ min was achieved. Tool life decreased to $T = 25$ min at cutting speed of 65 m/min. By increasing cutting speed chip formation difficulties are caused and chipping of tool material and catastrophic failure of tool was often occurring.

Machining the material X5 CrMnN 18 18 trial material with 0.57 wt.% N the tool life was $T = 10$ min. Tool life was increased when turning test material of higher nitrogen content. By cutting speed of $v_c = 60$ m tool life of $T = 22$ min was achieved. Cutting speeds of $v_c = 65$ and $v_c = 75$ m/min caused about 7 min tool life.

BUE formation decreased surface roughness. In analysing the samples with microhardness measurements, the presence of BUE was found. There were protuberance-like material formations on turned surfaces. Additionally there were microcracks. The evidence of BUE was focused on surfaces

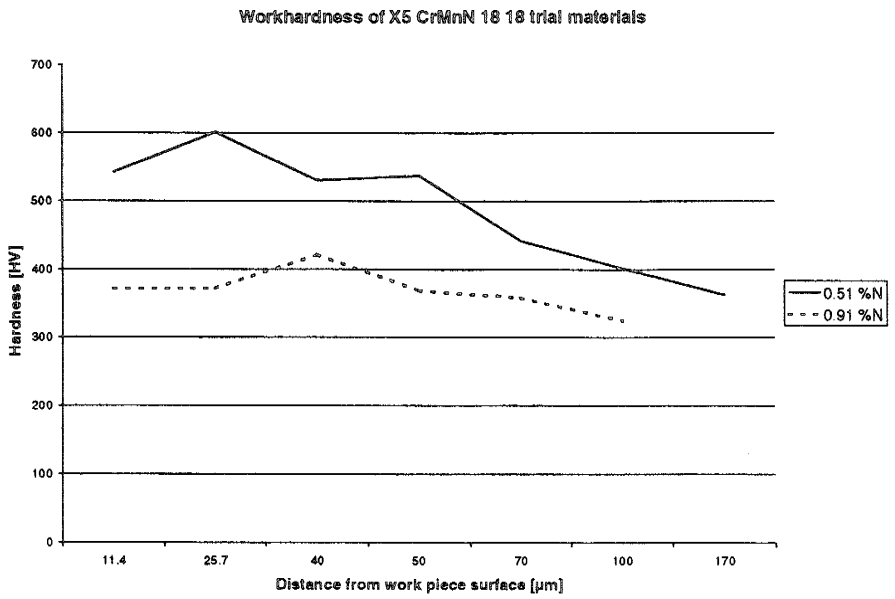

Fig. 10. Microhardness (20*g*) values of X5 CrMnN 18 18 trial material surfaces.

of X5 CrMnN 18 18 trial material with 0.57 wt.% N. Small amounts of trial material were also found from cracked edge areas. Workpiece surfaces were measured by microhardness testing device with video camera system. Results from the measurements are presented in Fig. 10.

The maximum microhardness value measured from X5 CrMnN 18 18 trial material with 0.57 wt.% N was approximately 600 HV. The microhardness curves show descending trend if measured in the direction of the surface normal. The other trial material with 0.91 wt.% N shows hardness values just below 400 HV. Comparing these two materials in Fig. 10 a work hardened surface of 0.1 mm thickness can be found from the trial material with 0.57 wt.% N.

4. Conclusions

From the results obtained in the present work the following conclusions may be drawn:

1. In the turning tests of X5 CrMnN 18 18 trial materials wear mechanisms were catastrophic failure of tool nose due to high cutting forces and sharp edge chipping.
2. The presence of BUE was decreasing the machinability of X5 CrMnN 18 18 trial materials.
3. There was a difference in machinability between X5 CrMnN 18 18 trial materials. Tool life T when machining the trial material with 0.91 wt.% N was 30 min and decreased to 10 min when the trial material with 0.57 wt.% N was applied with depth of cut, $a = 1.6$ mm and $v_f = 0.24$ mm/r.
4. Increasing the cutting speed from $v_c = 60$ to 70 m/min, the tool life of X5 CrMnN 18 18 trial material with 0.57 wt.% N decreased rapidly from 10 to 5 min.
5. There is a difference in cutting force between X5 CrMnN 18 18 trial materials. In turning X5 CrMnN 18 18 trial material with 0.91 wt.% N tangential force $F_y = 2.4–3.5$ kN and when turning X5 CrMnN 18 18 trial material with 0.57 wt.% N tangential force $F_y = 1.8–2.2$ kN was achieved, respectively.

Acknowledgements

The authors are thankful to Dr. I. Hucklenbroich from VSG Energie- und Schmiedetechnik GmbH for providing the X5CrMnN 18 18 trial materials.

References

[1] P.J. Uggowitzer, M.O. Speidel, Ultrahigh-strength austenitic steels, in: Proceedings of the Second International Conference on High Nitrogen Steels, HNS90, Aachen, October 10–12, 1990, pp. 156–158.
[2] E. Werner, P.J. Uggowitzer, M.O. Speidel, Mechanical properties and ageing behaviour of nitrogen alloyed austenitic steels, in: Proceedings of the Fifth International Conference on Mechanical Behaviour of Materials, Bejing, June 3–6, 1987, pp. 419–427.
[3] M.A. Harzenmoser, P.J. Uggowitzer, Neue aufgestickte austenitische rostfreie Stähle und Duplexstähle, in: P.J. Uggowitzer (Ed.), Ergebnisse der Werkstoff-Forschung, Band 1, Moderne Stähle, Verlag Thubal Kain, Zürich, 1987, pp. 219–247.

PUBLICATION IV

Tool wear and machinability of HIPed P/M and conventional cast duplex stainless steels

In: Wear 2001. Vol. 249, pp. 279–284.

ELSEVIER

Wear 249 (2001) 279–284

WEAR

www.elsevier.com/locate/wear

Tool wear and machinability of HIPed P/M and conventional cast duplex stainless steels

Jukka Paro [a,*], Hannu Hänninen [b], Veijo Kauppinen [a]

[a] *Laboratory of Workshop Technology, Helsinki University of Technology, Espoo, Finland*
[b] *Laboratory of Engineering Materials, Helsinki University of Technology, Espoo, Finland*

Abstract

In this study, active wear and failure mechanisms of TiN-coated cemented carbide tools with internal coolant supply when drilling of HIPed P/M Duplok 27 and conventionally-produced duplex stainless steel ASTM A8190 1A have been investigated. Stainless steels are often considered as poorly machinable materials. In P/M-produced duplex stainless steels, there are more hard oxide particles causing machining difficulties from the wear point of view. High strength and work hardening rate cause also difficulties from the machining point of view. In this study, drilling tests carried out by using a machining centre and optical microscope are presented. Chips were analysed by SEM electron microscopy and EDS-analysis. The machinability of duplex stainless steels is examined based on tool life and cutting speed presented by v–T-diagrams. The effect of cutting speed and the differences between powder metallurgically and conventionally-produced duplex stainless steels are also analysed by chip formation and tool wear mechanisms. Based on the cutting tests, cutting speeds of 20–100 m/min, feed rate of 0.15–0.25 mm and solid carbide drills, diameter of 8.6 mm, can be applied from machinability point of view. P/M duplex stainless steels with hard oxides decrease machinability. Tool wear criterion, VB-value of 0.3 mm, is reached after drilling time of 10 min, when 50 m/min cutting speed and 0.2 mm/r feed rate are utilised.

Keywords: Drilling; Machinability; Stainless steels; Tool wear

1. Introduction

Austenitic stainless steels are considered to be difficult to machine. Built-up edge (BUE) and irregular wear are often faced in machining operations. Difficulties from the machining point of view increase when duplex and high-strength stainless steels are to be machined. Machinability is often compared to the pitting corrosion resistance equivalent (PRE)-value representing the alloying content of the stainless steel.

Modern duplex stainless steel grades tend to be difficult to machine, by virtue of their higher austenite and nitrogen contents and with increasing alloy content, the machinability decreases rapidly [1].

Stainless steels are normally recognized as difficult materials to machine because of their high toughness, low thermal conductivity and high degree of work hardening. Stainless steels can be regarded as poorly machinable materials, because of their

- high tensile strength leading to high cutting forces and severe tool wear;
- high work hardening rates, especially for austenitic grades, and low thermal conductivity leading to high cutting temperatures and hence accelerated tool wear;
- high fracture toughness resulting in high temperatures, poor chip breakability and poor surface finish;
- abrasive carbide particles present in the high alloyed stainless steels causing tool wear;
- tendency to the BUE formation, which contrary to that in conventional steels, is present even at high cutting speeds due to the high fracture toughness and work hardening coefficient of these steels; the presence of the BUE impairs markedly the surface finish.

Due to the presence of porosity and structure of sintered powder metallurgy (P/M) steels, the machinability of such materials often bears a little resemblance to materials of similar composition of cast or wrought origin. It is generally accepted that the porosity causes a constantly interrupted cutting, which causes tool chatter and accelerates tool wear [2]. The porosity causes also a decrease in the thermal conductivity [2,3], which leads to an increase in the cutting temperature with a corresponding decrease in tool life. In hot isostatic pressed (HIP) P/M steels no porosity is expected to be present, but due to an increased oxygen content, large

* Corresponding author. Tel.: +358-9-456-5414; fax: +358-9-463-118.
E-mail address: jukka.paro@vtt.fi (J. Paro).

0043-1648/01/$ – see front matter
PII: S0043-1648(01)00570-1

Table 1
Chemical compositions of the studied stainless steels (wt.%)

Code	C	Si	Mn	P	S	Cu	Cr	Ni	Mo	V	Al	N	O
Duplok 27	0.03	0.2	0.7	0.02	0.001	2.3	26.5	7.0	3.0	–	–	0.3	–
A890 1A	0.03	0.74	0.63	0.026	0.006	3.01	25.0	5.54	2.03	–	–	–	–

amounts of hard oxide inclusions are present causing increased wear of tools.

New generation solid carbide drills with internal coolant supply providing efficiency in drilling operations are often utilised when hard to cut new high-strength stainless steels are to be machined. There is a need to understand materials aspects affecting tool wear and tool life of cemented carbide drills, when the high alloy austenitic and duplex stainless steels are machined. The differences in machinability between HIPed P/M stainless steel with hard oxide particles and cast stainless steel are studied to find tool wear behaviour.

2. Experimental details

2.1. Test materials

The workpiece materials were HIPed P/M super duplex Duplok 27 and conventionally-produced A8910 1A stainless steels. The chemical compositions are given in Table 1. The microstructures of the steels are shown in Figs. 1 and 2, respectively.

The microstructure of Duplok 27 stainless steel consists of lighter austenite phase and darker ferrite phase. The microstructure of A890 1A stainless steel consists of oriented dendritic austenite and ferrite phases.

2.2. Tool life testing and analyses

Drilling tests were carried out with a machining centre. Solid carbide drills were clamped on a high accuracy collet holder. Cutting speeds of 20–100 m/min, feed rate of 0.15–0.25 mm and solid carbide drills, diameter of 8.6 mm were used. Tool wear criterion applied was VB-value of 0.3 mm. The measurements were carried out by an optical microscope without releasing the drill from the tool holder. Drills and chips were analysed by SEM electron microscopy.

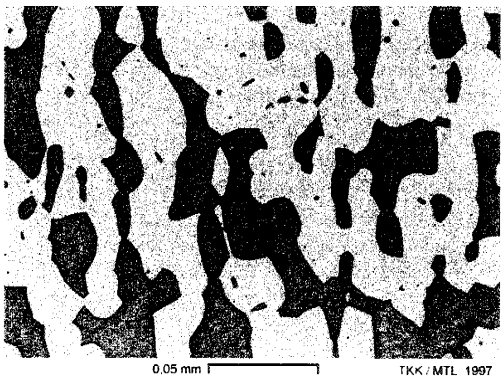

Fig. 1. The microstructure of HIPed P/M Duplok 27 stainless steel.

Fig. 2. The microstructure of cast A890 1A stainless steel.

3. Results

3.1. Tool life testing

Tool life v–T-curves of Duplok 27 and A890 1A steels are presented in Fig. 3. In the drilling of Duplok 27 steel with the cutting speed of 40 m/min, the drilling length was 4.4 m. Increasing the cutting speed to 60 m/min, the drilling length decreased to 1.9 m. Tool life shortened from 10 to 5 min. In the drilling of A890 1A steel with the cutting speed of 40 m/min, the drilling length was 6.4 m. Increasing the cutting speed to 60 m/min, the drilling length decreased to 2.5 m. Tool life shortened from 20 to 6 min. Comparing conventionally-produced stainless steel A890 1A to HIPed P/M Duplok 27 stainless steel, tool life and drilled hole length increased 50%.

3.2. Tool wear mechanisms

Tool wear proceeded continuously, firstly flute tip was rounded and after a few holes, the cutting edge was affected

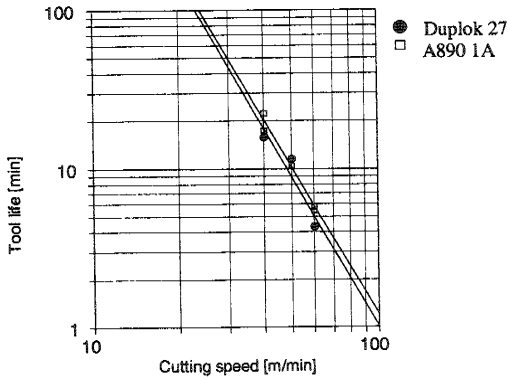

Fig. 3. Drilling of Duplok 27 and A890 1A stainless steels by Titex Alpha4 + DX45 Ø 8.5 mm P40; feed rate 0.2 mm/r.

by the formation of BUE. Due to presence of built-up edge in rake and flank face, there is possibility to adhesion wear of both surfaces near cutting edge. Because of internal cutting, fluid supply lowering the cutting temperature, the amount of oxidation and diffusion wear is supposed to be limited.

There was a higher tendency to built-up edge formation in A8910 1A stainless steel than in HIPed P/M super duplex Duplok 27 stainless steel. The formation of built-up edge in the drilling of A890 1A stainless steel with cutting speed of 40 m/min and feed rate of 0.2 mm/r with solid carbide drill Titex Alpha4 + DX45 is shown in Fig. 4.

The increase of cutting speed increased the BUE formation on the rake face. Compared to Duplok 27, no breaking of chisel edge corner existed in drilling of A890 1A steel. The formation of built-up edge into rake face has also altered tool geometry causing chipping of cutting edge, shown in Fig. 5.

To analyse tool wear from cemented carbide drills, SEM was used. BSE-images of rake surfaces of drills from drilling tests of HIPed P/M Duplok 27 stainless steel and cast A890 1A steel are presented in Figs. 5 and 6.

3.3. Chip morphology

To analyse chip morphology, SEM was used for both Duplok 27 and A890 1A steels with cutting speeds of 40, 50 and 60 m/min. The chips from HIPed P/M Duplok 27 steel are presented in Figs. 7 and 8 and the chips from cast A890 1A in Figs. 9 and 10. Convex and concave surfaces of the chips are presented. Tool wear increased, when cutting speed was increased from 40 to 60 m/min. There was a higher tendency to built-up edge formation in A8910 1A stainless steel than in super duplex HIPed P/M Duplok 27 stainless steel. The microstructure of A890 1A stainless steel is typical cast structure, shown in Fig. 2.

Fig. 7 presents the effect of cutting speed into the surface texture of Duplok 27 chips. There are grooves formed in the interaction between chip and rake face. The concave side of chips presented in Fig. 8 shows the change of chip lamella thickness when the cutting speed is increased.

Higher tendency to BUE formation of cast A890 1A steel chips in Figs. 9 and 10 can be compared to smoother Duplok 27 steel chips in Figs. 7 and 8. The decrease of machinability comparing A890 1A to Duplok 27 steel can be observed from the strongly serrated chip when comparing chips presented from the convex chip surfaces in Figs. 7 and 9.

In Fig. 9, is presented the bottom of A890 1A chip. Compared to Duplok 27 chips, there are burrs and grooves. The chip formation is affected by the instabilites of cast structure. Compared to Duplok 27 steel chips, the increased presence of built-up edge in the drilling of A890 1A stainless steel is shown by convex surface of chips in Fig. 9.

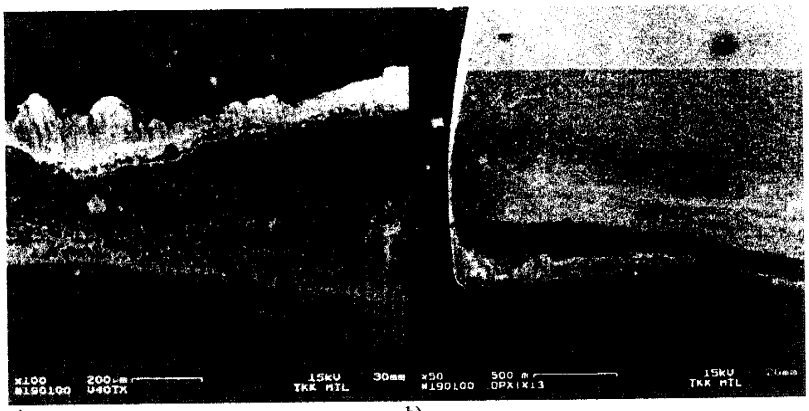

Fig. 4. The formation of built-up edge in drilling of cast A890 1A stainless steel with cutting speed of 40 m/min and feed rate of 0.2 mm/r. Solid carbide drill Titex Alpha4 + DX45 was used.

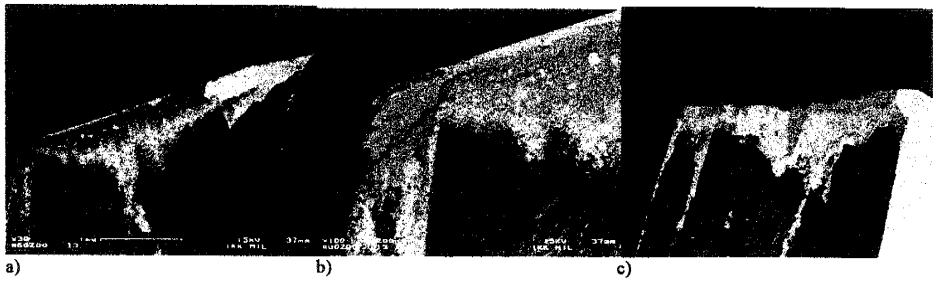

Fig. 5. SEM (BSE)-images of drills from drilling tests of HIPed P/M Duplok 27 stainless steel. Cutting speeds of $v_c = 40$ (a), 50 (b) and 60 m/min (c) and feed rate $v_f = 0.20$ mm/r were used.

Fig. 6. SEM (BSE)-images of drills from drilling tests of cast A890 1A steel. Cutting speeds of $v_c = 40$ (a), 50 (b) and 60 m/min (c) and feed rate $v_f = 0.20$ mm/r were used.

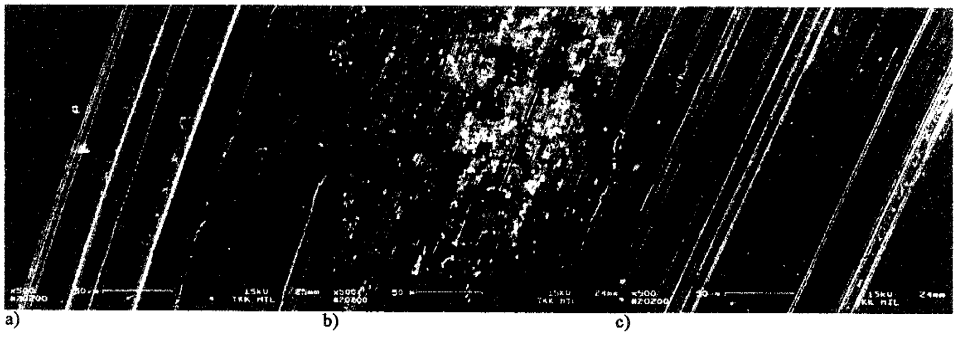

Fig. 7. SEM-images of HIPed P/M Duplok 27 steel chips from the convex side. Cutting speeds of $v_c = 40$ (a), 50 (b) and 60 m/min (c) and feed rate $v_f = 0.20$ mm/r were used.

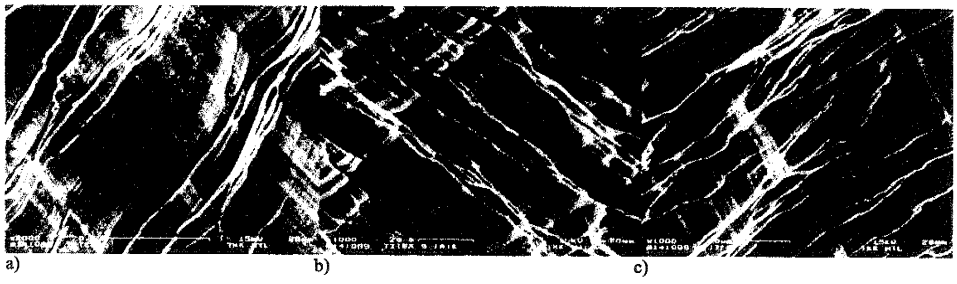

Fig. 8. SEM-images of HIPed P/M Duplok 27 steel chips from the concave side. Cutting speeds of $v_c = 40$ (a), 50 (b) and 60 m/min (c) and feed rate $v_f = 0.20$ mm/r were used.

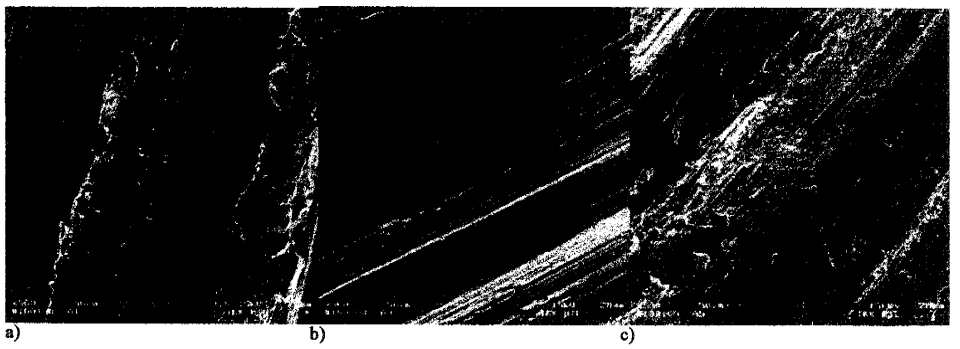

Fig. 9. SEM-images of chips from the convex side of chips of cast A890 1A steel. Cutting speeds of $v_c = 40$ (a), 50 (b) and 60 m/min (c) and feed rate $v_f = 0.20$ mm/r were used.

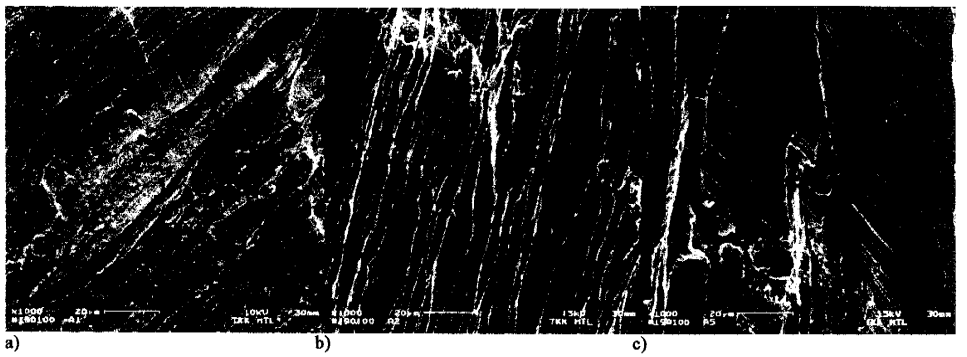

Fig. 10. SEM-images from the concave side of chips of cast A890 1A steel. Cutting speeds of $v_c = 40$ (a), 50 (b) and 60 m/min (c) and feed rate $v_f = 0.20$ mm/r were used.

4. Discussion

Machinability of stainless steels is often compared to the pitting resistance equivalent, PRE-value representing the alloying content of the steel. The pitting resistance equivalent (PRE) index, PRE = wt.% Cr + 3.3 × wt.% Mo + 13 × wt.% N, together with the tool life of Titex Alpha4 + DX45 for the drilling of test materials with cutting speed of v_c = 40 m/min and feed rate f = 0.2 mm/r are presented in Table 2. The PRE of HIPed P/M Duplok 27 stainless steel is 25% higher than the PRE-value of cast A890 1A stainless steel. Tool life decreases 40% when HIPed P/M Duplok 27 stainless steel is machined compared to cast A890 1A stainless steel.

Table 2
Pitting resistance equivalent (PRE) index, PRE = wt.% Cr + 3.3 × wt.% Mo + 13 × wt.% N, together with the tool life of Titex Alpha4+DX45 in drilling of test materials with cutting speed of v_c = 40 m/min and feed rate f = 0.2 mm/r

Test material	PRE index	Tool life (min)
Duplok 27	39.4	4.4
A890 1A	31.7	6.4

Tool wear proceeded continuously in drilling of both materials by solid carbide drills with internal coolant supply. Compared to that at fast cutting speeds, plastic deformation of the tool takes place, in combination with flaking of the insert coating and frittering [1], the tool wear is affected by formation BUE and flaking of coating.

Stainless steels undergo marked work hardening during machining. Work hardening of stainless steels during machining can be observed from the microhardness values of the chip bottom, because the chip bottom can be considered to be the most highly deformed zone of the chips. From the drilling tests with v_c = 50 m/min, A890 1A steel chips show microhardness values; austenite 452 HV (20 g) and ferrite 372 HV (20 g) and if measured from chip bottom; austenite 505 HV (20 g) and ferrite 445 HV (20 g). Duplok 27

chips are more strongly deformed than A890 1A chips; the chip bottom of austenite in Duplok 27 605 HV (20 g) (original microhardness 370 HV (20 g)) versus austenite phase of A890 1A steel 505 HV (20 g).

5. Conclusions

From the results obtained in the present work, the following conclusions can be drawn:

1. The machinability of Duplok 27 and A890 1A stainless steels is affected by the formation of BUE. There is a higher tendency to formation of BUE in A890 1A than in Duplok 27 steel.
2. The tool life when using solid carbide drills with internal coolant supply is between 5 and 12 min in machining of Duplok 27 stainless steel.
3. The tool life when using solid carbide drills with internal coolant supply is between 7 and 20 min in machining of A890 1A stainless steel.
4. The formation of BUE causing adhesion wear is supposed to be the dominant failure mechanism of solid carbide drills when drilling Duplok 27 and A890 1A stainless steels.

Acknowledgements

The authors are thankful to Ahlstrom Pumps and Rauma Materials Technology for providing the test materials.

References

[1] R. Gunn, Duplex Stainless Steels, Abington Publishing, Cambridge, England, 1997, p. 204.
[2] L. Jiang, H. Hänninen, J. Paro, V. Kauppinen, Active wear and failure mechanisms of TiN coated high speed steel and TiN-coated cemented carbide tools when machining powder metallurgically made stainless steels, Metall. Mater. Trans. 27A (9) (1996) 2796–2808.
[3] H. Chandrasekaran, J. Johansson, Chip flow and notch wear mechanisms during the machining of high austenitic stainless steels, Annals CIRP 43 (1) (1994) 101–105.

PUBLICATION V

Drilling of conventional cast stainless steel with HIPed NiTi coating

In: Journal of Materials Processing Technology 2004.
Vol. 153–154, pp. 622–629.

ELSEVIER

Journal of Materials Processing Technology 153–154 (2004) 622–629

Journal of Materials Processing Technology

www.elsevier.com/locate/jmatprotec

Drilling of conventional cast stainless steel with HIPed NiTi coating

J.A. Paro*, T.E. Gustafsson, J. Koskinen

VTT Industrial Systems, VTT Manufacturing Technology, Materials and Manufacturing Technology, P.O. Box 1703, Espoo VTT 02044, Finland

Abstract

This study investigated suitability of TiN- and TiCN-coated cemented carbide tools in the machining of conventionally produced stainless steel with hot isostatic pressed (HIPed) NiTi coating. Near-equiatomic nickel–titanium alloy (NiTi) has many attractive material properties, such as pseudo-elasticity and shape memory effects, which result into beneficial engineering properties, e.g. as cavitation resistant coatings in addition to its well-known shape memory properties. Stainless steels are often considered to be poorly machinable materials; materials with high elasticity are also difficult to machine. In drilling stainless steel with a pseudo-elastic-coating material, machinability difficulties are caused by the high strength and work hardening rate of steel and the pseudo-elastic properties of the coating material. In this study, drilling tests were carried out by a machining center. The machinability was studied by analyzing cemented carbide drills and chips. The interface between stainless steel and NiTi coating was examined with scanning electron microscopy (SEM) and energy dispersive spectroscopy (EDS) analysis. The effect of feed rate on chip formation and tool wear was analyzed. The cutting tests indicated that cutting speeds of 50 m/min, a feed rate of 0.1–0.2 mm/rev, and solid carbide drills can be applied, from a machinability standpoint. A HIPed pseudo-elastic coating decreases machinability. When effective cutting speeds and feed rates were utilized, optimal tool life was achieved without a decrease in coating properties.

Keywords: Drilling; Stainless steel; NiTi coating

1. Introduction

Austenitic stainless steels are considered to be difficult to machine. Built-up edge (BUE) and irregular wear situations are often faced in machining operations. Difficulties from the machining point of view increase when duplex and high-strength stainless steels are to be machined [1].

One important characteristic of shape memory alloys (SMAs) is their super-elastic property. The NiTi polycrystalline SMA has, due to its unique bio-compatibility and super-elasticity, been successfully used to manufacture medical devices in recent years. One of the most dramatic-appearing examples is the utility of super-elastic coatings. Near-equiatomic nickel–titanium alloys (NiTi) have many attractive properties for engineering applications, such as pseudo-elasticity and good cavitation resistivity, in addition to their more well-known shape memory properties [2,3]. Nevertheless, both technical and commercial limitations arise when NiTi is considered as a material for large engineering components. Consequently, interest in NiTi-coating technologies is on the rise.

One of the principal challenges in NiTi coating is how to achieve adequate adhesion between NiTi and the substrate material. Explosive welding has been used successfully as a NiTi-coating method [4,5]. However, due to the nature of explosive welding, the surface to be coated must not have a very complex geometry. Thermal spraying has also been investigated, but, unfortunately, thermally sprayed NiTi on steel substrates has been reported to have poor adhesion. It has been suggested that the poor adhesion is due to a thermal expansion mismatch between the coating and the substrate [5]. Fusion-welded coatings suffer from poor adhesion because of the formation of brittle inter-metallic reaction layers [6].

It is known that hot isostatic pressing (HIP) can be used to produce bulk NiTi components from powders [7–9]. In the present study, machining of NiTi-coated stainless steels has been investigated as a potential NiTi-coating method for stainless steels.

* Corresponding author. Tel.: +358-9-456-5414; fax: +358-9-463-118.
E-mail address: jukka.paro@vtt.fi (J.A. Paro).

0924-0136/$ – see front matter © 2004 Elsevier B.V. All rights reserved.
doi:10.1016/j.jmatprotec.2004.04.100

Table 1
The nominal composition (%) of the steel used in the drilling experiment

C	0.03
Mn	1.20
S	0.015
P	0.04
Cr	18.4
Ni	9.2
Si	0.4
V	0.06

2. Materials

The samples used in the drilling tests were firstly machined from the stainless steel blocks (X2CrNi 1911). The nominal composition of the test steel is presented in Table 1. The capsule (Fig. 1a) for HIP operation was welded from stainless steel plate (AISI 316) onto this block. The capsule was filled with rotating disc atomized NiTi powder (FUKUDA®) with an average particle size of 0.23 mm and composition 49.4 ± 4.7 at.% Ni and 50.6 ± 4.7 at.% Ti. The target bulk material composition (Ni/Ti) is 50/50 at.%, which is 55/45 wt.% (see Fig. 1b). After the HIPing of the NiTi powder onto the block, the capsule was removed with a solid carbide milling tool for later drilling tests.

3. Methods

The HIP treatment was used to sinter coatings from NiTi powder on the base material block. These samples were mounted in a stainless steel capsule that was evacuated to a pressure of 10^{-5} mbar. The HIPing parameters were 900 °C, 100 MPa, and 3 h. The cooling rate was 4.6 K/min.

Drilling tests were carried out using a horizontal machining center. The tests used TiCN- and TiN-coated cemented carbide drills with a diameter of ∅ 8.5 mm, at a cutting speed of 50 m/min and feed rates of 0.1, 0.15, and 0.2 mm/rev. Drilling tests were done both with and without through-spindle cooling. Pseudo-elasticity of the HIPed NiTi coating was tested with Vickers hardness measurements, using a load of 9.81 N.

From the drilled test piece, cross-sectional samples were cut out along the drill axis. These samples were polished and etched with picric acid and with NaOH–water solution with electrolytic etching.

The NiTi powder and HIPed coating cross-sections, and cross-sections of the drilling test samples, were studied in detail with an optical microscope (OM) and scanning electron microscope (SEM). The NiTi powder was collected on an electrically conductive graphite adhesive, and the powder sample on the adhesive was studied with the SEM and analyzed with an X-ray analyzer (EDS), which can detect sodium (Na) and elements heavier than that. The compositions of the particles ($N = 15$) and that of the details in the drilling test cross-sections were determined from the X-ray spectra using a correction factor program (ZAF). The X-ray lines used in the analysis were iron (Fe), chromium (Cr), manganese (Mn), nickel (Ni), titanium (Ti), and silicon (Si). To calibrate the magnification of the microscope and to perform the X-ray analysis, ASTM practices E766-98, E1508-98, when applicable were used, respectively. In SEM images obtained with a 25 kV acceleration voltage at a working distance of 20 mm, the error in the magnification is ±2%. The smallest detectable content in the X-ray analysis is approximately 0.3–0.5% for metals, depending on the composition of the material analyzed.

4. Results

The HIPed NiTi coating is shown in Fig. 2. The NiTi powder has sintered into solid material, in which only some inter-granular pores could be detected. The hardness was tested with a Vickers-hardness measuring device, from both

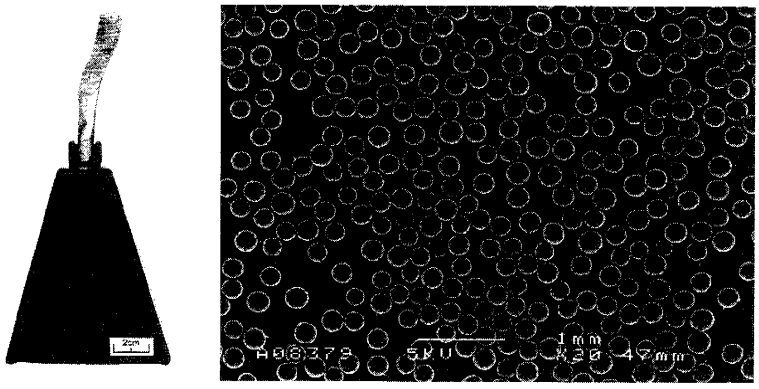

(a) (b)

Fig. 1. (a) The HIPing capsule and (b) NiTi powder used in the experiment.

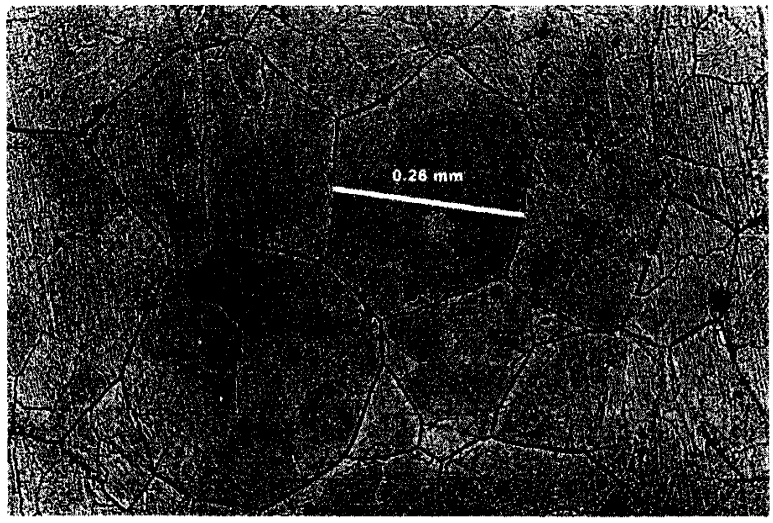

Fig. 2. NiTi coating after HIPing—magnification 200×.

the steel and the NiTi coating. The hardness print of the steel shows a typical Vickers imprint (Fig. 3a) on the steel surface, whereas the imprint on the NiTi coating shows retraction of the material on the imprint edges (Fig. 3b). The retraction is due to the pseudo-elastic nature of the NiTi coating.

The interface between the coating and the steel was studied after making longitudinal polished and etched cross-sections from the drilled hole edge and drilling chips. The interface between the coating and base material is shown in Fig. 4a and b.

The interface between the HIPed NiTi coating and the steel showed two distinct features. First, there was a layer of iron that diffused into the NiTi coating; this had a thickness of approximately 20 μm. The second feature is the layer on the steel side, which was enriched in chromium to a level of 28.4% Cr due to the diffusion of iron into the NiTi coating (Table 2, Fig. 4b). Also, titanium diffusion into the steel surface layer, a few micrometers in thickness, was observed. A more detailed study of the interface layer on the steel side showed internal structure in the layer, which seems to form more easily in the ferrite phase than in the austenite phase of the steel (Fig. 5a and b).

The results presented in Table 2, from the points in Fig. 4b, show diffusion of iron and chromium into NiTi. The diffusion of iron is stronger than that of the chromium, leading to the observed chromium enrichment at the steel-edge layer (Figs. 4b and 6, points 21–25).

The cutting edges with TiN and TiCN-coated drills that were examined by SEM analysis are shown in Fig. 7a and b. Fig. 7a shows the unused cutting edge of a solid carbide drill, and Fig. 7b shows the edge after drilling without internal through-spindle cooling and with a machining speed of 50 m/min and feed rate of 0.1 mm/rev. The same cutting edge was analyzed with SEM and EDS (Fig. 8b).

A nickel- and titanium-rich layer was found at the cutting edge between the edge and the steel chip adhering to it (Fig. 8a and b).

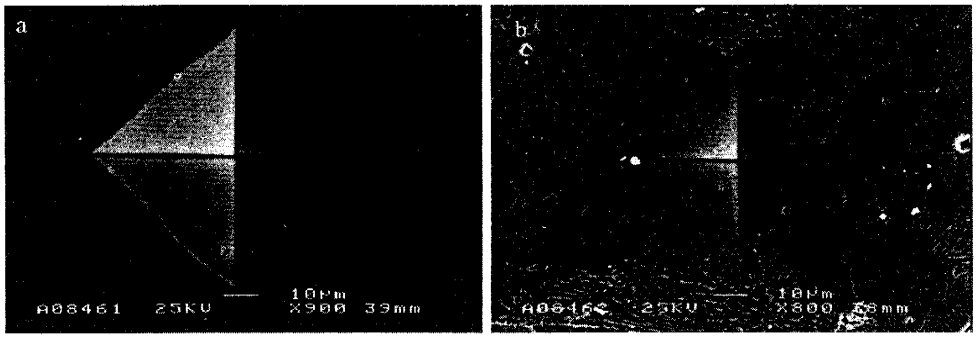

Fig. 3. SEM images of (a) the Vickers hardness indentation (HV1) in the steel and (b) Vickers hardness indentation (HV1) in the NiTi coating.

Table 2
The EDS element analysis at points presented in Fig. 4b

Analysis	Fe (%)	Cr (%)	Ni (%)	Mn (%)	Si (%)	Ti (%)
Points 1–5	1.8 ± 0.1	n.d.	49.8 ± 2.5	n.d.	n.d.	48.1 ± 2.4
Points 6–10	5.1 ± 0.1	0.4 ± 0.1	46.0 ± 0.5	n.d.	n.d.	48.4 ± 0.5
Points 11–15	8.5 ± 0.2	0.7 ± 0.1	42.4 ± 0.3	n.d.	n.d.	48.3 ± 0.4
Points 16–20	40.6 ± 2.4	7.5 ± 0.4	12.2 ± 1.0	0.4 ± 0.1	~0.3	38.9 ± 2.7
Points 21–25	51.7 ± 3.2	28.4 ± 1.9	5.1 ± 0.4	0.8 ± 0.1	~0.2	13.8 ± 5.4
Points 26–30	67.5 ± 0.2	19.3 ± 0.5	11.6 ± 0.5	~1.0	~0.3	~0.3

A change in chip morphology was detected between the NiTi coating and steel chips. First, when the NiTi coating is drilled, the chip is deformed strongly. The chips are conical and strongly spiral in form. Second, when the drill has reached the interface between the NiTi coating and stainless steel, the shape becomes that of conventional stainless steel chips. The chips encountered during the drilling operation were also red-hot. These chips, produced at a cutting speed of 50 m/min and feed rate of 0.1 mm/rev, are shown in Fig. 9a.

In Fig. 9b is presented a stainless steel and NiTi chip boundary. A detailed image of the interface (Fig. 10a) shows good adhesion between the materials, even when the NiTi's pseudo-elasticity has been exceeded during the drilling (Fig. 10b).

Fig. 11a and b shows the influence of feed rate on the NiTi coating's structure after drilling. In Fig. 11b, a cutting speed of 50 m/min and feed rate of 0.1 mm/rev were used, whereas for Fig. 10a the feed rate was increased to 0.3 mm/rev. Cutting fluid through spindle during these drilling operations was not applied. Fig. 11b also shows the points for EDS analyses, with results listed in Table 3. No apparent diffusion of steel or NiTi elements over the adhered interface was found. The NiTi grains nearest to the drill hole showed a size increase on account of heat. This was not found in the bulk material.

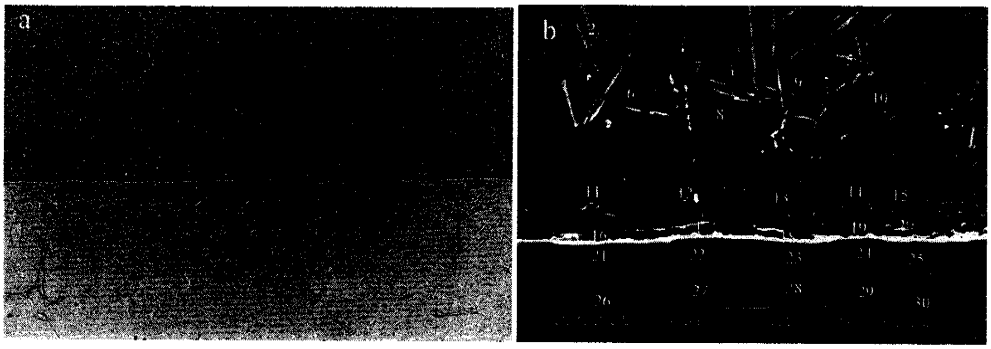

Fig. 4. (a) Optical micrograph of the NiTi coating and stainless steel interface and (b) an SEM image of the interface with points used for quantitative EDS element analysis. Etched with picric acid.

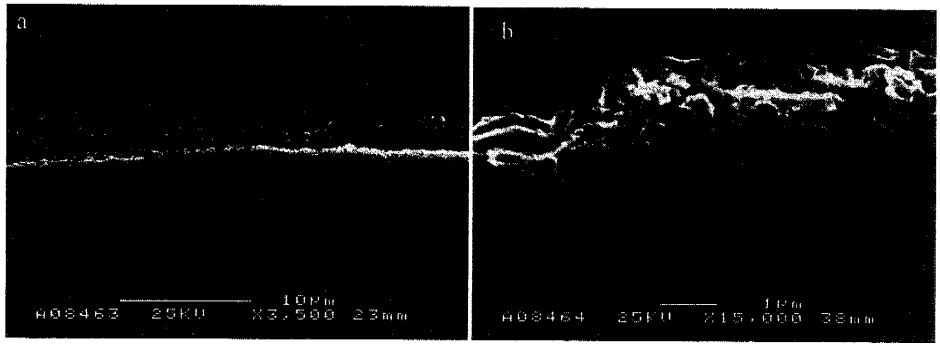

Fig. 5. (a) The NiTi coating and steel interface after electrolytic etching in NaOH–water solution and (b) a detail from the interface on the steel side in the layer with analysis points 21–25 in Fig. 4b.

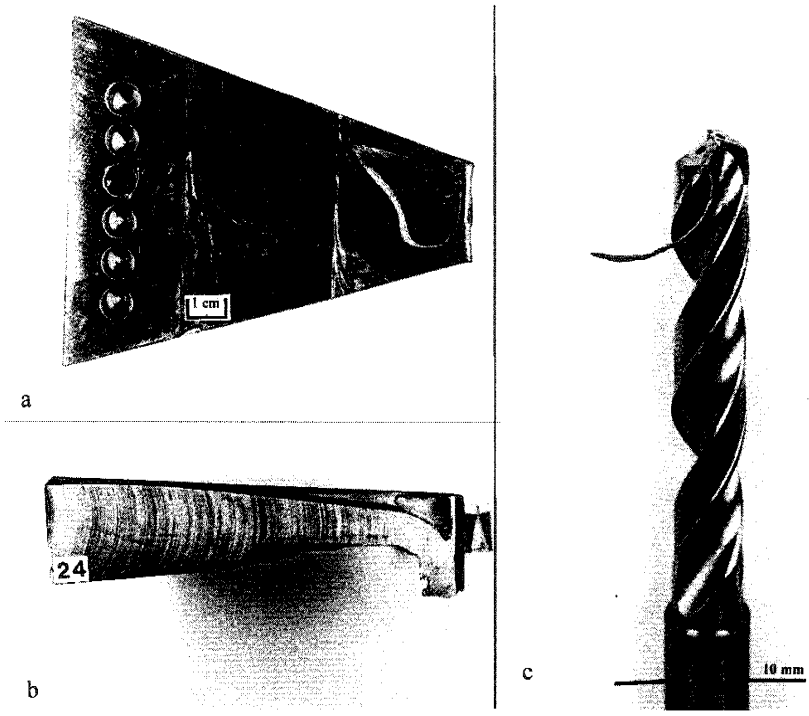

Fig. 6. (a, b) The workpiece of stainless steel with NiTi coating used in drilling tests and (c) a TiN-coated ∅ 8.5 mm solid carbide drill used in drilling tests showing chip buildup on the cutting edge.

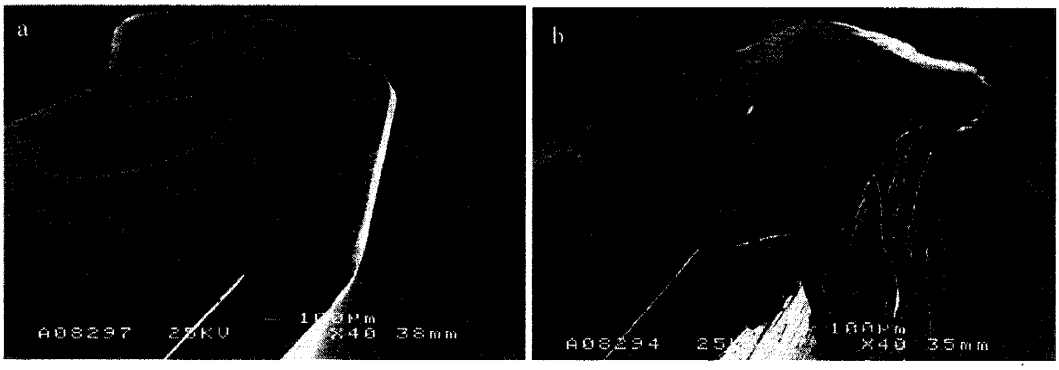

Fig. 7. (a) SEM image of an unused TiCN- and TiN-coated solid carbide drill's cutting edge and (b) the built-up edge (BUE).

With optimum machining parameters, some expiration of the grain boundaries of NiTi was detected (Fig. 12a and b). This sample was produced at a cutting speed of 50 m/min and feed rate of 0.1 mm/rev by applying coolant through the spindle. In comparing Figs. 11b and 12a, the effect of cooling can be seen in decreased steel buildup on the NiTi. Also, the surface topography was found to be much smoother than with inferior cooling properties or higher feed rates.

5. Discussion

The stainless steel workpiece with NiTi coating was produced by HIP treatment, and sufficient adhesion properties were achieved. After a machining operation was performed on the capsule, the interface between the stainless steel block and NiTi coating was intact. The drilling experiments showed that the tool wear mechanism for NiTi-coated stainless steel was similar to that with conventional stainless steel.

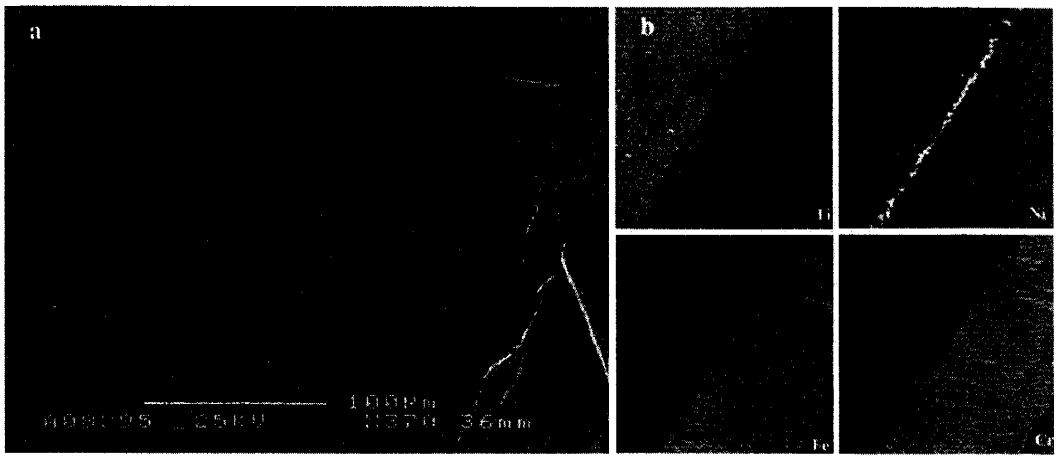

Fig. 8. (a) The cutting edge of a solid carbide drill with BUE and (b) EDS analyses showing the distribution of Ti, Ni, Fe, and Cr within the field of view.

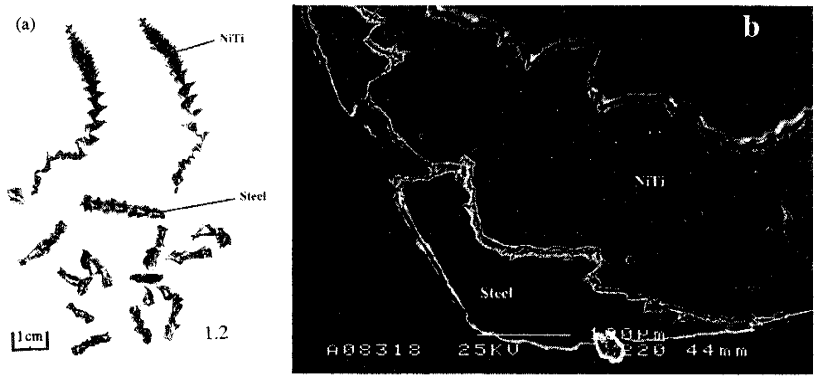

Fig. 9. (a) Chips from drilling of NiTi-coated stainless steel and (b) an SEM image of the deformation of the interface between the steel and NiTi coating.

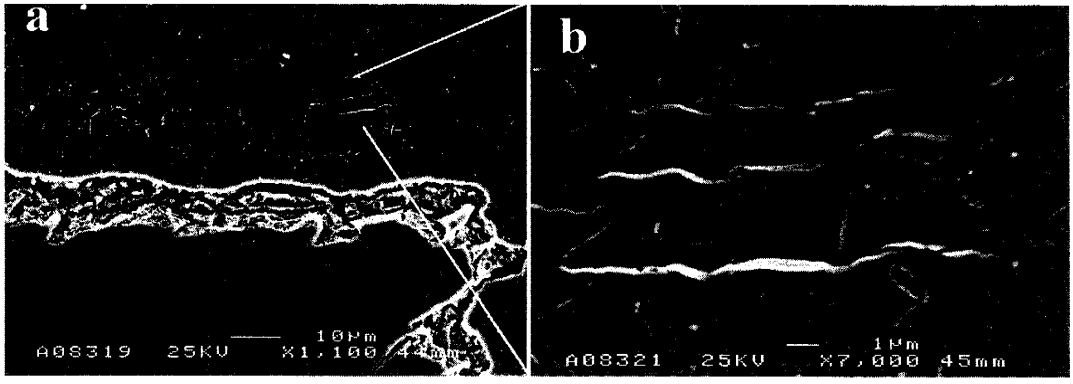

Fig. 10. (a) A detail from Fig. 9b, showing deformation of the stainless steel and NiTi interface in the chip and (b) a detail of the deformed NiTi coating detected in the chip when the load had exceeded the pseudo-elasticity of NiTi during drilling.

Table 3
Point analyses of drilled NiTi hole with stainless steel buildup layer (Fig. 11b)

Analysis	Fe (%)	Cr (%)	Ni (%)	Mn (%)	Si (%)	Cu (%)	Ti (%)
Points 1–5	68.2 ± 0.2	19.8 ± 0.5	10.6 ± 0.5	~0.9	~0.3		
Points 6–10	0.8 ± 0.3	0.2	55.1 ± 0.2			~0.2	43.7 ± 0.2
Points 11–15			55.1 ± 0.3				44.7 ± 0.3

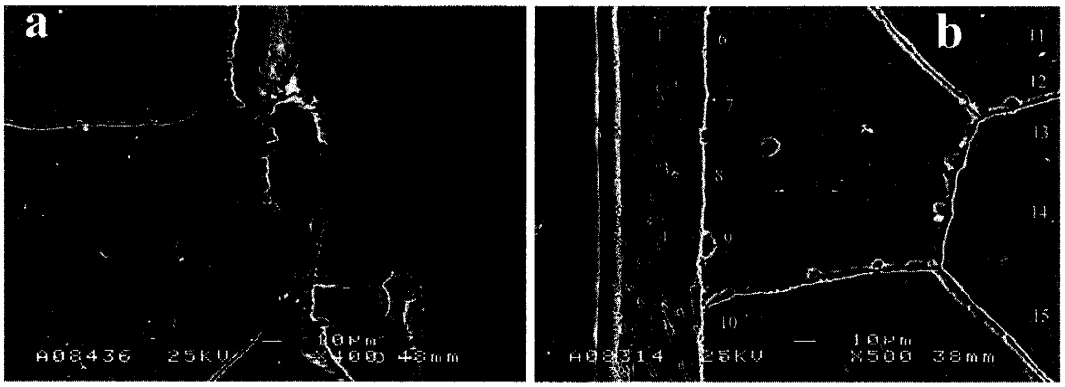

Fig. 11. SEM images of holes drilled in the NiTi coating: (a) cutting speed of 50 m/min and feed rate of 0.2 mm/rev, showing rough surface structure; (b) 0.1 mm/rev, showing steel buildup on the drilled hole wall.

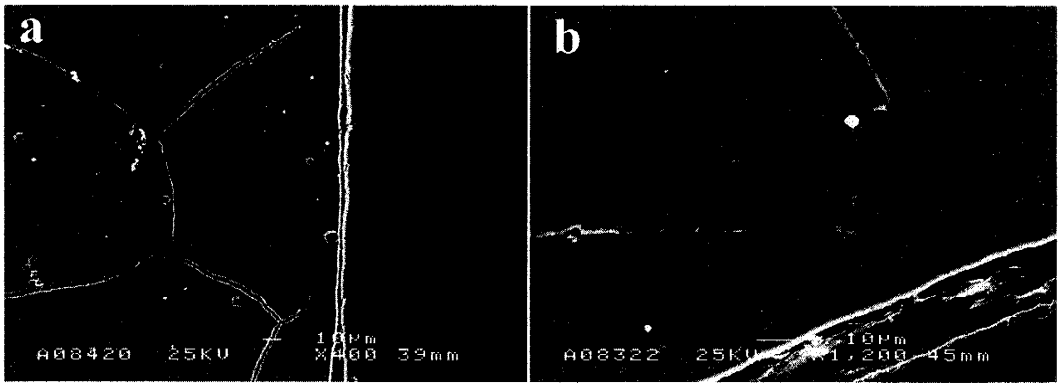

Fig. 12. SEM images of drilled NiTi coating with optimum cutting speed of 50 m/min and feed rate of 0.1 mm/rev, with cutting fluid applied through the spindle.

The interface between steel and the NiTi coating was studied via SEM and EDS analyses. For future investigation of the microstructure of the interface between stainless steel and NiTi coating, transmission electron microscopy (TEM) should be carried out to map out the microstructure in heat-affected diffusion layers originating from the HIPing process.

The first drilling showed strongly deformed chips which have been red-hot. Their deformation may be related to shape memory effects. The opening chips also showed good adhesion between NiTi and stainless steel, as these chips were found to be unbroken. The formation of the BUE detected in drills might have been enhanced by the tool coating (TiCN and TiN), which in turn also merits further investigation.

When sensitive feed rate values are used, the drilled hole wall remains smooth, with only a small amount of steel stuck to the NiTi. Increasing the feed rate causes the surface topography to be roughened. Using internal cooling through the spindle in solid carbide drills makes the hole surface topography even smoother.

The NiTi diffusion layers were found to be affected by the heat from HIPing, and the NiTi grain boundaries affected by the strong plastic deformation during drilling operations in the vicinity of the hole wall.

6. Conclusions

From the results obtained in the study, the following conclusions were drawn. The drilling of NiTi-coated stainless steel with sufficient cutting parameters is possible without severe tool wear. A cutting speed of 50 m/min and feed rate between 0.1 and 0.2 mm/rev with solid carbide drills and through-spindle cooling should be applied. Tool wear mechanisms in through-spindle cooling are similar to those encountered with stainless steel.

The macroscopic geometry of stainless steel chips with NiTi coating differs from conventional stainless steel chips. The opening chips are constructed from the NiTi concatenated with conventional long stainless steel chips, and the adhesion in the interface layer between NiTi coating and stainless steel remains intact in the chip formation process.

There are stainless steel residues on NiTi drilled hole walls. An increased supply of cutting fluid has an advantageous effect on the surface properties of the hole. The amount of stainless steel adhering to the NiTi walls is decreased when cutting fluid is injected through the spindle. An increase in feed rate will decrease the surface quality of the drilled hole.

Strongly deformed layer on the drilled surface of NiTi was observed been deformed in excess of the pseudo-elasticity.

There is a diffusion layer of iron in the NiTi coating, and there is also a layer extending inward on the steel side, which has been enriched in chromium due to the HIP process.

Acknowledgements

The authors are thankful to Sulzer Pumps, Finland, for providing the tested stainless steel materials.

References

[1] L. Jiang, H. Hänninen, J. Paro, V. Kauppinen, Active wear and failure mechanisms of tin-coated high speed steel and tin-coated cemented carbide tools when machining powder metallurgically made stainless steels, Metall. Mater. Trans. A 27 (9) (1996) 2796–2808.

[2] Z. Li, Q. Sun, Growth of macroscopic martensite band in nano-grained NiTi microtube under tension, Int. J. Plast. 18 (2002) 1481–1498.

[3] D. Starosvetsky, I. Gotman, TiN coating improves the corrosion behaviour of superelastic NiTi surgical alloy, Surf. Coat. Technol. 148 (2001) 268–276.

[4] C. Zimmerly, T. Inal, R. Richman, Explosive welding of a near-equiatomic nickel–titanium alloy to low-carbon steel, Mater. Sci. Eng. A 188 (1994) 251–254.

[5] R. Richman, A. Rao, D. Kung, Cavitation erosion of NiTi explosively welded to steel, Wear 181–183 (1995) 80–85.

[6] P. Jardine, Y. Field, H. Herman, D. Marantz, K. Kowalsky, Processing and properties of arc-sprayed shape memory effect NiTi, Scripta Met. Mater. 24 (1990) 2391–2396.

[7] G. Wang, Welding of nitinol to stainless steel, in: Proceedings of the SMST-97, 1997, pp. 131–136.

[8] J. Koskinen, E. Haimi, A. Mahiout, V. Lindroos, S.-P. Hannula, Superelastic NiTi coatings with good corrosive wear resistance, in: Proceedings of the International Conference on Martensitic Transformations (ICOMAT'02), Espoo, 2002, pp. 10–14.

[9] J. Koskinen, E. Haimi, Method for forming a nickel–titanium plating, US Patent 6,458,317 (2002).

PUBLICATION VI

Chip morphology in drilling of conventional cast stainless steel with HIPed NiTi coating

In: Proceedings of the 3rd International Conference on Research and Development in Mechanical Industry, RaDMI 2003. Predrag, Dasic (ed.). Herceg Novi, Serbia and Montenegro, 19–23 September 2003. Pp. 1–8. ISBN 86-83803-06-6 in hard copy and ISBN 86-83803-10-4 in electronic form on CD-ROM.

3rd International Conference
"Research and Development in Mechanical Industry"
RaDMI 2003
19 - 23. September 2003, Herceg Novi, Serbia and Montenegro

Plenary paper

CHIP MORPHOLOGY IN DRILLING OF CONVENTIONAL CAST STAINLESS STEEL WITH HIPED NiTi COATING

J. A. Paro, T. E. Gustafsson, J. Koskinen
VTT Industrial Systems, Espoo, FINLAND; Email: jukka.paro@vtt.fi

Summary: *This study investigated chip morphology in drilling of HIPed (Hot Isostatic Pressed) NiTi-coated conventionally cast stainless steels with TiN and TiCN-coated cemented carbide tools. Near-equiatomic nickel-titanium alloy (NiTi) has many attractive material properties, such as pseudo-elasticity and shape memory effects, which result in properties beneficial for use in cavitation-resistant coatings in addition to its well-known shape memory properties. Stainless steels are often considered to be poorly machinable materials; materials with high elasticity are also difficult to machine. In the drilling of stainless steel with a pseudo-elastic coating material, machinability difficulties are caused by the high strength and work hardening rate of steel and the pseudo-elastic properties of the coating material. In this study, drilling tests were carried out by a machining centre. The chip morphology was studied by analysing cemented carbide drills and chips. The interface between stainless steel and NiTi coating was examined using SEM (Scanning Electron Microscopy) and EDS (Energy Dispersive Spectroscopy) analysis. The effect of feed rate and cutting fluid supply on chip formation and tool wear was analysed. The cutting tests indicated that cutting speeds of 50 m/min, a feed rate of 0.1-0.2 mm/rev, and solid carbide drills can be applied, from a machinability standpoint. A HIPed pseudo-elastic coating decreases machinability. When effective cutting speeds and feed rates were used, optimal tool life was achieved without a deterioration in coating properties.*
Keywords: *drilling, stainless steel, NiTi coating*

1. INTRODUCTION

Austenitic stainless steels are considered to be difficult to machine. Built-up edge (BUE) and irregular wear situations are often faced in machining operations. Difficulties from the machining point of view increase when duplex and high-strength stainless steels are to be machined. [1] In the drilling operation, small, well-broken chips are desirable. During drilling and formation, the chips rotate with the drill and impact the hole wall or interior of the flute. Once the bending moment has caused the critical strain, fracturing will occur.
One important characteristic of Shape Memory Alloys (SMAs) is their super-elastic property. The NiTi polycrystalline SMA has, due to its unique bio-compatibility and super-elasticity, been successfully used to manufacture medical devices in recent years. One of the most dramatic examples is the utility of super-elastic coatings. Near-equiatomic nickel-titanium alloys (NiTi) have many properties that make them attractive for engineering applications, such as pseudo-elasticity and good cavitation resistivity, in addition to their more well-known shape memory properties [2, 3], while both technical and commercial limitations arise when NiTi is considered as a material for large engineering components. Consequently, interest in NiTi-coating technologies is on the rise.
One of the principal challenges in NiTi coating is how to achieve adequate adhesion between NiTi and the substrate material. It is known that Hot Isostatic Pressing (HIP) can be used to produce bulk NiTi components from powders [4, 5, 6]. In the present study, machining of NiTi-coated stainless steels is investigated as a potential NiTi-coating method for stainless steels.

2. MATERIALS

First, the samples used in the drilling tests were machined from the stainless steel blocks (X2CrNi 19 11). The nominal composition of the test steel is presented in Table 1. The capsule (Figure 1a) for HIP operation was welded from stainless steel plate (AISI 316) onto this block. The capsule was filled with rotating disc atomised

NiTi powder (FUKUDA®) with an average particle size of 0.23 mm and composition 49.4±4.7 at-% Ni and 50.6±4.7 at-% Ti. The target bulk material composition (Ni/Ti) in at-% is 50/50, which in wt-% is 55/45. After the HIPing of the NiTi powder onto the block, the capsule was removed with a solid carbide milling tool for later drilling tests.

Figure 1: The HIPing capsule

Table 1: The nominal composition of the steel used in the drilling experiment

% C	% Mn	% S	% P	% Cr	% Ni	% Si	% V
0.03	1.20	0.015	0.04	18.4	9.2	0.4	0.06

3. METHODS

The HIP treatment was used to sinter coatings from NiTi powder onto the base material block. These samples were mounted in a stainless steel capsule that was evacuated to a pressure of 10^{-5} mbar. The HIPing parameters were 900 °C, 100 MPa, and 3 h. The cooling rate was 4.6 K/min.
Drilling tests were carried out using a horizontal machining centre. The tests used TiCN- and TiN-coated cemented carbide drills with a diameter of Ø8.5 mm, at a cutting speed of 50 m/min and feed rates of 0.1, 0.15, and 0.2 mm/rev. In the tests used cemented carbide drill material with coating layers is presented in Figure 2.

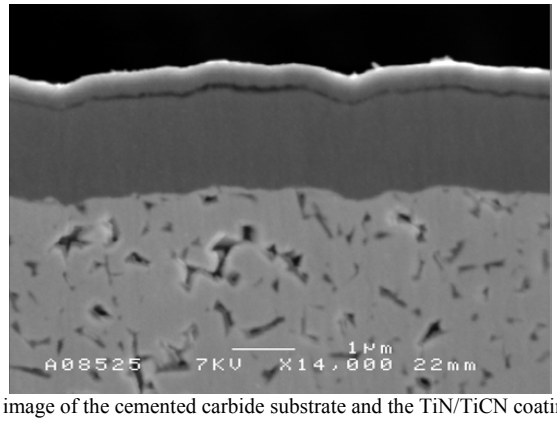

Figure 2: An SEM image of the cemented carbide substrate and the TiN/TiCN coating layers on the drill used in the tests

Drilling tests were done both with and without through-spindle cooling. The pseudo-elasticity of the HIPed NiTi coating was tested with Vickers hardness measurements, using a load of 9.81 N. From the chips and drilled test piece, cross-sectional samples were produced. These samples were polished and etched with picric acid and with a NaOH/water solution with electrolytic etching.

4. RESULTS

The microstructure of HIPed NiTi coating is shown in Figure 3. The NiTi powder has sintered into solid material, in which only some inter-granular pores could be detected. The hardness was tested with a Vickers-hardness measuring device, from both the steel and the NiTi coating. The hardness print of the steel shows a typical Vickers imprint (Figure 4a) on the steel surface, whereas the imprint on the NiTi coating shows retraction of the material on the imprint edges (Figure 4b). The retraction is due to the pseudo-elastic nature of the NiTi coating.

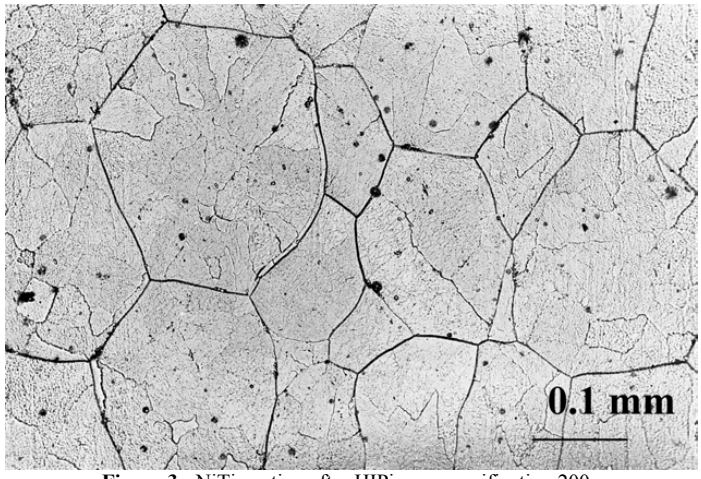

Figure 3: NiTi coating after HIPing - magnification 200x

The interface between the coating and the steel was studied after making longitudinal polished and etched cross-sections from the drilled hole edge and chips. The interface between the coating and base material is shown in Figure 5a and Figure 5b. Numbers in the Figure 5b indicate EDS analysis, which shows diffusion of iron and chromium into NiTi..

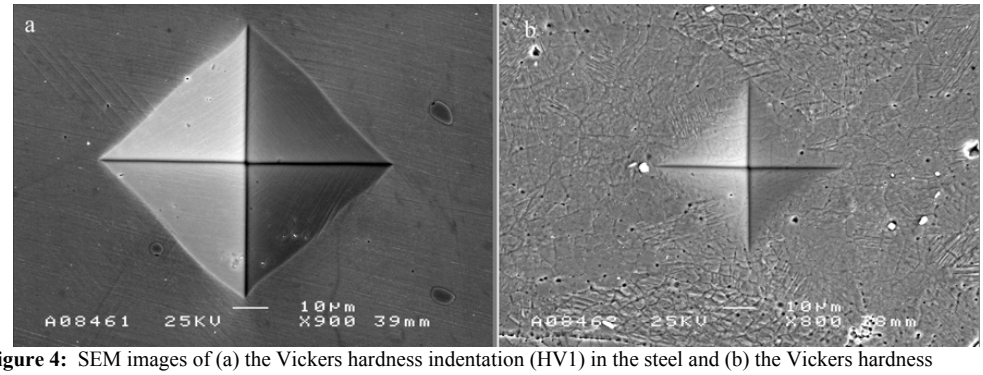

Figure 4: SEM images of (a) the Vickers hardness indentation (HV1) in the steel and (b) the Vickers hardness indentation (HV1) in the NiTi coating

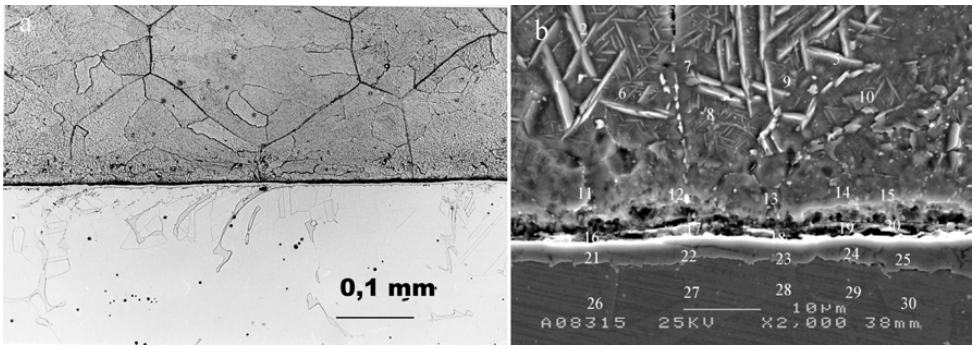

Figure 5: (a) Optical micrograph of the NiTi coating and stainless steel interface and (b) an SEM image of the interface with points used for Quantitative EDS element analysis. Etched with picric acid

The cutting edges of TiN and TiCN-coated drills that were examined by SEM analysis are shown in Figure 6a, Figure 6b, and Figure 6c. Figure 6a shows the unused cutting edge of a solid carbide drill, and (b) the edge after drilling without internal through-spindle cooling and with a machining speed of 50 m/min and feed rate of 0.1 mm/rev. Figure 6c shows a cutting tool after drilling operation with the same cutting parameters but using internal through-spindle cooling. Figure 7a and Figure 7b show the effect of cutting fluid on the drill surface. Figure 8 shows an SEM image of the wear to the drill surface. The cemented carbide tool´s TiCN and TiN coating layers experience wear when NiTi-coated stainless steel is drilled with a cutting speed of 50 m/min and a feed rate of 0.15 mm/rev.

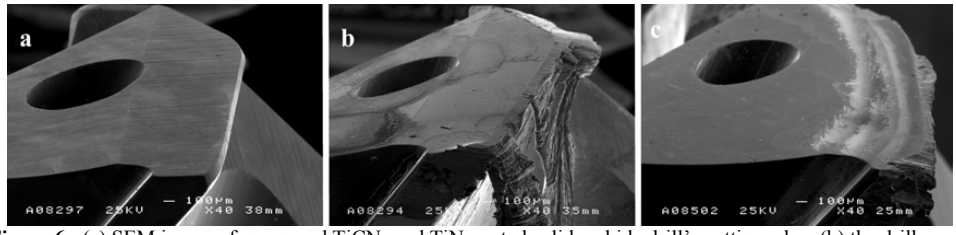

Figure 6: (a) SEM image of an unused TiCN- and TiN-coated solid carbide drill's cutting edge, (b) the drill after drilling without built-up edge (BUE), and (c) the drill after use of internal cooling

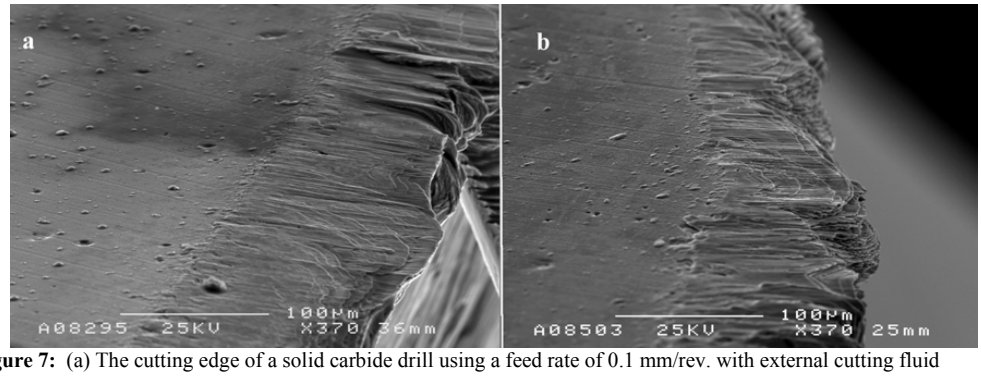

Figure 7: (a) The cutting edge of a solid carbide drill using a feed rate of 0.1 mm/rev. with external cutting fluid supply and (b) the cutting edge with a feed rate of 0.1 mm/rev. and internal cutting fluid supply

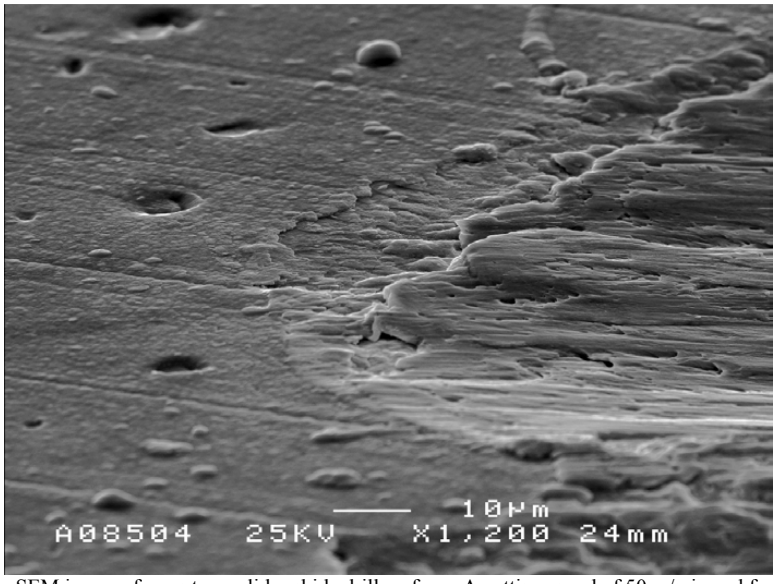

Figure 8: An SEM image of wear to a solid carbide drill surface. A cutting speed of 50 m/min and feed rate of 0.15 mm/rev were applied

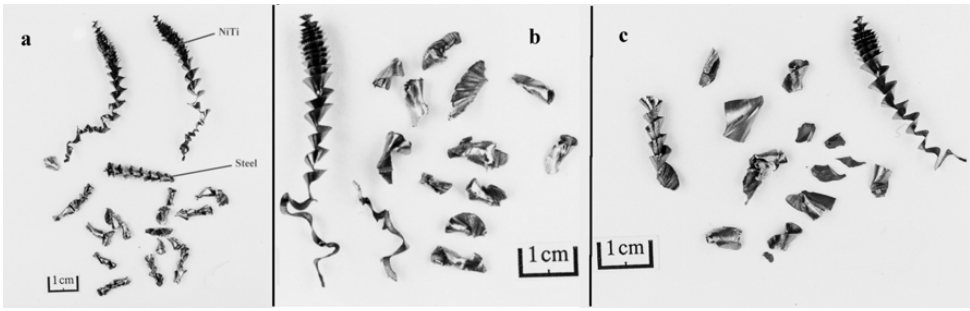

Figure 9: (a) The drilling chips with feed rate of 0.1 mm/rev., (b) drilling chips with a feed rate of 0.15 mm/rev. and (c) with 0.2 mm/rev. A cutting speed of 50 m/min was used. Conventional cutting fluid supply was used

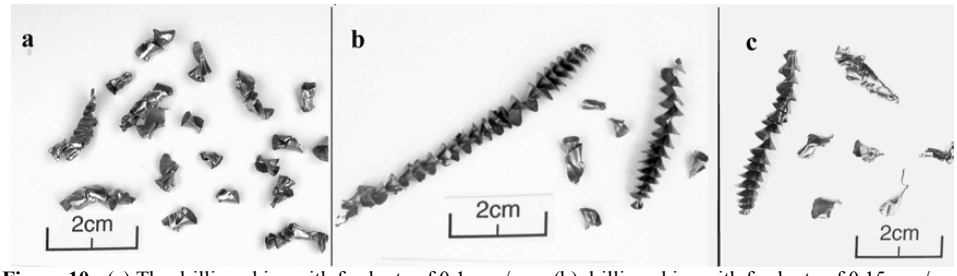

Figure 10: (a) The drilling chips with feed rate of 0.1 mm/rev., (b) drilling chips with feed rate of 0.15 mm/rev. and (c) with 0.2 mm/rev. A cutting speed of 50 m/min was used. Through-spindle cutting fluid supply was used

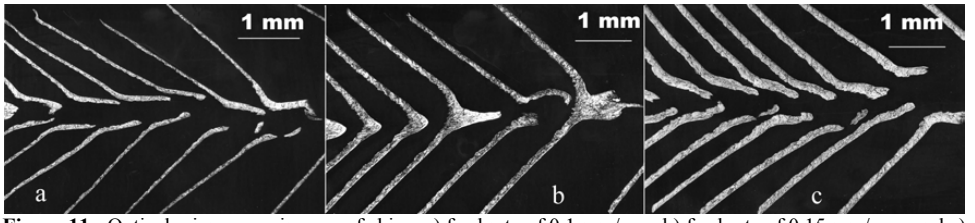

Figure 11: Optical microscope images of chips: a) feed rate of 0.1 mm/rev., b) feed rate of 0.15 mm/rev., and c) feed rate of 0.2 mm/rev

The formation of chips was also analysed from polished chip samples. An SEM image of the deformation of the interface between the steel and NiTi coating is shown in Figure 12.

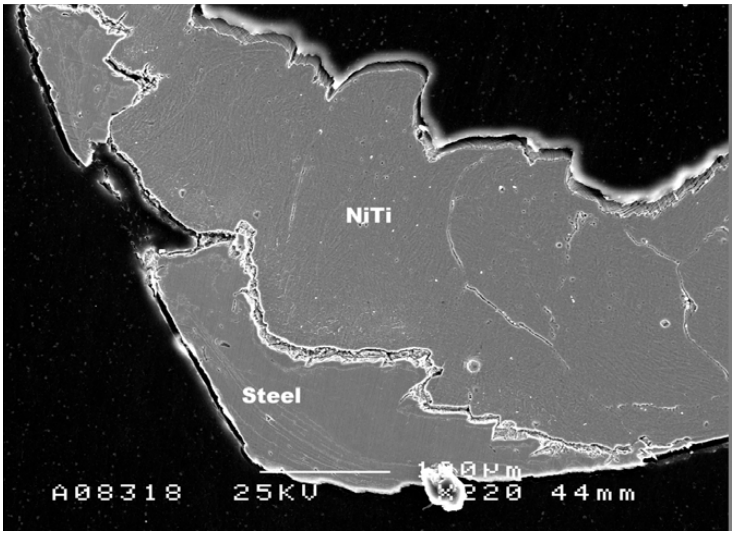

Figure 12: An SEM image of the deformation of the interface between the steel and NiTi coating

A change in chip morphology was detected between the NiTi coating and steel chips. Firstly, when the NiTi coating is drilled, the chip is deformed strongly. The chips are conical and highly spiral in form. Secondly, when the drill has reached the interface between the NiTi coating and the stainless steel, the shape becomes that of conventional stainless steel chips. The chips encountered during the drilling operation were also red-hot. These chips, produced at a cutting speed of 50 m/min and feed rate of 0.1 mm/rev, are shown in Figure 9a, Figure 9b, and Figure 9c. Figure 10a, Figure 10b, and Figure 10c present the macroscopic chip geometry when internal through-spindle cutting fluid is applied. In the opening chip, the NiTi spiral (Figure 10b and Figure 10c) stays open and is not packed.

The effect of feed rate on NiTi chip formation is shown in Figure 11a. Figure 12 presents a stainless steel and NiTi chip boundary. Figure 13a and Figure 13b present a NiTi chip. Figure 13a shows the chip formation with external cutting fluid supply and Figure 13b the chip formation with internal cutting fluid supply.

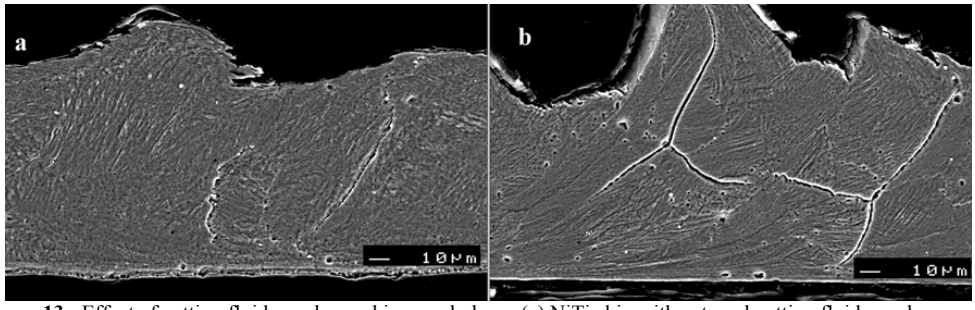

Figure 13: Effect of cutting fluid supply on chip morphology: (a) NiTi chip with external cutting fluid supply and (b) NiTi chip with internal through-spindle cutting fluid supply

5. DISCUSSION

The stainless steel work piece with NiTi coating was produced by HIP treatment, and sufficient adhesion properties were achieved. After a machining operation was performed on the capsule, the interface between the stainless steel block and NiTi coating was intact. The drilling experiments showed that the tool wear mechanism affected by built-up edge formation on the cutting tool for NiTi-coated stainless steel was similar to that with conventional stainless steel.

The opening chips also showed good adhesion between NiTi and stainless steel, as these chips were found to be unbroken. The formation of the BUE detected in drills might have been enhanced by the tool coating (TiCN and TiN), which also merits further investigation.

Chip morphology and chip dimensions were studied. After chip observation for chips formed at different feed rates, the macroscopic aspects can be studied. It is recognised that during machining, two mechanisms of chip formation can apply. For ductile materials, the chip formation was followed by a shearing in the plastic region. For these materials, the length of the chip and its thickness depend on the material´s elasto-plastic behaviour. An increase in plasticity leads to the formation of a chip that is difficult to break [7]. As an opening chip that was formed when a hole was drilled through the NiTi layer, the chip was formed fan concatenated with long tubular stainless steel, chip which was after that broken into smaller chips.

Figure 12a and Figure 12b show the difference in chip formation when cutting fluid supply switches from external conventional supply to internal cutting fluid flow. The effect of chip size on hole surface finish was not examined.

The first drilling showed strongly deformed chips that went through a red-hot stage. Their deformation could be related to shape memory effects. Shape memory effects arise also when chip micrographs with external and internal cutting fluid supply are compared (see Figure 13a and Figure 13b). Figure 13a shows a more strongly deformed microstructure than Figure 13b. The influence of cutting fluid could have affected the strongly deformed chip microstructure, causing it propably to remain in martensitic phase. Figure 13a shows the retired structure of the chip after drilling with less cooling.

6. CONCLUSIONS

From the results obtained in the study, the following conclusions were drawn.

The drilling of NiTi-coated stainless steel with appropriate cutting parameters is possible without severe tool wear. A cutting speed of 50 m/min and feed rate between 0.1 and 0.2 mm/rev with solid carbide drills and through-spindle cooling should be applied.

Tool wear mechanisms in through-spindle cooling are affected by built up edge formation

The effect of cutting parameters on chip size and formation was examined. The macroscopic geometry of stainless steel chips with NiTi coating differs from that of conventional stainless steel chips. The opening chips form from the NiTi concatenated with conventional long stainless steel chips.

Cutting-fluid presence significantly affected the predominant NiTi chip size and geometry. When internal cooling is applied, the geometry of NiTi chips remains open-spiral and the microstructure with deformed grains. When external cooling is applied, NiTi chips are strongly deformed and packed.

Feed rate does not have a significant effect on NiTi chip geometry.

ACKNOWLEDGEMENTS

The authors are thankful to Sulzer Pumps Finland for providing the stainless steel materials that were tested.

REFERENCES

[1] L. Jiang, H. Hänninen, J. Paro, and V. Kauppinen, *Active Wear and Failure Mechanisms of TiN-Coated High Speed Steel and TiN-Coated Cemented Carbide Tools When Machining Powder Metallurgically Made Stainless Steels.* Metallurgical and Materials Transactions, 27A (1996) 9, 2796-2808.
[2] Z. Li and Q. Sun, *The initation and growth of macroscopic martensite band in nano-grained NiTi microtube under tension.* International Journal of Plasticity 18 (2002), 1481-1498.
[3] D. Starosvetsky and I. Gotman, *TiN coating improves the corrosion behaviour of superelastic NiTi surgical alloy.* Surface and Coatings Technology 148 (2001), 268-276.
[4] G. Wang, *Welding of Nitinol to Stainless Steel.* Proceedings of SMST-97, 1997, 131-136.
[5] J. Koskinen, E. Haimi, A. Mahiout, V. Lindroos, and S-P. Hannula, *Superelastic NiTi coatings with good corrosive wear resistance.* Proceedings of the International Conference on Martensitic Transformations (ICOMAT 02). Espoo, 2002, 10-14.
[6] J. Koskinen, E. Haimi, *Method for Forming a Nickle-Titanium Plating*, US Patent 6,458,317 (2002).
[7] H., Schulz, *Hochgeschwindigkeitsfräsen metalischer und nichtmetallischer Werkstoffe. Carl Hanser Verlag 1989. München Wien. 348 p.*

PUBLICATION VII

Deformation effects on the interface between X2CrNi 19 11 stainless steel and HIPed NiTi coating in machining

In: Proceedings of the 18th International Conference on Production Research. Salerno, Italy, 31st July – 4th August 2005. 5 p.

DEFORMATION EFFECTS ON THE INTERFACE BETWEEN X2CrNi 19 11 STAINLESS STEEL AND HIPED NiTi COATING IN MACHINING

J.A. Paro, T.E. Gustafsson, and J. Koskinen
VTT Industrial Systems, Technical Research Centre of Finland
P.O. Box 1703, 02044 VTT, Espoo, Finland

Abstract
This study investigated the deformation effects of the interface between conventionally produced stainless steel X2crNi 19 11 and HIPed NiTI coating (Hot Isostatic Pressed). Near-equiatomic nickel-titanium alloy (NiTi) has many attractive material properties, such as pseudo-elasticity and shape memory effects, which result into beneficial engineering properties e.g. as cavitation resistant coatings in addition to its well-known shape memory properties. Stainless steels are often considered to be poorly machinable materials; materials with high elasticity are also difficult to machine. In drilling stainless steel with a pseudo-elastic coating material, machinability difficulties are caused by the high strength and work hardening rate of steel and the pseudo-elastic properties of the coating material. The deformation effects were studied by analyzing cemented carbide drills and chips. The interface between stainless steel and NiTi coating was examined with SEM (Scanning Electron Microscopy) and EDS (Energy Dispersive Spectroscopy) analysis. The effect of feed rate on chip formation was analyzed. The cutting tests indicated that cutting speeds of 50 m/min, a feed rate of 0.1-0.2 mm/rev, and solid carbide drills can be applied, from a machinability standpoint. A HIPed pseudo-elastic coating decreases machinability. When effective cutting speeds and feed rates were utilized, optimal tool life was achieved without severe decrease in coating properties.

Keywords:
machinability, stainless steel, NiTi coating

1 INTRODUCTION

Shape memory alloys (SMA) are functional materials which are well known for their unique mechanical properties. The shape memory effects of these materials are caused by a reversible martensitic transformation. This functional material is very difficult to machine because of its high ductility, its different shape memory properties in dependence on temperature and the strong work hardening when this material is deformed. Austenitic stainless steels area also considered to be difficult to machine. Built-up edge (BUE) and irregular wear situations are often faced in machining operations. Difficulties from the machining point of view increase when duplex and high-strength stainless steels are to be machined. [1] In the drilling operation, small, well-broken chips are desirable. During drilling and formation, the chips rotate with the drill and impact the hole wall or interior of the flute. In addition to this NiTi possesses a high ductility and tends to strong work hardening when deformed [2, 3].

Shape memory alloys based on NiTi have a large variety of applications. One of the principal challenges in NiTi coating is how to achieve adequate adhesion between NiTi and the substrate material. It is known that Hot Isostatic Pressing (HIP) can be used to produce bulk NiTi components from powders [4, 5, 6]. The objective is to investigate the machinability of NiTi coating. The machinability is evaluated with respect to chip deformations and stainless steel and NiTi coating interface studied from chip samples.

2 MATERIALS

The samples used in the drilling tests were produced from the stainless steel blocks. The nominal composition of the stainless steel (AISI 304) blocks was 0.03%C, 1.20%Mn, 0.015%S, 0.04%P, 18.4%Cr, 9.2%Ni, 0.4%Si and 0.06%V. The capsule for HIP operation was welded from stainless steel plate (AISI 316) onto this block. The capsule was filled with rotating disc atomised NiTi powder (FUKUDA®) with an average particle size of 0.23 mm and composition 49.4±4.7 at-% Ni and 50.6±4.7 at-% Ti. The target bulk material composition (Ni/Ti) in at-% is 50/50, which in wt-% is 55/45. After the HIPing of the NiTi powder onto the block, the capsule was removed and the sample face milled for drilling tests. The evacuation pressure for HIPing was 10^{-5} mbar and treatment parameters were 900 °C, 100 MPa, and 3 h. The cooling rate was 4.6 K/min.

3 METHODS

Drilling tests were carried out using a horizontal machining centre equipped with 12 000 rpm, 22 kW spindle. The tests used TiCN- and TiN-coated cemented carbide drills with a diameter of Ø8.5 mm, at a cutting speed of 50 m/min and feed rates of 0.1, 0.15, and 0.2 mm/rev were used with through spindle coolant supply. In the tests used cemented carbide drill with built-up edge is presented in Figure 1.

The pseudo-elasticity of the HIPed NiTi coating was tested with Vickers hardness measurements, using a load of 9.81 N. From the chips cross-sectional samples were produced. These samples were polished and etched with picric acid and with a NaOH/water solution with electrolytic etching.

Samples were SEM and EDS analysed. The drill head and chip build-up was studied in detail with a scanning electron microscope (SEM) and analyzed with an X-ray analyzer (EDS), which can detect carbon (C) and elements heavier than that. The compositions were determined from the X-ray-spectra using a correction factor program $\Phi(\rho z)$. The X-ray lines used in the analysis were chromium (Cr), iron (Fe), nickel (Ni), and titanium (Ti). The quantitative result results were normalised to 100 %. To calibrate the magnification of the microscope and to perform the X-ray-analysis ASTM E766-98 and E1508-98 were used.

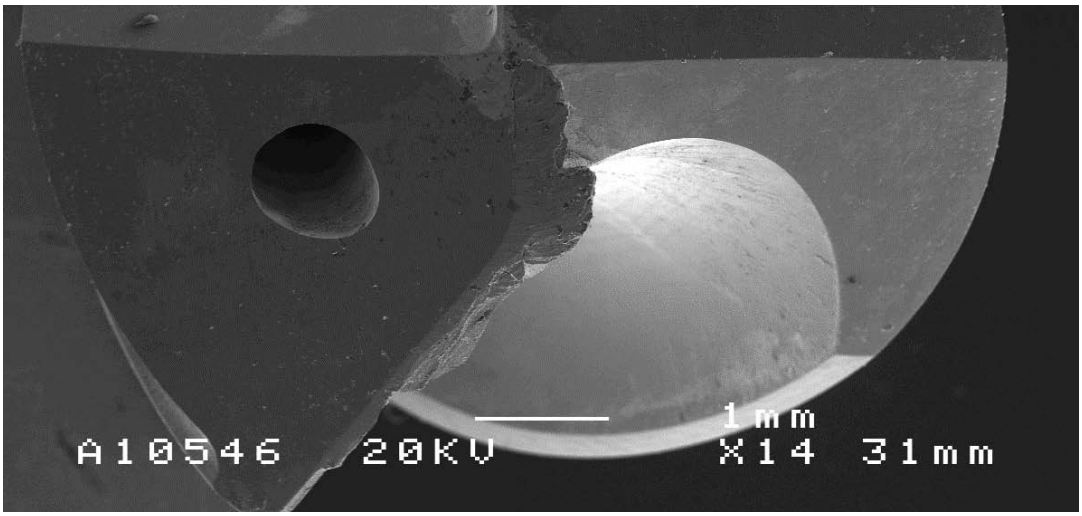

Figure 1: The drill used in cutting tests. The formation of built-up edge (BUE) is present.

In SEM-images obtained with a 25 kV acceleration voltage at a working distance of 39 mm, the error in the magnification is ± 4 %. The smallest detectable content in the X-analysis is approx. 0.3-0.5 % for metals depending on the composition of the analyzed material. Quantitative line scans were obtained utilizing Point Tagged Spectroscopy (PTS) in X-ray analysis. The quantitative line scans were used to estimate Cr-rich surface layer thickness on the in the stainless steel and Fe diffusion depth into the NiTi coating. The measurements were performed across the NiTi/Stainless Steel-interface. Chip thickness was measured from nine positions from both 0.1 and 0.2 mm/rev chips.

4 RESULTS

The microstructure of HIPed NiTi coating is shown in Figure 2. The NiTi powder has sintered into solid material, in which only some inter-granular pores could be detected.

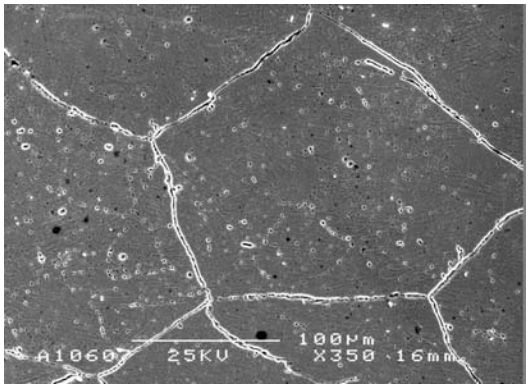

Figure 2: NiTI coating after HIPing-magnification 240x.

On the cutting edge of in Figure 1. presented solid carbide drill with TiN and TICN coating was SEM and EDS analysed. It was found that NiTi between TiN-coating and steel built-up edge (BUE) acts as an adhesive. Cutting speed 50 m/min and feed rate 0.2 mm/rev was used. Figure 4a shows a SEM image of a chip with a cutting speed of 50 m/min and feed rate of 0.1 mm/rev. Figure 4b shows the EDS line scan location resulting in Figure 4c. Figure 5a shows a SEM image of a chip with a cutting speed of 50 m/min and feed rate of 0.2 mm/rev. Figure 5b. shows the EDS line scan location resulting in Figure 5c. In Table 1. is presented the influence of feed rate on the thickness of Cr-rich layer and the diffusion of Fe into NiTi and chip thickness. It was found a wider Cr-rich interface in Figure 5b and Figure 5c with feed rate of 0.2 mm/rev was used in drilling than in Figure 5b and Figure 5c when feed rate of 0.1 mm/rev was used in drilling. Chip thickness with feed rate of 0.1 mm/rev was 88.8 µm and 171 µm with feed rate of 0.2 mm/rev. Figure 6 presents the micro hardness measurements performed across the NiTi/stainless steel interface with drilling feed rate value of 0.1 mm/rev and Figure 7 presents the micro hardness measurements performed across the NiTi/stainless steel interface with drilling feed rate value of 0.2 mm/rev. In Table 1 is presented dimensions of Fe-diffusion and Cr-rich layers are also approximately marked in Figure 6 and Figure 7. Figure 6 shown micro hardness values are between 420 HV and 501 HV. The measured micro-hardness value near the interface is higher than the value of NiTi chip. In Figure 7 shown micro hardness values are between 402 HV and 420 HV.

Table 1: Characteristics of the chip and NiTi/Steel interface.

Chip thickness (µm)	88.8	171
Feed rate (mm/rev)	0.1	0.2
Cr-rich layer (µm)	2.1	4.5
Fe-diffusion layer (µm)	4.3	27

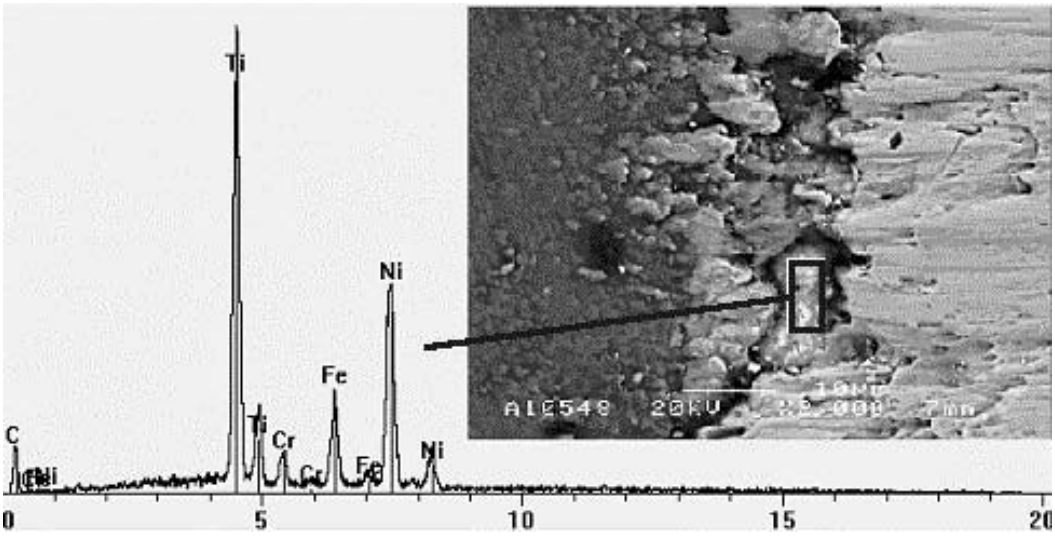

Figure 3: SEM image and EDS mapping of the built up edge formed in the cutting edge of the drill. Cutting speed 50 m/min and feed rate 0.2 mm/rev. Magnification-2 000x.

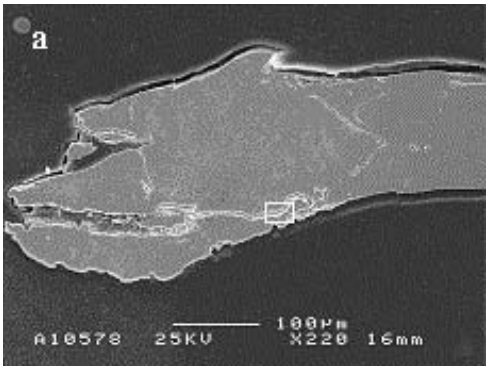

Figure 4a: NiTi and stainless steels interface with cutting speed of 50 min and feed rate of 0.1 mm/rev.

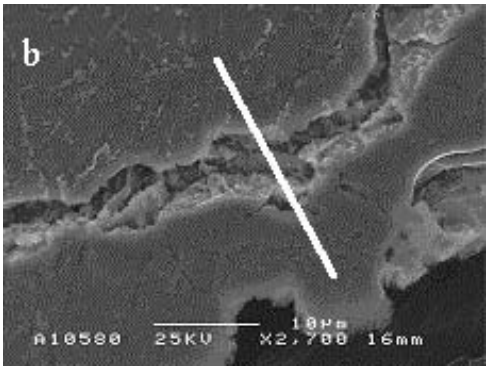

Figure 4b: Line scanning location across the NiTi and stainless steel interface.

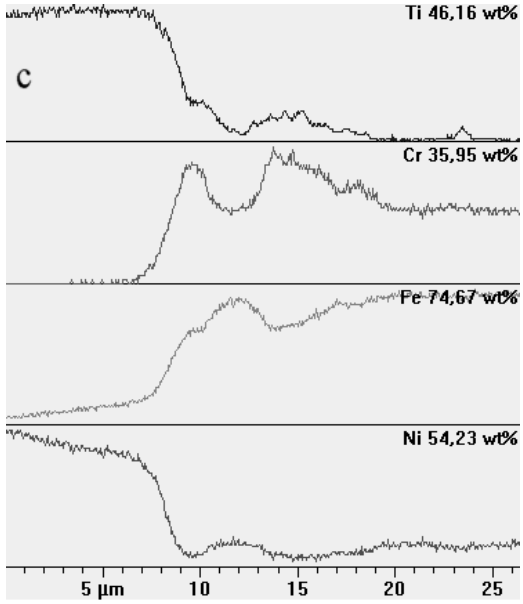

Figure 4 c: Element wt% along the line presented in Figure 4b.

It is also observed a strong deformation of NiTi coating and stainless steel chip. Grain boundaries were formed. The interface also seems to withstand the deformation without break down with feed rates of 0.1 mm/rev and 0.2 mm/rev.

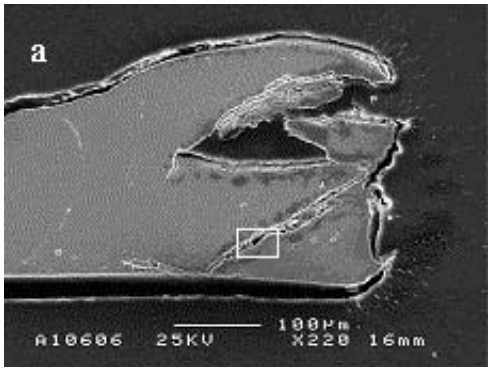

Figure 5a: NiTi and stainless steels interface with cutting speed of 50 min and feed rate of 0.2 mm/rev.

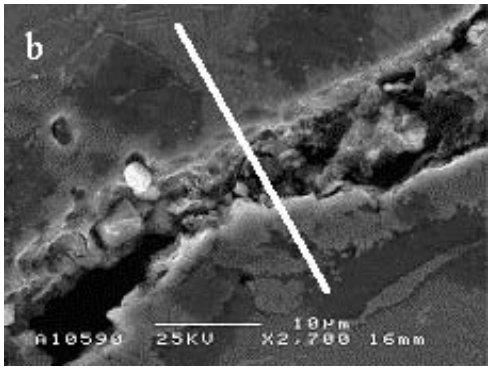

Figure 5b: Line scanning location across the NiTi and stainless steel interface.

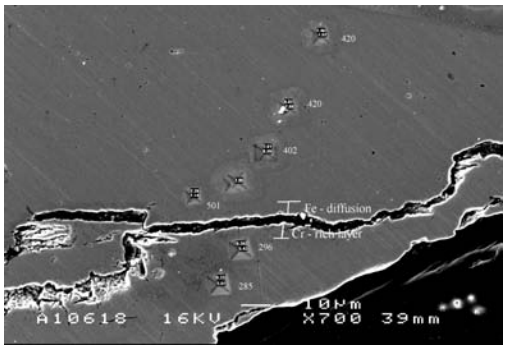

Figure 6: Micro hardness measurements across NiTi and stainless steel interface with feed rate of 0.1 mm/rev.

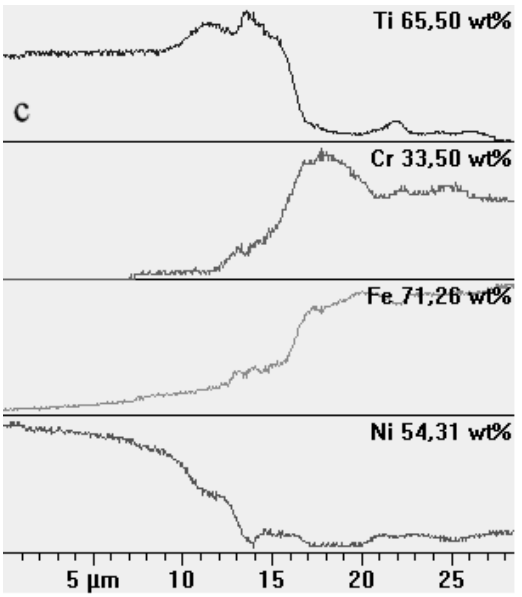

Figure 5c: Element wt% along the line presented in Figure 5b.

Chip thicknesses of deformed chips were measured from SEM images using in Figure 4a and Figure 5a shown chip samples. A chromium rich layer on the steel side and iron diffusion layer into the NiTi were detected from both 0.1 and 0.2 mm/rev feed rate chips. Measured chip thickness, thickness of Cr-rich layer and Fe-diffusion layer were found increasing when feed rate was increased.

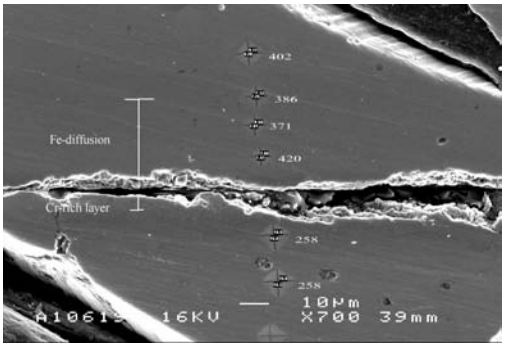

Figure 7: Micro hardness measurements across NiTi and stainless steel interface with feed rate of 0.2 mm/rev.

5 DISCUSSION

The machinability of stainless steel work piece with HIPed NiTi coating with solid carbide drill was examined. The experiments showed that the tool wear mechanism affected by built-up edge formation on the cutting tool for NiTi-coated stainless steel was similar to that with conventional stainless steel. Also according to Weinert et al. (2004) the special properties of NiTi shape memory alloys lead to a difficult processing of these intermetallic compounds [7].

The interface between steel and the NiTi coating was studied via SEM and EDS analyses. It was noticed that the chips became work hardened during drilling process for both cutting parameters. The deformation of the chips has been studied and micro hardness alteration has been found because of work hardening and the diffusion of Fe into NiTi. Chromium rich layer forms on the steel during HIPing, when also iron diffuses into NiTi. The work hardening of NiTi observed in this study is due to the drilling. The increase of feed rate increases the depth of work hardened layer of NiTi coating.

The interface between NiTi and steel is strong enough to withstand shear stresses caused by drilling forces and therefore the drilling process can be optimised according to difficult to machine base materials.

The diffusion mechanism during HIPing and work hardening merits further investigation.

According to Weinert et al. (2004) best results concerning work piece quality and tool costs can be obtained when applying coated cemented carbide tools is used. Common cutting materials for machining Ni- or Ti-based alloys can be applied [8,9] This work also shows machinability of NiTi-alloy and tool wear mechanism affected by BUE and deformation capability of NiTi coating and stainless steel interface detected from chips.

6 CONCLUSIONS

From the results obtained in the study, the following conclusions were drawn.

The work hardening rate of NiTi coating chip is increased when feed rate is increased from 0.1 mm/rev into 0.2 mm/rev. The NiTi coating adhesion into stainless steel is not affected by diffusion of Fe into NiTi or Cr-rich layer in the steel.

The drilling of NiTi coated stainless steel with appropriate cutting parameters is possible without severe tool wear. A cutting speed of 50 m/min and feed rate between 0.1 and 0.2 mm/rev with solid carbide multilayer coated drills and through-spindle cooling should be applied.

Tool wear mechanisms are affected by built-up edge (BUE) formation of NiTi and stainless steel on the TiN coating of solid carbide drill.

7 ACKNOWLEDGEMENTS

The authors are thankful to Sulzer Pumps Finland for providing the stainless steel materials that were tested.

8 REFERENCES

[1] L. Jiang, H. Hänninen, J. Paro, and V. Kauppinen, Active Wear and Failure Mechanisms of TiN-Coated High Speed Steel and TiN-Coated Cemented Carbide Tools When Machining Powder Metallurgically Made Stainless Steels. Metallurgical and Materials Transactions, 27A (1996) 9, 2796-2808.

[2] K. Weinert, V., Petzoldt, V., D. Kötter, Truning and Drillign of NiTi Shape Memory Alloys. Annals of the CiRP 53/1/2004 pp. 65-68

[3] D. Starosvetsky and I. Gotman, TiN coating improves the corrosion behaviour of superelastic NiTi surgical alloy. Surface and Coatings Technology 148 (2001), 268-276.

[4] G. Wang, Welding of Nitinol to Stainless Steel. Proceedings of SMST-97, 1997, 131-136.

[5] J. Koskinen, E. Haimi, A. Mahiout, V. Lindroos, and S-P. Hannula, Superelastic NiTi coatings with good corrosive wear resistance. Proceedings of the International Conference on Martensitic Transformations (ICOMAT 02). Espoo, 2002, 10-14.

[6] J. Koskinen, E. Haimi, Method for Forming a Nickle-Titanium Plating, US Patent 6,458,317 (2002).

[7] H., Schulz, Hochgeschwindigkeitsfräsen metalischer und nichtmetallischer Werkstoffe. Carl Hanser Verlag 1989. München Wien. 348 p.

[8] Hanasaki, S., Fujiwara, J., Touge, M., Hasegawa, Y., 1990, Tool Wear of Coated Tools when Machining of a high Nickels Alloy, Annals of the CIRP, 39/1: 77-80

[9] Corduan, N., himbert, T., Poulachon, G., Dessoly, M., Vigneau, J., Payoux, B., 2003 Wear Mechanisms pf New Tool Materials of Ti-6Al-4V High Performance Machining, Annals of the CIRP, 52/1: 73-76

Published by

Series title, number and report code of publication

VTT Publications 610
VTT–PUBS–610

Author(s)
Paro, Jukka

Title

Machinability effects of stainless steels with a HIPed NiTi coating in high-efficiency machining operations

Abstract

The machinability effects of new high-strength stainless steels are studied due to specific properties arising from their structure. In the grinding operations HIPed austenitic 316L, duplex 2205 and super duplex 2507 and as-cast 304 stainless steel; in turning HIPed 316L, duplex stainless steel 2205 and X5 CrMnN 18 18 stainless steel; and in drilling HIPed PM Duplok 27 and duplex stainless steel ASTM8190 1A and X2CrNi 1911 with a HIPed NiTi coating were studied in revised machining testing environments by tool life testing, and chip and work piece surface morphology analysis. Chips, work piece surfaces and cutting tools were analysed by scanning electron microscopy (SEM) and EDS.

High toughness, work hardening and low heat conductivity have a synergistic effect in inducing machinability difficulties. An increased amount of alloying elements is found to decrease machinability in the forms of increased cutting force and work hardening rate of machined surface, and decreased tool life and surface roughness. Powder metallurgically produced stainless steels introduce increased machinability difficulties caused by more hard oxide particles included in PM-produced stainless steels. The formation of built-up edge is found to affect the machinability and tools of the tested high-strength stainless steels.

In grinding operations, HIPed austenictic 316L and duplex 2205 stainless steel are rated according to cutting force, work hardening rate and the amount of microvoids and microcracks in the ground surfaces. In turning operations, HIPed 316L, duplex stainless steel 2205 and X5 CrMnN 18 18 stainless steels are assessed in machinability order. The machinability of conventional cast duplex stainless steel ASTM8910 and HIPed duplex stainless steel Duplok27 were sorted according to their PRE-value.

Finally, in this study the suitability of coated cemented carbide tools in the drilling of conventionally produced cast stainless steels with a HIPed NiTi coating was investigated. In the drilling of difficult-to-cut X2CrNi 19 11 stainless steel with a pseudo-elastic coating, effective cutting parameters that maintain the adhesion layer between the NiTi coating and the stainless steel with advantageous surface finish were generated.

Keywords
stainless steels, machinability, machine tools, wear, surface coating, grinding, turning, drilling, nickel-titanium alloys

ISBN
951–38–6853–2 (soft back ed.)
951–38–6854–0 (URL: http://www.vtt.fi/publications/index.jsp)

Series title and ISSN	Project number
VTT Publications 1235–0621 (soft back ed.) 1455–0849 (URL: http://www.vtt.fi/publications/index.jsp)	

Date	Language	Pages	Price
October 2006	English, Finnish abstr.	51 p. + app. 82 p.	C

Contact
VTT Technical Research Centre of Finland,
Metallimiehenkuja 8, P.O. Box 1000,
FI-02044 VTT, Finland
Phone internat. +358 20 722 111
Fax +358 20 722 3349

Sold by
VTT Technical Research Centre of Finland
P.O.Box 1000,
FI-02044 VTT, Finland
Phone internat. +358 20 722 4404
Fax +358 20 722 4374

Julkaisija

VTT

Julkaisun sarja, numero ja raporttikoodi

VTT Publications 610
VTT–PUBS–610

Tekijä(t)
Paro, Jukka

Nimeke

Isostaattisella kuumapuristusmenetelmällä NiTi-pinnoitetun ruostumattoman teräksen suurtehotyöstön lastuttavuusvaikutuksia

Tiivistelmä

Uusien lujien ruostumattomien terästen ominaisuuksilla on suuri vaikutus niiden lastuttavuuteen. Tässä työssä tutkittiin isostaattisella kuumapuristuksella (HIP) valmistettujen austeniittisen 316L, duplex 2205 ja super duplex 2507 sekä valetun 304 ruostumattomien terästen hiontaa, HIP-menetelmällä valmistetun 316L ruostumattoman teräksen ja X5 CrMnN 1818 -typpiteräksen sorvausta sekä HIP-menetelmällä valmistetun Duplok 27 -teräksen ja ruostumattoman duplex-teräksen ASTM8190 1A porausta. Lisäksi tutkittiin HIP-menetelmällä valmistetun NiTi-pinnoitteella pinnoitetun X2CrNi 1911 ruostumattoman teräksen porausta. Lastuttavuutta selvitettiin sovelletuin testein tutkimalla terän kestoaikaa, analysoimalla lastujen ja työkappaleen pinnan morfologiaa. Lastuja, työkappaleiden pintoja sekä teriä tukittiin pyyhkäisyelektronimikroskoopilla (SEM) ja energiadispersiivisellä alkuaineanalyysillä (EDS).

Tutkittujen terästen ominaisuuksista suuri sitkeys, muokkauslujittuminen sekä matala lämmönjohtavuus aiheuttavat lastuttavuusongelmia. Runsaan seostuksen on todettu huonontavan lastuttavuutta, sillä lastuamisvoimat kasvavat, terien kestoajat lyhentyvät, koneistetut pinnat muokkauslujittuvat sekä työkappaleen pinnanlaatu huononee. Pulverimetallurgisesti valmistetuttujen ruostumattomien terästen mikrorakenteen kovat oksidit vaikeuttavat myös koneistettavuutta. Irtosärmän muodostumisen todettiin myös heikentävän testattujen terästen lastuttavuutta.

Tässä työssä havaittiin suurten lastuamisvoimien sekä hiotun pinnan muokkauslujittumisen ja mikrohalkeamien ja -säröjen muodostumisen vaikuttavan 316L sekä duplex 2205 ruostumattoman teräksen hiottavuuteen. Sorvaustutkimuksissa selvitettiin 316L:n, 2205:n sekä X5 CrMnN 1818:n lastuttavuuteen vaikuttavia tekijöitä, terän kestoaikoja sekä kulumismekanismeja. Porauksessa arvioitiin myös perinteisen valetun duplex-teräksen sekä HIP-menetelmällä valmistetun duplex ruostumattoman teräksen lastuttavuutta PRE-arvon (Pitting Resistance Equivalent) avulla. Lopuksi selvitettiin pinnoitettujen kovametalliporien soveltuvuutta pseudoelastisella NiTi-pinnoitteella pinnoitettujen valettujen ruostumattomien terästen poraukseen. Työssä löydettiin menetelmät ja lastuamisarvot, joilla voidaan saavuttaa riittäviä terien kestoaikoja ja pitää NiTi-pinnoitteen ja ruostumattoman teräksen välinen adheesiokerros vaurioitumatta sekä reikien pinnanlaatu hyvänä.

Avainsanat

stainless steels, machinability, machine tools, wear, surface coating, grinding, turning, drilling, nickel-titanium alloys

ISBN
951–38–6853–2 (nid.)
951–38–6854–0 (URL: http://www.vtt.fi/publications/index.jsp)

Avainnimeke ja ISSN			Projektinumero
VTT Publications 1235–0621 (nid.) 1455–0849 (URL: http://www.vtt.fi/publications/index.jsp)			
Julkaisuaika Lokakuu 2006	Kieli Englanti, suom. tiiv.	Sivuja 51 s. + liitt. 82 s.	Hinta C

Yhteystiedot	Myynti
VTT Metallimiehenkuja 8, PL 1000, 02044 VTT Puh. vaihde 020 722 111 Faksi 020 722 3349	VTT PL 1000, 02044 VTT Puh. 020 722 4404 Faksi 020 722 4374

The machinability effects of new high-strength stainless steels are studied due to specific properties arising from their structure. In the grinding operations HIPed austenitic 316L, duplex 2205 and super duplex 2507 and as-cast 304 stainless steel; in turning HIPed 316L, duplex stainless steel 2205 and X5 CrMnN 18 18 stainless steel; and in drilling HIPed PM Duplok 27 and duplex stainless steel ASTM8190 1A and X2CrNi 1911 with a HIPed NiTi coating were studied in revised machining testing environments by tool life testing, and chip and work piece surface morphology analysis. Chips, work piece surfaces and cutting tools were analysed by scanning electron microscopy (SEM) and EDS.

High toughness, work hardening and low heat conductivity have a synergistic effect in inducing machinability difficulties. An increased amount of alloying elements is found to decrease machinability in the forms of increased cutting force and work hardening rate of machined surface, and decreased tool life and surface roughness. Powder metallurgically produced stainless steels introduce increased machinability difficulties caused by more hard oxide particles included in PM-produced stainless steels. The formation of built-up edge is found to affect the machinability and tools of the tested high-strength stainless steels.

In grinding operations, HIPed austenictic 316L and duplex 2205 stainless steel are rated according to cutting force, work hardening rate and the amount of microvoids and microcracks in the ground surfaces. In turning operations, HIPed 316L, duplex stainless steel 2205 and X5 CrMnN 18 18 stainless steels are assessed in machinability order. The machinability of conventional cast duplex stainless steel ASTM8910 and HIPed duplex stainless steel Duplok27 were sorted according to their PRE-value.

Finally, in this study the suitability of coated cemented carbide tools in the drilling of conventionally produced cast stainless steels with a HIPed NiTi coating was investigated. In the drilling of difficult-to-cut X2CrNi 19 11 stainless steel with a pseudo-elastic coating, effective cutting parameters that maintain the adhesion layer between the NiTi coating and the stainless steel with advantageous surface finish were generated.

Tätä julkaisua myy

VTT
PL 1000
02044 VTT
Puh. 020 722 4404
Faksi 020 722 4374

Denna publikation säljs av

VTT
PB 1000
02044 VTT
Tel. 020 722 4404
Fax 020 722 4374

This publication is available from

VTT
P.O. Box 1000
FI-02044 VTT, Finland
Phone internat. +358 20 722 4404
Fax +358 20 722 4374

ISBN 951–38–6853–2 (soft back ed.)
ISSN 1235–0621 (soft back ed.)

ISBN 951–38–6854–0 (URL: http://www.vtt.fi/inf/pdf/)
ISSN 1455–0849 (URL: http://www.vtt.fi/inf/pdf/)